

# Dissertation

## **Node Coordination and Cooperation in Multiuser Wireless Communications**

ausgeführt zum Zwecke der Erlangung des akademischen Grades  
eines Doktors der technischen Wissenschaften

eingereicht an der  
Technischen Universität Wien  
Fakultät für Elektrotechnik und Informationstechnik

von  
Roland Tresch

Wien, 1. April 2011



TECHNISCHE  
UNIVERSITÄT  
WIEN

Vienna University of Technology

Supervisor

Prof. Christoph Mecklenbräuer

Institut für Nachrichtentechnik und Hochfrequenztechnik

Technische Universität Wien, Austria

Examiner

Prof. Ana Isabel Pérez-Neira

Dept. of Signal Theory and Communications

Universitat Politècnica de Catalunya (UPC), Barcelona, Spain

FTW Dissertation Series

Roland Tresch

# **Node Coordination and Cooperation in Multiuser Wireless Communications**



telecommunications research center Vienna

This work was carried out with funding in parts from the STREP project IST-026905 (MASCOT) within the FP6 programme of the European Commission, from the Vienna Science and Technology Fund (Wiener Wissenschafts-, Forschungs- und Technologiefonds, WWTF) within the project "Cooperative Communications in Traffic Telematics", from the Austrian Science Fund (Fonds zur Förderung der wissenschaftlichen Forschung FWF) through the grant NFN SISE (S106) and by the COMET competence center program of the Austrian government and the City of Vienna through the FTW I0 strategic project.

Supervisor at FTW: Maxime Guillaud and Thomas Zemen

This thesis has been prepared using L<sup>A</sup>T<sub>E</sub>X.

April 2011

1. Auflage

Alle Rechte vorbehalten

Copyright © 2011 Roland Tresch

Herausgeber: FTW Forschungszentrum Telekommunikation Wien GmbH

Printed in Austria

ISBN 3-902477-22-9

# Abstract

Most wireless networks are fundamentally interference limited. Interference management has become a prerequisite for a wide class of emerging systems with full reuse of the wireless spectrum, heterogeneous node deployment, the lack of centralized medium access and power control. Signals from concurrent transmissions, separated only in space, are added to the intended signal at the receivers. Hence, high spectral efficiency in such systems necessitates distributed, low complexity interference management algorithms with limited communication overhead. Sophisticated multiuser detection and interference cancellation schemes are prohibited. In this thesis, interference mitigation techniques for multiuser systems are proposed, investigated and analyzed that exclude sharing of user payload data among the transmitters and render joint signal processing at the receivers unnecessary.

A promising approach to achieve high spectral efficiency under the aforementioned conditions is the use of multiple antenna (MIMO) systems. Computationally simple linear beamforming allows to separate spatially the transmitted signals of different users. This manuscript focuses on the MIMO broadcast channel (MIMO-BC) and the  $K$ -user MIMO interference channel (MIMO-IC). Random beamforming using finite rate channel state feedback is studied for point-to-multipoint systems and interference alignment (IA) for independent point-to-point communication. Alignment-based precoding limits the necessary backhaul communication compared to joint MIMO transmission.

In the first part, an improved channel state information (CSI) feedback metric in a MIMO-BC is designed. The data transmission to different users is organized through random beams. The CSI feedback method of random beamforming is extended to cope with noisy MIMO channel observations. The proposed feedback estimation method is based on the perturbation of the measured channel. The resulting signal-to-interference-plus-noise ratio (SINR) feedback can noticeably reduce the outage probability. The increased transmission reliability is achieved at the cost of a minor reduction of the achievable goodput compared to state-of-the-art link quality estimation methods.

In the second part, IA over the  $K$ -user MIMO-IC is studied. In a fully connected  $K$ -user IC with global CSI, alignment achieves virtually interference-free communi-

cation over a dimension reduced channel and maximizes the achievable multiplexing gain. MIMO-IA avoids long symbol extensions that are necessary to achieve the optimal multiplexing gains in single-antenna systems. Closed-form IA solutions for the  $K$ -user MIMO-IC for an arbitrary number of users are found and the sensitivity of alignment-based precoding to imperfect CSI feedback is studied.

The application of IA in practical systems operating at non-asymptotic signal-to-noise ratio (SNR) is explored. To this end, the idealized model thoroughly studied in the IA literature where all desired and interfering signals are of comparable strength is extended and spatial networks are considered, with geographical node distributions and a link model with distance dependent pathloss and fading. In a large network with numerous transmitters and without preexisting infrastructure, a stochastic model is introduced and tools to analyze the performance of clustered node cooperation. The deleterious effect of uncoordinated interference is assessed through the model parameters. Formulas for the link outage probability of IA inside the clusters are established. This modular IA strategy is chosen in order to keep the number of antennas that need to be deployed per node and the IA training overhead finite. The benefit of IA with receive diversity that increases the link reliability is depicted. The aggregate network throughput per unit area can be increased, albeit fewer users per cluster are active.

# Acknowledgement

I would like to thank Maxime Guillaud for his continuous encouragement and devoted guidance. His supervision together with Professor Christoph Mecklenbräuker and Thomas Zemen shaped my knowledge and skills, and their passion for research inspired and motivated me. I wish to thank all of them for their feedback on my work. I wish to express my gratitude to Professor Ana Isabel Pérez-Neira for being a co-examiner of my thesis. I also wish to thank Giusi Alfano and Erwin Riegler for their collaboration and advice.

It is a pleasure to thank all those people who made the daily life at FTW truly enjoyable. In the order of appearance during one of my typical working days: I am grateful to Sebastian Egger and Matthias Baldauf for the morning coffee jour-fixes, Laura Bernadó, Paolo Castiglione and Paul Fuxjäger for many enriching discussions as well as all the members of the FTW soccer group. Furthermore, thanks to Alexander Paier for many helpful advices and sharing his experience in the final stage of the thesis.

Most of all, I would like to thank Ana and my family for their love and support.





# Contents

|  |               |
|--|---------------|
| <b>Abstract</b>  | <b>iv</b>     |
| <b>Acknowledgement</b>   | <b>vi</b>     |
| <b>1 Introduction</b>  | <b>1</b>      |
| 1.1 Objectives . . . . .   | 2             |
| 1.2 Related Work . . . . .   | 3             |
| 1.2.1 Broadcast Channel . . . . .  | 3             |
| 1.2.2 Interference Channel . . . . .   | 5             |
| 1.3 Methodology . . . . .  | 9             |
| 1.3.1 Channel State Information . . . . .  | 11            |
| 1.4 Outline and Contributions . . . . .  | 12            |
| <br><b>I Opportunistic Interference Mitigation in MIMO Broadcast Channels</b>                | <br><b>15</b> |
| <b>2 SINR Estimation in Random Beamforming with Noisy Channel Measurements</b>               | <b>17</b>     |
| 2.1 Random Beamforming for MIMO Broadcast Channels . . . . .                                 | 18            |
| 2.2 SINR Perturbation . . . . .  | 20            |
| 2.2.1 Stochastic Bound . . . . .   | 23            |
| 2.2.2 Perturbation of the SINR . . . . .   | 24            |
| 2.3 Simulation Results . . . . .   | 24            |
| 2.4 Appendix: Stochastic SINR Metric . . . . .   | 28            |
| <br><b>II MIMO Interference Alignment: Feasibility, Algorithms and Large System Analysis</b> | <br><b>31</b> |
| <b>3 Introduction to Interference Alignment</b>  | <b>33</b>     |

|          |  |           |
|----------|--|-----------|
| 3.1      | K-user Interference Channel . . . . .                        | 33        |
| 3.1.1    | Interference Alignment . . . . .                             | 35        |
| 3.2      | Degrees of Freedom of the SISO $K$ -user IC . . . . .        | 38        |
| 3.3      | Degrees of Freedom of the MIMO $K$ -user IC . . . . .        | 42        |
| 3.4      | Linear Algebra Background . . . . .                          | 45        |
| 3.4.1    | SISO and MIMO Interference Alignment Conditions . . . . .    | 48        |
| <b>4</b> | <b>MIMO Interference Alignment</b>                           | <b>53</b> |
| 4.1      | MIMO Interference Channel . . . . .                          | 53        |
| 4.1.1    | Opportunistic Beamforming . . . . .                          | 55        |
| 4.2      | Alignment-Based Interference Management . . . . .            | 55        |
| 4.2.1    | Feasibility Conditions . . . . .                             | 57        |
| 4.2.2    | Projection Receiver . . . . .                                | 59        |
| 4.3      | Alignment Procedures . . . . .                               | 60        |
| 4.3.1    | Iterative Alignment Procedure . . . . .                      | 60        |
| 4.3.2    | Constructive Alignment Procedures . . . . .                  | 61        |
| 4.4      | Ergodic Performance . . . . .                                | 64        |
| 4.4.1    | Noisy Channel State Information . . . . .                    | 65        |
| 4.4.2    | Bounds of Ergodic Rate with Imperfect CSI . . . . .          | 66        |
| 4.5      | Simulation Results . . . . .                                 | 68        |
| 4.5.1    | Beamforming with Perfect Channel State Information . . . . . | 69        |
| 4.5.2    | Multuser Diversity-Multiplexing Trade-off . . . . .          | 71        |
| 4.5.3    | Imperfect Channel State Information . . . . .                | 72        |
| 4.6      | Appendix: Proof of Theorem 4 . . . . .                       | 76        |
| 4.6.1    | Lower Bound of the Ergodic Mutual Information . . . . .      | 76        |
| 4.6.2    | Upper Bound of the Ergodic Mutual Information . . . . .      | 77        |
| <b>5</b> | <b>Interference Alignment in Cellular Networks</b>           | <b>79</b> |
| 5.1      | Large Cellular Network Model . . . . .                       | 80        |
| 5.1.1    | Clustered Base Station Cooperation . . . . .                 | 81        |
| 5.2      | Simulation Results . . . . .                                 | 83        |
| 5.2.1    | Frequency Reuse Scheme . . . . .                             | 83        |
| 5.2.2    | Performance Evaluation . . . . .                             | 84        |
| <b>6</b> | <b>Interference Alignment in Clustered Ad Hoc Networks</b>   | <b>91</b> |
| 6.1      | Stochastic Geometry . . . . .                                | 92        |
| 6.1.1    | Point Processes . . . . .                                    | 92        |
| 6.2      | Clustered Wireless Ad Hoc System . . . . .                   | 95        |
| 6.2.1    | Intra-cluster IA and Feasible Cluster Settings . . . . .     | 98        |

|          |   |            |
|----------|---|------------|
| 6.2.2    | Analysis of the Equivalent Channel . . . . .                              | 100        |
| 6.3      | Transmission Success Probability . . . . .                                | 102        |
| 6.3.1    | Intra-Cluster IA with $d'=1$ and Bounds . . . . .                         | 102        |
| 6.3.2    | Bounds on the Transmission Success Probability for $d'=1$ . . .           | 103        |
| 6.3.3    | Intra-Cluster IA with Diversity Receiver . . . . .                        | 105        |
| 6.3.4    | Dominant Eigenmode Transmission . . . . .                                 | 107        |
| 6.4      | Transmission Capacity . . . . .   | 108        |
| 6.5      | Simulation Results . . . . .  | 109        |
| 6.5.1    | Link Level Performance of IA for $d'=1$ and Bounds . . . . .              | 109        |
| 6.5.2    | Link Level Performance of IA with Receive Diversity . . . . .             | 112        |
| 6.5.3    | High Reliability Regime and Large System Analysis . . . . .               | 114        |
| 6.6      | Appendix: Integral Expressions for $\mathbb{P}(\text{success})$ . . . . . | 119        |
| <b>7</b> | <b>Summary and Conclusions</b>  | <b>123</b> |
| <b>A</b> | <b>Notation, Abbreviations</b>  | <b>127</b> |
|          | <b>Bibliography</b>   | <b>131</b> |



# List of Figures

|     |  |    |
|-----|--|----|
| 1.1 | Multiuser network scenarios. . . . .                                       | 10 |
| 2.1 | Feedback mechanism in random beamforming. . . . .                          | 20 |
| 2.2 | Illustration of perturbation weight vector. . . . .                        | 22 |
| 2.3 | Performance of SINR feedback metric, $2 \times 2$ -case. . . . .           | 26 |
| 2.4 | Performance of SINR feedback metric, $4 \times 2$ -case. . . . .           | 27 |
| 3.1 | The $K$ -user IC and message flow. . . . .                                 | 34 |
| 3.2 | Resource sharing strategies in a $K$ -user IC. . . . .                     | 36 |
| 3.3 | Singe-user communication system. . . . .                                   | 38 |
| 3.4 | Competition for limited resources of a $K$ -user IC . . . . .              | 39 |
| 3.5 | IA solution for a SISO-IC. . . . .   | 50 |
| 3.6 | IA solution for a MIMO-IC. . . . .   | 51 |
| 4.1 | The $K$ -user MIMO-IC and message flow. . . . .                            | 54 |
| 4.2 | MIMO-IA with or without receive diversity. . . . .                         | 59 |
| 4.3 | Alignment in the $(3 \times 3, 1, 2)^3$ -IC and effective channel. . . . . | 60 |
| 4.4 | IA based on imperfect CSI. . . . .   | 66 |
| 4.5 | Ergodic sum-rate in the $K = 3$ -user MIMO-IC. . . . .                     | 69 |
| 4.6 | Ergodic sum-rate in the $K = 5$ -user MIMO-IC. . . . .                     | 70 |
| 4.7 | Ergodic per-user and sum-rates illustrating DMT. . . . .                   | 74 |
| 4.8 | Ergodic rates for IA based on imperfect CSI with $\beta = 1$ . . . . .     | 75 |
| 4.9 | Ergodic rates for IA based on imperfect CSI with $\beta = 0.5$ . . . . .   | 75 |
| 5.1 | Large cellular network with base station cooperation. . . . .              | 82 |
| 5.2 | Large cellular network with frequency reuse three. . . . .                 | 85 |
| 5.3 | Ergodic throughput for cluster scenario A. . . . .                         | 88 |
| 5.4 | Ergodic throughput for cluster scenario B. . . . .                         | 89 |
| 5.5 | Relative ergodic throughput of IA w.r.t. frequency reuse. . . . .          | 90 |
| 6.1 | Definition of a two dimensional PP. . . . .                                | 93 |
| 6.2 | Snapshot of homogeneous and clustered PPP. . . . .                         | 95 |

|      |  |     |
|------|--|-----|
| 6.3  | Transmitter positions modeled as a Poisson cluster process. . . . .                      | 96  |
| 6.4  | Intended and interfering signals add up at receiver $i$ . . . . .                        | 97  |
| 6.5  | IA leads to coordinated and uncoordinated interference. . . . .                          | 99  |
| 6.6  | Signals in the receive signal space where intra-cluster IA is established.               | 100 |
| 6.7  | Feasible cluster setting for intra-cluster IA. . . . .                                   | 101 |
| 6.8  | Comparison of $\mathbb{P}(\text{success})$ for SISO and MIMO clustered networks. . .     | 110 |
| 6.9  | Different cluster sizes and comparison to established bounds. . . . .                    | 111 |
| 6.10 | Sample realization of considered clustered networks for DMT inves-<br>tigations. . . . . | 113 |
| 6.11 | Comparison of link performance for non-/overlapping clusters for $\alpha = 4$ .          | 115 |
| 6.12 | Comparison of link performance for non-/overlapping clusters for $\alpha = 3$ .          | 116 |
| 6.13 | Approximation of link performance in the high reliability regime. . .                    | 117 |
| 6.14 | Term related to diversity gain allocation. . . . .                                       | 117 |
| 6.15 | Area spectral efficiency as a function of the SIR threshold $T$ . . . . .                | 118 |

# List of Tables

|     |  |     |
|-----|--|-----|
| 3.1 | Parameter set of the SISO and MIMO $K$ -user IC. . . . .                                     | 48  |
| 4.1 | Feasibility of an IA solution in different $K$ -user MIMO-ICs. . . . .                       | 58  |
| 4.2 | Closed-form IA solutions for the $(M \times M, 1)^K$ -IC. . . . .                            | 64  |
| 5.1 | Parameters for the considered scenarios with base station cooperation.                       | 85  |
| 5.2 | System parameters for the considered large cellular network with<br>hexagonal cells. . . . . | 86  |
| 6.1 | Feasible number of cluster points for intra-cluster IA. . . . .                              | 112 |
| A.1 | Symbols used throughout this manuscript. . . . .   | 127 |
| A.2 | Notation used throughout this manuscript. . . . .  | 128 |
| A.3 | Abbreviations A-L used throughout this manuscript. . . . .                                   | 129 |
| A.4 | Abbreviations M-Z used throughout this manuscript. . . . .                                   | 130 |





# 1 Introduction

The omnipresence of interference is one of the most challenging features of communication over wireless channels. In the recent years, interference management techniques have gained importance due to a strong increase in the number of wireless devices, a densification of wireless access networks and the development of novel communication paradigms such as mobile ad-hoc, vehicle-to-vehicle communication and sensor networks. Standards for future generation cellular architectures, such as the long term evolution of UMTS, study the deployment of relay nodes, repeaters and femtocells (small home base-stations) in order to meet the requirement with respect to spectral efficiency and to guarantee ubiquitous user experience [1–3]. Due to the scarceness of available spectrum and the limited performance of conventional orthogonal resource sharing, concurrent transmissions consequently occur simultaneously in the same frequency band, separated only geographically. Thus, many interfering signals are added to the intended signal at the receivers and lead to larger areas where the transmission is limited by interference. As a consequence, more sophisticated capabilities need to be embedded in the infrastructure where a trend towards self organizing networks with decentralized medium access and resource sharing is observable [2, 3].

We focus on two multiuser network scenarios that comprise the underlying aspects and allow to analyze how to deal with interference in multiuser communications in a canonical way. Firstly, we consider the broadcast channel (point-to-multipoint communication). A broadcast channel has one transmitter and multiple receivers. This model has applications in, e.g. the downlink of a cellular system or infrastructure-to-vehicle communication. Simultaneous transmission of signals carrying messages for the receivers creates co-channel interference. Secondly, we consider the interference channel (multiple point-to-point communication). An interference channel has multiple independent transmitter-receiver pairs. Applications of this model range from cellular systems, vehicle-to-vehicle communication systems to mobile ad-hoc and sensor networks.

We study the case where all nodes in the network are equipped with multiple antennas. Besides the thoroughly studied potential to increase spectral efficiency in single-user (point-to-point) multiple-input multiple-output (MIMO) systems, the

use of multiple antennas in multiuser systems enables interference management approaches in the spatial domain. Beamforming of the transmitted signals allows to separate spatially the signals of different users which is especially beneficial in distributed networks with a lack of joint pre/post processing of the transmitted data. Hence, we put our attention on distributed systems where the user data is not exchanged among nodes, saving on the amount of backhaul communication. Furthermore, we circumvent computationally expensive multiuser precoding and detection schemes and restrain on single-user linear precoding and simple linear filtering at the receiver side.

The distributed nature of the considered networks uncovers new challenges that are by far not as distinctive as in single-user systems. Throughout this manuscript, we will address the importance of channel state information (CSI) at the transmitter side. In the broadcast network, low-rate feedback about the link quality to different users allows for opportunistic scheduling of the best users and achieves multiuser diversity. In the interference channel scenario, we study interference alignment (IA) which is based on channel state acquisition and feedback about the interfering links. Using alignment-based precoding with full CSI, it is possible to achieve sum-rate capacity that scales with the number of users in the networks in the high signal-to-noise ratio (SNR) regime. We assess the performance of interference alignment in practical systems operating at non-asymptotic SNR and propose clustered cooperation in large networks where IA is applied among groups of users. In order to model a practically feasible cooperation scheme, we assume that CSI is available only inside the clusters.

### 1.1 Objectives

The high-level goals of this thesis are as follows:

- We analyze the perturbation of the measured MIMO channel in a broadcast network. We conjecture that additional information about the channel enables the receiver to design an improved channel feedback metric, leading to refined scheduling decision and a reduced probability of link outages.
- We assess the application of alignment-based interference management in the multiuser MIMO interference channel at non-asymptotic SNR. We seek for closed form interference alignment solutions that facilitate a reduction of training overhead compared to iterative alignment procedures. We claim that interference alignment is a promising candidate to improve the spectral efficiency in future cellular systems.

- We analyze the performance of clustered interference alignment in a network with accumulation of transmitting nodes in certain geographical areas. We claim that intra-cluster interference alignment has the potential to suppress the dominant interference coming from nearby transmitters, while the cluster nodes enjoy the interference alignment multiplexing gains and full spectral reuse. We conjecture that interference alignment in conjunction with diversity techniques significantly improves the link reliability.

## 1.2 Related Work

In this section, we summarize lines of work studying multiple-antenna systems in a multiuser network environment. We focus on literature that is closely related to the scope of this thesis. In Subsection 1.2.1, we provide references that characterize the sum-rate capacity in a MIMO broadcast channel and refer to capacity achieving transmission schemes that are based on perfect channel state information at the transmitter. In the first part of this manuscript, we investigate random beamforming, a transmission scheme that employs only partial channel state information thereby achieving the optimal sum-rate scaling. Random beamforming transmits to users with the most favorable channel conditions through simple superposition coding. In Subsection 1.2.2, we present related work on the multiuser single-input single-output (SISO) and MIMO interference channel. The state of the art is briefly outlined, with an emphasis on a novel interference management technique that is based on alignment of all interfering signals. This stunning idea is the inspiration for the work in the second part of this thesis.

### 1.2.1 Broadcast Channel

The notion of a broadcast channel was introduced by Cover in [4]. A broadcast channel is a multiuser network comprised of a transmitter and multiple receivers. We consider point-to-multipoint data transmission over wireless links where transmitting and receiving nodes are equipped with multiple antennas and impaired by receive-side additive white Gaussian noise, i.e. the MIMO Gaussian broadcast channel. Joint signal processing is omitted among the receivers. There has been a line of work studying the sum-rate capacity and the capacity region of a MIMO broadcast channel [5,6]. The sum-rate capacity is the highest achievable sum rate in the network where all receivers are able to decode their data with zero decoding error probability and constitutes one particular point in the capacity region. The capacity region is the union of all possible achievable rate tuples. It has been shown that

dirty paper coding [6] achieves the sum-rate capacity and any point in the capacity region of the Gaussian MIMO broadcast channel [5]. Dirty paper coding is a technique that allows the receiver to cancel the effect of interference without knowing the interference state. However, the channel state has to be known perfectly at the transmitter and the coding scheme is computationally extremely intensive.

In MIMO broadcast channels, the multiuser capacity strongly depends on whether the transmitter knows the channel coefficient to each user [7]. The increased throughput by scheduling those users with the most favorable channel conditions is referred to as multiuser diversity [8]. Here, we leverage the channel fading as opposed to single-user systems where diversity techniques are used to improve the reliability of communication impaired by fading effects [8].

A transmission technique that exploits multiuser diversity and requires only finite-rate feedback about the channel state is introduced by Sharif and Hassibi and denoted as random beamforming [9]. They propose to use random beams and serve the users with the highest signal-to-interference plus noise ratios (SINRs). The required feedback compared to full CSIT is considerably reduced since each user needs to feed back one real number (its best SINR) and the corresponding index of the desired beam. It is shown that the proposed scheme achieves the same sum throughput scaling as obtained with perfect CSI using dirty paper coding [9]. Transmission of data using one random beam is also proposed in [10]. The scheme aims at inducing faster and larger fluctuations in the receive SNR of the users and improving the fairness in the system. Sharif and Hassibi show that fairness in their random beamforming scheme is guaranteed asymptotically for infinite number of transmit antennas. In this regime, the probability that users with different SNR are chosen is equal [9].

### 1.2.1.1 Imperfect Receive-Side Channel Knowledge

The throughput analysis in [9] is based on perfect CSI at the receiver and error free feedback links. Imperfect SINR feedback is considered in [11–13] and leads to a mismatch between reported link quality, and the data rate that the channel can currently support. Inaccuracy of the feedback information leads to improper scheduling decisions if a user with an overestimated SINR claims a beam and prevents the scheduling of the legitimate user with the best channel. In addition, overestimated link quality can generate outages if adaptive modulation and coding is used. An SINR back-off scheme based on the knowledge of the variance of the estimation error is proposed in [12] to tackle the problem, and in [11] and [13] a rate back-off mechanism is investigated.

### 1.2.2 Interference Channel

A long-standing open problem in information theory is the capacity of the interference channel [14]. An interference channel (IC) has two transmitters and two receivers, and transmitter  $i$  sends its message to receiver  $i$  for  $i = 1, 2$ . The transmissions interfere with each other. Achievable rates regions, different capacity outerbounds and the underlying transmission and coding schemes of the SISO-IC with deterministic channel gains and the SISO Gaussian IC are outlined in [14–16] and references therein.

The second part of this manuscript deals with the  $K$ -user SISO interference channel. This network model is a generalization of the IC, which has  $K$  transmitters and  $K$  receivers, and transmitter  $i$  sends its message to receiver  $i$  for  $i = 1, 2, \dots, K$ . All transmissions interfere with each other. Cadambe and Jafar showed in their landmark paper [17] that using interference alignment a sum-rate multiplexing gain of  $K/2$  per time or frequency dimension can be achieved. In comparison, independent operation of  $K$  isolated point-to-point links would incur a sum-rate multiplexing gain of  $K$  per dimension. This indicates that IA allows virtually interference-free communications, at the cost of halving the multiplexing gains with respect to what users could achieve over isolated point-to-point links. Thus, the loss in number of degrees of freedom of each user, caused by the distributed nature of the IC that prohibits joint signal processing at transmitter and receiver side, is independent of  $K$  and much smaller than previously conjectured [18].

The terminology "interference alignment" is first used in [19] to describe the idea of overlapping interference spaces [20]. In [19], the authors consider IA for the two-user MIMO X channel with an arbitrary number of antennas per user  $M > 1$ . It is shown that IA achieves the maximum of  $4/3M$  degrees of freedom achievable on this channel. The X channel has two transmitters and two receivers, and transmitter  $i$  sends messages to receiver  $j = 1, 2$  for  $i = 1, 2$ .

#### 1.2.2.1 Interference Alignment through Symbol Extension

The aforementioned maximum multiplexing gains in the SISO-IC are achieved by simple linear precoding at the transmitters and zero-forcing of the aligned interference at the receivers. So called super symbols, which result from low rank precoding of each users data symbols, are transmitted over multiple channel accesses where the super symbols experience different fading [21]. The linear precoders allow to steer the supersymbol in different dimensions. The precoders are designed, based on perfect knowledge about the coefficients of the extended channel of all interfering links, such that the super symbols align at each unintended receiver in a subspace of mini-

imum dimension. The matrices that describe the extended channels are diagonal and non-degenerate. Asymptotically large symbol extensions and alignment-based precoding lead to the situation that the interfering super symbols span approximately half of the dimension of the extended channel at each unintended receiver simultaneously [17]. The remaining dimensions can be used for interference-free communication with the intended receiver. Cadambe and Jafar demonstrate an IA precoder design for a three dimensional extended channel where noncausal channel knowledge is not required [17]. However, the achievability of the number of degrees of freedom per user in the  $K$ -user SISO-IC is based on an asymptotically large extended channel where the presented precoder design [17] is based on noncausal knowledge of the channel state. Furthermore, the constructive precoder matrices cause a high implementation complexity because of their nonorthogonality.

### 1.2.2.2 Interference Alignment in the Spatial Domain

We now consider a  $K$ -user MIMO-IC, where transmitters and receivers are equipped with multiple antennas. Interference alignment in the spatial domain can be achieved through transmit beamforming of the users data streams. All interfering streams are aligned in a subspace of minimum dimension at each unintended receiver and can be removed through interference suppression filtering, rendering a dimension-reduced equivalent channel for interference-free communication [17, 22–26]. The matrices that describe the MIMO channels are fully populated. Symbol extensions can be avoided, which is referred to as IA over the constant  $K$ -user MIMO-IC [22].

In the  $K$ -user Gaussian MIMO-IC, under mild hypotheses on the distribution of the channel coefficients, the existence with probability one of a solution to the IA problem depends only on the dimensions of the problem, i.e. the number of users  $K$  and the number of antennas at each node. An existence criterion is introduced in [27, 28].

Given a feasible network setting, alignment is achieved by one of the following methods. Iterative minimization of an interference leakage metric is introduced in [22, 23], alternate optimization of the interference power in [24] and modified metrics taking into account additive colored noise or joint MMSE receive filter design are used in [25, 26]. The proposed interference alignment scheme [29] extends conventional spatial interference alignment in order to keep the signal space of the desired signal as orthogonal as possible to the received interference subspace.

Closed-form IA solutions are reported for certain particular network cases in [22, 28, 30], i.e. the  $K = 3$ -user MIMO-IC with an arbitrary number of antennas per user  $M > 1$  [22] and the  $K = 4$ -user MIMO-IC with different number of antennas per

transmitter and receiver [28, 30]. In Chapter 4, we derive a closed form IA solution for a network with an arbitrary number of users, when all nodes have  $M = K - 1$  antennas.

The high SNR performance of IA is thoroughly studied in the literature. Using IA, the sum capacity scales linearly with SNR in dB and its slope is equal to the number of degrees of freedom of the IC. However, many practical systems operate at medium or low SNR and little is known about how fast the performance of IA degrades in the presence of noise and uncoordinated interference caused by users that are not participating in the alignment procedure. An attempt to apply IA to the MIMO-IC at non-asymptotic SNR is undertaken in [31]. IA is generalized to the case where the receiver exploits diversity inside the interference-free subspace created by IA. By virtue of additional receive diversity, the codimension of the interference-free subspace at each receiver must be larger than the number of streams from the intended transmitter. Feasibility conditions of an IA solution are derived for this case in [31]. It is shown that for a fixed antenna configuration, there is a tradeoff between the number of users that can be accommodated in the alignment procedure and the diversity gain per user. The per user ergodic rate of IA with receive diversity is shown in [31] to be increased compared to conventional IA over the whole range of SNR. However, the per user performance gain comes with the price of a decreased sum-rate in the network.

### 1.2.2.3 Large Network Analysis

Let us now consider spatial networks. In order to assess the critical role of interference in large wireless networks, a tradeoff between analytical tractability and accurate modeling of the network geometry has to be made. A model based on statistical node distributions can account for the variety of possible network topologies.

An introduction to spatial modeling and the analysis of fundamental performance limits in wireless networks is given in [32] and [33]. Analytically tractable models based on *stochastic geometry* [34, 35] and the theory of *point processes* are instrumental to assess different interference management strategies. [36] outlines results on interference distributions, link outages and network capacity for networks whose underlying node deployment is ranging from deterministic grids to complete spatial randomness. The mathematical foundation of point processes is introduced as well as an assessment of different medium access schemes.

The most popular spatial model for networks where transmitters and receivers are located randomly over a large area with a pure random channel access is the homogeneous Poisson point process. It reflects complete spatial randomness and is

analytically tractable. Assuming single-antenna nodes, a standard power law for the pathloss and Rayleigh fading, a closed-form expression for the Laplace transform of the interference was found [32, 37]. Closed-form expressions for the interference distribution exist for special cases. The characterization of the interference in the Laplace domain is instrumental for deriving the probability of a link outage. Here, properties of Poisson point processes can be used to derive the transmission success probability for a network using ALOHA channel access. Introducing attraction between nodes, a Poisson cluster process serves as an appealing model for sensor networks, military platoons or urban networks with dense hot-spots. Closed-form integral expressions for the probability of non-outage can be derived for the above assumptions on fading and network configuration [38].

Stochastic geometry and the techniques for characterizing interference and outage can be used to determine the area spectral efficiency in ad hoc networks, i.e. the data rate per bandwidth that can be transmitted in a given area. The metric used for the large system performance analysis is the transmission capacity that was introduced by Weber et al. in [39]. It measures the maximum spatial density of active links given a link outage constraint for a SINR target. Networks where the underlying transmitter distribution is a homogeneous Poisson point process were analyzed for single antenna networks in [39] and in [40] for nodes employing multiple antenna diversity techniques. The generalization to clustered and inhomogeneous networks has been undertaken in [38]. In order to circumvent the analytical difficulties for modeling interference in inhomogeneous networks, outage probability and capacity analysis was proposed by Ganti, Andrews and Haenggi for the so called high-reliability regime [41], i.e. a regime where the interferer density goes to zero. The link analysis for general networks and MAC schemes was carried out in [42]. The extension to the transmission capacity was undertaken in [43], based on the second order product density of the underlying node distribution.

The theory of stochastic geometry and its associated techniques have been applied to cellular systems [32] and emerging network architectures such as femtocells, hot-spots and relay networks. The deleterious effect of the distributed, opportunistic and uncoordinated deployment of transmission nodes on reliable communication in existing cellular infrastructures [44] was analyzed.

Attempts to apply IA to large networks can be found in [45] and [46]. Both papers consider a finite (unit-square) area where single-antenna terminals are deployed independently at random. The channel gains are modeled using a distance dependent pathloss model and random fast fading phases. However, random fading amplitudes are omitted in their analysis. The authors of [45] show that if the number of transmitter-receiver pairs tends to infinity, the average per-user capacity converges



in probability to half the capacity that can be achieved by an isolated pair. The achievability of their result is based on the ergodic IA scheme introduced in [47]. This ergodic IA scheme introduces coding delays that grow exponentially with the number of transmitter-receiver pairs. Furthermore, full channel state information at all nodes is necessary.

## 1.3 Methodology

In this section, we outline the multiuser networks that we investigate in the course of this manuscript and the modeling assumptions of the wireless channel between nodes.

Fig. 1.1 shows deployments of transmitters (circles) and receivers (boxes) of the considered scenarios. The broadcast channel with  $K$  receivers, depicted in Fig. 1.1(a), is investigated in Chapter 2. The transmitter simultaneously sends data to all receivers using superposition coding. The desired and interfering signals at receiver  $i$  are received over the link depicted by solid and dashed lines, respectively. The  $K$ -user interference channel is shown in Fig. 1.1(b) and is the underlying model for the research in Chapter 3 and 4. In this scenario, each sender transmits data intended only for one receiver. The intended signal is received over the wireless links depicted by solid lines along with interference from  $K - 1$  transmitters over the interfering (dashed) links. In Chapter 5 and 6 we consider a network with many user pairs that are grouped into cooperation clusters. Each cluster, surrounded in Fig. 1.1(c), forms an interference channel. Interference from transmitters in the same cluster is received along with interference from neighboring clusters, visualized in 1.1(c) as a compound dashed arrow between the clusters.

Let us now focus on the wireless links between nodes in Fig. 1.1. We consider a discrete-time complex baseband input/output model incorporating additive white Gaussian noise. This model is the building block of the discussions in the following chapters. The pulse-shaping filters at the transmitter side and the front end filter at each receiver are chosen such that the *Nyquist criterion* [48] is satisfied, e.g. square-root raised-cosine filters. Let  $\phi$  denote the set of indices of the transmitters in the network.  $N_T$  and  $N_R$  denote the number of antennas at transmitter  $j$  and receiver  $i$ , respectively. Using the vector representation, the received signal for user  $i$  at discrete-time  $m$  is

$$\underline{\mathbf{y}}_i[m] = \sum_{j \in \phi} \gamma_{ij} \mathbf{H}_{ij}[m] \underline{\mathbf{x}}_j[m] + \underline{\mathbf{n}}_i[m], \quad (1.1)$$

with  $\underline{\mathbf{y}}_i[m] = [y_i[m](1), \dots, y_i[m](N_R)]^T$ ,  $\underline{\mathbf{n}}_i[m] = [n_i[m](1), \dots, n_i[m](N_R)]^T$  and

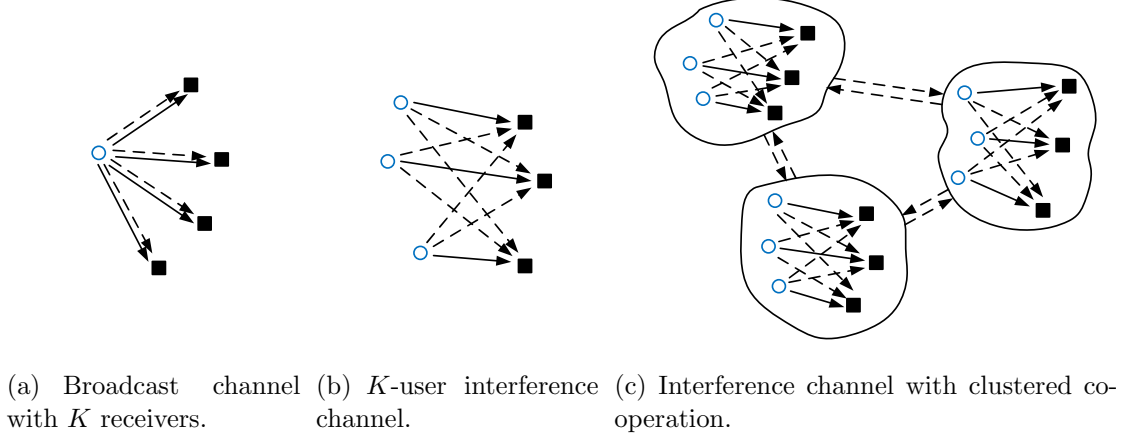


Figure 1.1: Considered multiuser network scenarios.

$\mathbf{x}_j[m] = [x_j[m](1), \dots, x_j[m](N_T)]^T$  denoting the receive signal vector, additive noise and transmit symbol vector from transmitter  $j$  and receive  $i$ , respectively.  $y_i[m](n_r)$ ,  $n_i[m](n_r)$  and  $x_j[m](n_t)$  are the received signal, additive noise and transmit symbol from receive antenna  $n_r$  and transmit antenna  $n_t$ , respectively.  $\mathbf{n}_i[m]$  is circular symmetric additive white Gaussian noise (AWGN) satisfying  $\mathbb{E}[\mathbf{n}_i[m]\mathbf{n}_{i'}[m]^H] = \sigma_n^2 \mathbf{I}_{N_R} \delta[i - i']$ .  $\gamma_{ij}$  is a distance dependent pathloss on the link between transmitter  $j$  and receiver  $i$ , and the MIMO channel matrix in (1.1) is

$$\mathbf{H}_{ij}[m] = \begin{bmatrix} h_{ij}[m](1, 1) & h_{ij}[m](1, 2) & \dots & h_{ij}[m](1, N_T) \\ h_{ij}[m](2, 1) & h_{ij}[m](2, 2) & \dots & h_{ij}[m](2, N_T) \\ \vdots & \vdots & \ddots & \vdots \\ h_{ij}[m](N_R, 1) & h_{ij}[m](N_R, 2) & \dots & h_{ij}[m](N_R, N_T) \end{bmatrix}, \quad (1.2)$$

with  $h_{ij}[m](n_r, n_t)$  the discrete-time channel gain from transmit antenna  $n_t$  of transmitter  $j$  to receive antenna  $n_r$  of receiver  $i$ . Note that for the broadcast channel introduced in Subsection 1.2.1  $\phi = \{1\}$ ,  $i = 1, \dots, K$  and  $\mathbf{x}_j[m]$  is carrying the messages for all receivers whereas for the  $K$ -user interference channel introduced in Subsection 1.2.2  $\phi = \{1, \dots, K\}$ ,  $i = 1, \dots, K$  and  $\mathbf{x}_j[m]$  is carrying the messages only for receiver  $j$ .

Throughout this thesis, we assume i.i.d. *Rayleigh fading* channels [8, 49], an adequate model for scattering mechanisms where there exist many small reflectors. It specifies the entries of the channel gain matrix  $\mathbf{H}_{ij}[m]$  in (1.2) as i.i.d. circular symmetric complex Gaussian. Due to the uniform phase,  $h_{ij}[m](n_r, n_t)$  is circular symmetric  $\mathcal{CN}(0, 1)$  and its magnitude  $|h_{ij}[m](n_r, n_t)|$  is a *Rayleigh* random variable, i.e. has density  $x \exp\{-x^2/2\}$ ,  $x \geq 0$  and its squared magnitude  $|h_{ij}[m](n_r, n_t)|^2$  is

exponentially distributed with density  $\exp\{-x\}$ ,  $x \geq 0$ .

We assume a flat fading channel model. This channel model can represent narrow-band systems (e.g. GSM) where the multipath delay spread (typically around one or two microseconds for cellular or wireless local area networks [8]) is negligible with respect to the symbol duration. Furthermore, the same model can be used for wideband systems where orthogonal frequency division multiplexing is used (OFDM) in combination with MIMO technology (MIMO-OFDM [50]) is used. This approach turns a frequency selective channel into a number of narrowband parallel non-interfering sub-channels with input-output relation (1.1) per sub-carrier in the frequency domain.

We consider a slow time-varying channel, i.e. the coherence time, defined as the interval over which  $\mathbf{H}_{ij}[m]$  changes significantly as a function of  $m$ , is much larger than the delay requirement of the data transmission. In this situation a *block fading model* captures the important aspects [8]. It asserts that the channel remains constant for the coherence time and a block of successive received symbols can be decoded under the assumption that they experienced the same channel conditions. Successive blocks experience independent and identically distributed fading realizations.

Throughout this work, we consider rate achieving Gaussian codebooks. In Chapter 2 we assume adaptive modulation and coding, based on channel quality feedback and outage based communication. In Chapter 3, 4 and 5 we assume that the encoder can track the link quality and adaptively adjust the users data rate. In Chapter 6, we assume that the data rate of all transmitter-receiver pairs is fixed and an outage occurs whenever the channel is too poor to support the SNR threshold that corresponds to the data rate.

### 1.3.1 Channel State Information

The amount of channel state information (CSI) is a performance determining metric in a wireless communication systems [7, 9]. In single-user systems, multiple-antenna communication with channel state information at the receiver increases the capacity of the channel by a factor equal to the minimum of the number of transmit/receive antennas [51]. In multiuser MIMO systems, additionally, CSI at the transmitter (CSIT) is gaining fundamental significance. In communication systems based on frequency division duplexing (FDD), CSI needs to be estimated and fed back to the transmitter in a compressed way through a feedback link. In systems based on time division duplexing (TDD), we can use the fact that the forward and reverse links often share the same fading distribution and we can exploit channel reciprocity to

acquire CSI. With knowledge of the channels at the transmitters, the system can exploit multiuser diversity. However, imperfect channel estimation and feedback has deleterious effects on the reliability and the achievable rates on the user's intended links and in addition may increase the interference level that is caused to other users in the network.

In Chapter 2 we investigate partial CSIT in the MIMO broadcast channel through a finite rate feedback link. In Chapter 3, we introduce interference alignment in the  $K$ -user IC assuming perfect CSIT. We investigate the effect of imperfect CSI at transmitter and receiver on the alignment gains in a MIMO-IC in Chapter 4. Chapter 5 and 6 focus on the large system performance of clustered IA at finite SNR, where we assume perfect CSIT inside the clusters, whereas knowledge about the inter-cluster interference power levels is assumed at the transmitters in Chapter 5 and no knowledge about the channels and interference power between clusters is assumed in Chapter 6.

## 1.4 Outline and Contributions

The thesis is organized into the following parts and chapters:

### Part I: Opportunistic Interference Mitigation in MIMO Broadcast Channels

#### Chapter 2: SINR Estimation in Random Beamforming with Noisy Channel

**Measurements** In this chapter, we design a novel channel quality feedback metric for random beamforming that reduces channel outages. Fewer retransmissions of the transmitted data blocks are attained, especially beneficial for safety and delay-critical applications. The receivers are equipped with multiple antennas. We derive a perturbation bound for the eigenspaces of an Hermitian matrix using the framework introduced in [52]. We apply the stochastic version of the bound for the evaluation of (respectively lower and upper) bounds on the received signal and interference plus noise terms of the SINR. This conservative estimate of the actual link quality exploits additional information provided by the analysis of the perturbation of the measured MIMO channel. The proposed SINR feedback metric refines scheduling decisions and provides a noticeable decrease in outage probability compared to rate back-off schemes, while incurring only a marginal goodput loss.

**Part II: MIMO Interference Alignment: Feasibility, Algorithms and Large System Analysis**

**Chapter 3: Introduction to Interference Alignment** In this chapter, we introduce approximate capacity characterization results of the  $K$ -user IC. The state of the art of interference alignment is outlined. The fundamentals of alignment-based linear precoding in the SISO- and MIMO-IC are discussed and we formulate alignment conditions applicable to both cases. We highlight the fundamental difference between MIMO-IA over constant channels and alignment in single-antenna systems. SISO networks require symbol extensions that grow exponentially with the number of users to achieve the maximum network multiplexing gain.

**Chapter 4 : MIMO Interference Alignment** In this chapter, we introduce feasibility conditions that specify the existence of a IA solution for the MIMO-IC. We distinguish the case where the receivers exploit spatial diversity inside the interference-free subspace created by IA and the case where IA attains solely multiplexing gains per user. We describe the multiuser diversity-multiplexing trade-off applicable to the MIMO-IC. For a special network setting, we develop a constructive closed-form solution for IA for an arbitrary number of users. We derive analytical expressions for the achievable ergodic sum-rate of IA with a projection receiver. Furthermore, the sensitivity of IA to noisy channel state feedback is investigated and we derive bounds on the achievable ergodic sum-rate of IA based on imperfect CSI.

**Chapter 5: Interference Alignment in Cellular Networks** We evaluate the applicability of interference alignment to cases representative of upcoming cellular networks. We propose a clustered base station cooperation strategy, whereby interference is aligned inside a cluster of base stations, while the rest of the network contributes non-coordinated interference.

**Chapter 6: Clustered Wireless Ad Hoc Networks** In this chapter, we investigate the theoretical performance limits of MIMO-IA at non-asymptotic SNR. In our model, a numerousness of transmitters is deployed on the infinite plane. The location of concurrent transmitters is modeled as a Poisson clustered process. MIMO-IA is applied among  $K$  transmitters which we group into clusters. The clusters of cooperating transmitters partition the network. This approach leads to coordinated intra-cluster interference that can be suppressed at each receiver by linear filtering and uncoordinated inter-cluster interference. The

inter-cluster interference, whose intensity is attenuated by a distance dependent pathloss, is treated as noise. We assume an outage-based model where the data on the link between transmitter  $i$  and receiver  $i$  is transmitted with a predefined data rate  $R$ , which translates into an SINR threshold that needs to be exceeded for a successful transmission. We characterize the link-level performance using techniques from stochastic geometry as a function of the density of the transmitters, the path-loss model and the fading distribution. Furthermore, we establish analytically tractable results for the outage probability for intra-cluster IA with receive diversity and expressions for the transmission capacity in the high-reliability regime. In this regime, where density of interferers goes to zero, we characterize the area spectral efficiency and the optimum SIR operating point.

## **Part I**

# **Opportunistic Interference Mitigation in MIMO Broadcast Channels**





## 2 SINR Estimation in Random Beamforming with Noisy Channel Measurements

In this chapter, we consider the multiple-input multiple-output (MIMO) broadcast channel. It is comprised of a transmitter that aims at delivering messages to multiple receiver nodes. The messages for the receivers are independent, i.e. every receiver is only interested in its own data. The receivers locations are spatially separated and there is no communication between the receiver nodes. Hence, joint receive signal processing is not possible. Simultaneous transmission of data using superposition coding for different users creates co-channel interference (CCI).

We investigate random beamforming [9], a transmission technique suitable for the broadcast channel with limited channel state information at the transmitter (CSIT). The scheme constructs random beams and transmits data to the subset of users that report the highest signal-to-interference plus noise ratios (SINRs). This fairly low amount of channel state feedback allows the transmitter to opportunistically serve those users whose channel state allows for high data rates and exploit multiuser diversity. We extend the analysis of [9] that is based on perfect CSI at the receiver to the case where the channel observation used to compute the SINRs is noisy. Inaccurate SINR estimation results in outages if adaptive coding and modulation is used. We propose an improved SINR metric as a conservative estimate of the true SINR based on the knowledge of the measured channel and the variance of the estimation error. We show by simulation that the use of the novel metric has the potential to noticeably reduce channel outages.

This reliability of the measured SINR is addressed in the case of a single antenna at the receiver, in [12] where a SINR back-off scheme is proposed, and in [11] and [13] with a rate back-off mechanism. However, we will demonstrate that when multiple antennas are present at the receiver, analysis of the perturbation of the measured channel can provide useful information about the true SINR. More specifically, the objective of this chapter is to investigate the mismatch between the measured SINR and the real SINR in the case of multiple receive antennas. We use results on the

perturbation of the eigenspaces of Hermitian matrices to account for the effect of noise on the MIMO channel estimate. The novel SINR metric is based on expectations of bounds on the signal and interference power and enables scheduling decisions that lead to fewer retransmission, which is especially beneficial for e.g. safety and delay-critical applications.

The topic of SINR perturbation is studied also in [53], however in this work the perturbation is on the beamforming vectors themselves (their orthogonality is relaxed into  $\epsilon$ -orthogonality), whereas we focus on perturbations of the channel itself. Note also that although the channel estimation error can have multiple causes, namely additive noise (which can be combated by increasing the energy dedicated to training) or variation of the channel between the training phase and the data transmission phase (which can be mitigated by reducing the time interval between the two). However, in the present chapter, we do not attempt to distinguish estimation error and actual channel variation, and rather choose to model the difference as zero-mean circularly symmetric Gaussian.

This chapter is organized as follows: the system model is introduced in Section 2.1, the SINR lower bound is established in Section 2.2, together with its expectation. A detailed derivation of the SINR lower bound can be found in Appendix 2.4. The influence of the proposed channel quality metric is studied in Section 2.3 by ways of simulation.

Results presented in this chapter were first published in [54].

## 2.1 Random Beamforming for MIMO Broadcast Channels

Let us consider the downlink of a wireless communications system. A transmitter is equipped with  $N_T$  antennas and  $K$  users with  $N_R$  antennas each. The discrete-time baseband model (1.1) for user  $i$  at time  $m$  is given by

$$\underline{\mathbf{y}}_i[m] = \gamma_i \mathbf{H}_i[m] \underline{\mathbf{x}}[m] + \underline{\mathbf{n}}_i[m], \quad (2.1)$$

where  $\underline{\mathbf{x}}[m]$  is an  $N_T$  dimensional vector representing the transmitted signal,  $\gamma_i$  and the  $N_R \times N_T$  matrix  $\mathbf{H}_i[m]$  represent the pathloss and fading of the MIMO channel<sup>1</sup> (assumed frequency-flat) experienced by user  $i$  at time  $m$ , and  $\underline{\mathbf{n}}_i[m]$  denotes the noise experienced by user  $i$ . Here, the noise is modeled as Gaussian i.i.d. with  $\mathbb{E}[\underline{\mathbf{n}}_i[m] \underline{\mathbf{n}}_i[m]^H] = \mathbf{I}_{N_R}$ . Note that we assume that all users have the same number  $N_R \geq 2$  of antennas purely for notational simplicity, and without loss of generality.

---

<sup>1</sup>In the BC we omit the index for the sole transmitter  $\phi = \{1\}$  in (1.1).

Let  $\tilde{\mathbf{H}}_i$  denote the channel estimated by user  $i$  during the SINR estimation phase of random beamforming. As noted before, in general,  $\tilde{\mathbf{H}}_i \neq \mathbf{H}_i$ , due to both estimation noise and time variation of the channel. Let  $\mathbf{E}_i = \tilde{\mathbf{H}}_i - \mathbf{H}_i$  denote the channel measurement error, and assume that it is a Gaussian random matrix with i.i.d. components of variance  $\sigma_E^2$ . Hence, our error model does not include measurement error correlation in the spatial or time domain.

The random beamforming method [9] operates as follows: the base station randomly picks a set of  $N_T$  orthogonal beamforming vectors  $\mathbf{v}_1, \dots, \mathbf{v}_{N_T}$ . Let  $\mathbf{V} = [\mathbf{v}_1 \dots \mathbf{v}_{N_T}]$  denote the unitary matrix of beamforming vectors. A number of independently encoded data streams are transmitted, each stream being associated to one of the beamforming vectors. Although not generally optimal in the case of a Gaussian vector broadcast channel (see [55]), this approach is of interest since the amount of channel knowledge required to make the scheduling decision is lower than the full channel knowledge required by optimal approaches, thus saving feedback bandwidth. In general, granting channel access to the best (in the highest achievable mutual information sense) users will maximize the sum-throughput of the system. More involved selection criteria involving e.g. fairness between users [56] or taking delay constraints into account are sometimes desirable, and require relaxing the goodput maximization requirement. In the present chapter, we will focus on the case where the SINR is used as the channel quality metric.

Let us further analyze the random beamforming mechanism, and let  $\mathbf{s}[m]$  denote the vector containing the  $N_T$  symbols associated to each stream and transmitted at time  $m$ . The signal received by user  $i$  is therefore a superposition of all  $N_T$  streams, with weights depending on the beamforming vectors and their own channel, as

$$\mathbf{y}_i = \sum_{l=1}^{N_T} \gamma_i \mathbf{H}_i \mathbf{v}_l s_l + \mathbf{n}_i = \gamma_i \mathbf{H}_i \mathbf{V} \mathbf{s} + \mathbf{n}_i. \quad (2.2)$$

The goal of the training phase in the random beamforming method is to associate each beamforming vector to a user (here we assume that the number of users, denoted by  $K$ , is at least  $N_T$ ). Assuming that all beams are always in use, and that the power budget  $\rho = \mathbb{E}[\text{Tr}(\mathbf{s}\mathbf{s}^H)]$  is split equally among streams, the SINR of stream  $l$  as experienced by user  $i$  can be written

$$\text{SINR}_{i,l} = \frac{\mathbf{v}_l^H \mathbf{H}_i^H \mathbf{H}_i \mathbf{v}_l}{\sum_{l'=1 \dots l-1, l+1 \dots N_T} \mathbf{v}_{l'}^H \mathbf{H}_i^H \mathbf{H}_i \mathbf{v}_{l'} + N_T / (\gamma_i \rho)}. \quad (2.3)$$

Each user feeds back the highest measured SINR value and the index of the beam that leads to this highest SINR value, i.e. for user  $i$ , the feedback values consist of  $(\text{SINR}_{i,b_i}, b_i)$ , where  $b_i = \arg\max_{l=[1, \dots, N_T]} \text{SINR}_{i,l}$ . Among all the users that fed

back the  $l$ -th beamforming vector, the scheduler selects the user  $\tilde{i}_l$  that leads to the highest SINR value for this particular beam, i.e. the use of beam  $l$  is granted to user  $\tilde{i}_l = \operatorname{argmax}_i(\operatorname{SINR}_{i,b_i}|b_i = l)$ . Data transmitted on beam  $l$  is encoded with rate  $R_l = \log_2(1 + \operatorname{SINR}_{\tilde{i}_l,l})$  bit/s/Hz. The transmission is in outage if  $R_l > \log_2(1 + \operatorname{SINR}_{\text{inst},l})$  with  $\operatorname{SINR}_{\text{inst},l}$  the true SINR value of the user  $\tilde{i}_l$  for beam  $l$ . Fig. 2.1 shows the broadcast channel with  $K$  users competing for  $N_T$  random beams.

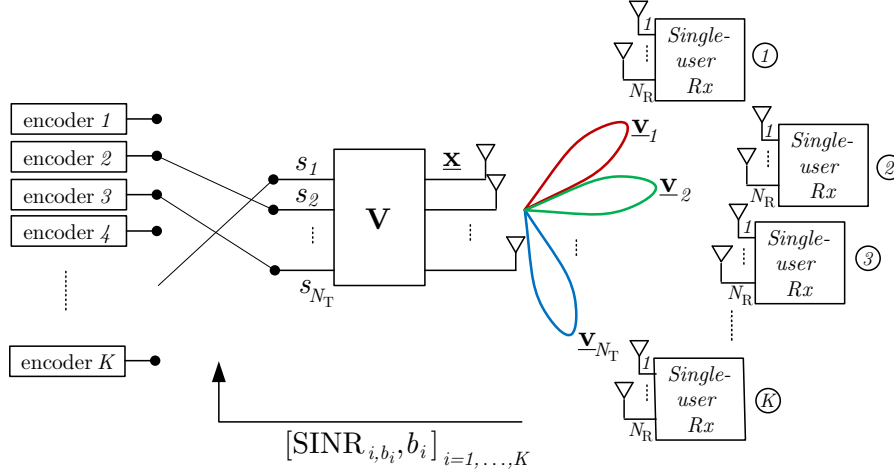


Figure 2.1: Broadcast channel with  $K$ -users competing for  $N_T$  random beams. During a training phase all users feed back the highest measured SINR value and the index of the corresponding beam.

Assuming (without loss of generality) that  $b = 1$ , and denoting  $\mathbf{V}_\perp = [\mathbf{v}_2 \dots \mathbf{v}_{N_T}]$ , this becomes

$$\operatorname{SINR}_{i,1} = \frac{\mathbf{v}_1^H \mathbf{H}_i^H \mathbf{H}_i \mathbf{v}_1}{\operatorname{Tr}(\mathbf{V}_\perp^H \mathbf{H}_i^H \mathbf{H}_i \mathbf{V}_\perp) + N_T/(\gamma_i \rho)}. \quad (2.4)$$

Note that if several streams can be assigned to the same user, SINR analysis based on the above formula is not sufficient, since joint decoding of the streams could effectively suppress part of the interference, depending on the receiver structure. However, as noted in [57], the probability of several beams being assigned to one user vanishes for large number of users, and we will therefore neglect this case.

We will now focus on the perturbation of this expression when  $\tilde{\mathbf{H}}$  is used instead of  $\mathbf{H}$  in the above formula.

## 2.2 SINR Perturbation

As already hinted in Sharif and Hassibi's paper [9], for a sufficiently large number of transmit antennas, the SINR in random beamforming systems is dominated by

interference, i.e. proper matching of a beam to the channel eigenmode (which enables interference nulling at the receiver) is more important than the actual received power alone. Therefore, our perturbation analysis will be based on the eigendecomposition of the Hermitian matrix  $\mathbf{A} = \mathbf{H}^H \mathbf{H}$ , i.e.  $\mathbf{A} = \mathbf{W} \mathbf{D} \mathbf{W}^H$  where  $\mathbf{W}$  is the unitary matrix containing the eigenvectors, and  $\mathbf{D}$  is the diagonal matrix containing the (non-negative) eigenvalues of  $\mathbf{A}$ .

The perturbation analysis that we propose in this section (and the stochastic version that follows) is largely inspired by the work of Stewart [52]. However, the analysis presented here is done for the particular case where both the original and the perturbed matrices are Hermitian, which is not the case in the original analysis.

Let us consider the perturbed matrix  $\tilde{\mathbf{A}} = \tilde{\mathbf{H}}^H \tilde{\mathbf{H}} = \mathbf{A} + \mathbf{B}$  where  $\mathbf{B} = \mathbf{E}^H \mathbf{H} + \mathbf{H}^H \mathbf{E} + \mathbf{E}^H \mathbf{E}$ . We will assume that  $\tilde{\mathbf{A}}$  is used during the training phase to estimate the SINR. We consider in particular its eigendecomposition  $\tilde{\mathbf{A}} = \tilde{\mathbf{W}} \tilde{\mathbf{D}} \tilde{\mathbf{W}}^H$ .

For simplicity, we investigate separately the perturbation of the numerator and denominator of the SINR formula (2.3). Since  $\tilde{\mathbf{W}}$  is unitary, one can always write the following expression for the received power (numerator)

$$P = \underline{\mathbf{v}}_1^H \mathbf{A} \underline{\mathbf{v}}_1 = \underline{\mathbf{v}}_1^H \tilde{\mathbf{W}} \tilde{\mathbf{W}}^H \mathbf{W} \mathbf{D} \underbrace{\mathbf{W}^H \tilde{\mathbf{W}}}_{\chi_2} \underbrace{\tilde{\mathbf{W}}^H \underline{\mathbf{v}}_1}_{\chi_1}, \quad (2.5)$$

and the following expression for the interference power

$$I = \text{Tr} [\mathbf{V}_\perp^H \mathbf{A} \mathbf{V}_\perp] = \text{Tr} \left[ \mathbf{V}_\perp^H \tilde{\mathbf{W}} \tilde{\mathbf{W}}^H \mathbf{W} \mathbf{D} \underbrace{\mathbf{W}^H \tilde{\mathbf{W}}}_{\chi_2} \underbrace{\tilde{\mathbf{W}}^H \mathbf{V}_\perp}_{\chi_1} \right]. \quad (2.6)$$

Interestingly, different terms can be isolated above: the terms denoted by  $\chi_1$  in (2.5) and (2.6) represent the mismatch between the beamforming vector of the first stream  $\underline{\mathbf{v}}_1$  and the eigenvectors  $\tilde{\mathbf{W}}$  of the measured channel matrix  $\tilde{\mathbf{H}}$ , and the mismatch between the beamforming vectors of the interfering streams and  $\tilde{\mathbf{W}}$  respectively. We denote

$$\tilde{\mathbf{W}}^H \underline{\mathbf{v}}_1 = \begin{bmatrix} f_1 \\ \underline{\mathbf{f}}_\perp \end{bmatrix} \text{ and } \tilde{\mathbf{W}}^H \mathbf{V}_\perp = \begin{bmatrix} \underline{\mathbf{g}}_1 \\ \mathbf{G}_\perp \end{bmatrix}. \quad (2.7)$$

$f_1$  is a scalar,  $\underline{\mathbf{f}}_\perp$  is a  $(N_T - 1) \times 1$  vector,  $\underline{\mathbf{g}}_1$  is a  $1 \times (N_T - 1)$  vector and  $\mathbf{G}_\perp$  is a  $(N_T - 1) \times (N_T - 1)$  matrix. For an SINR metric based on the knowledge of the measured channel  $\tilde{\mathbf{H}}$ , all terms in (2.7) can be measured during the training phase and  $\mathbf{D}$  can be approximated by  $\tilde{\mathbf{D}}$ . It remains to investigate the terms denoted by  $\chi_2$  in (2.5) and (2.6) which represent the subspace estimation error (indeed, if  $\mathbf{E} = 0$ ,  $\mathbf{W}^H \tilde{\mathbf{W}}$  becomes the identity matrix).

The bound presented below is based on the analysis of the first-order effects of  $\mathbf{E}$  on the product  $\mathbf{W}^H \tilde{\mathbf{W}}$ . Let us denote  $\mathbf{W} = [\underline{\mathbf{w}}_1 \mathbf{W}_\perp]$  where we separate the first eigenvector from the others and  $\mathbf{D} = \text{diag}\{[\lambda_1, \underline{\lambda}_\perp]\}$ .  $\underline{\lambda}_\perp$  is the  $1 \times (N_T - 1)$  vector  $[\lambda_2, \dots, \lambda_{N_T}]$ . Similarly,  $\tilde{\mathbf{W}} = [\tilde{\underline{\mathbf{w}}}_1 \tilde{\mathbf{W}}_\perp]$  and  $\tilde{\mathbf{D}} = \text{diag}\{[\tilde{\lambda}_1, \tilde{\underline{\lambda}}_\perp]\}$ . We will be concerned with the effect of  $\mathbf{B}$  to the subspace of  $\mathbf{A}$  spanned by  $\underline{\mathbf{w}}_1$  which we denote by  $\mathcal{S}(\underline{\mathbf{w}}_1)$ . The subspace spanned by  $\tilde{\underline{\mathbf{w}}}_1$  approaches  $\mathcal{S}(\underline{\mathbf{w}}_1)$  as  $\mathbf{B}$  approaches zero. Let us now characterize this perturbation more precisely: following [52], we consider the perturbation of the first invariant subspace of  $\mathbf{A}$ , through the first-order expansion of  $\tilde{\underline{\mathbf{w}}}_1$ :

$$\tilde{\underline{\mathbf{w}}}_1 = \underline{\mathbf{w}}_1 + \mathbf{W}_\perp \underline{\mathbf{p}}, \quad (2.8)$$

where  $\underline{\mathbf{p}}$  is a  $(N_T - 1) \times 1$  weight vector which is presumed small. A basis for the orthogonal complement of  $\mathcal{S}(\tilde{\underline{\mathbf{w}}}_1)$  is then given by the columns of

$$\tilde{\mathbf{W}}_\perp = \mathbf{W}_\perp - \underline{\mathbf{w}}_1 \underline{\mathbf{p}}^H. \quad (2.9)$$

Fig. 2.2 shows the weight vector in the orthogonal complement of  $\underline{\mathbf{w}}_1$ .

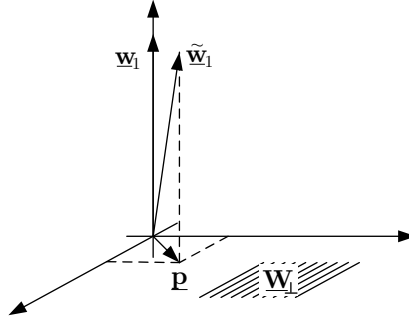


Figure 2.2: Weight vector  $\underline{\mathbf{p}}$  in the orthogonal complement  $\mathbf{W}_\perp$  of the eigenvector  $\underline{\mathbf{w}}_1$  closest to the beam.

The properties of the first order expansion of  $\tilde{\underline{\mathbf{w}}}_1$  introducing the weight vector  $\underline{\mathbf{p}}$  in Section 2.2 can be summarized as  $\tilde{\underline{\mathbf{w}}}_1^H (\mathbf{A} + \mathbf{B}) \tilde{\mathbf{W}}_\perp = \mathbf{0}_{N_T-1}$ , or

$$(\underline{\mathbf{w}}_1 + \mathbf{W}_\perp \underline{\mathbf{p}})^H (\mathbf{A} + \mathbf{B}) (\mathbf{W}_\perp - \underline{\mathbf{w}}_1 \underline{\mathbf{p}}^H) = \mathbf{0}_{N_T-1}. \quad (2.10)$$

Solving (2.10) for  $\underline{\mathbf{p}}$ , we will find a measure of the distance between  $\mathcal{S}(\underline{\mathbf{w}}_1)$  and  $\mathcal{S}(\tilde{\underline{\mathbf{w}}}_1)$ , i.e. the perturbation of the eigenvalue  $\lambda_1$ . Let us define

$$\begin{bmatrix} b_{11} & \underline{b}_{12} \\ \underline{b}_{21} & B_{22} \end{bmatrix} = \begin{bmatrix} \underline{\mathbf{w}}_1^H \\ \mathbf{W}_\perp^H \end{bmatrix} \mathbf{B} \begin{bmatrix} \underline{\mathbf{w}}_1 & \mathbf{W}_\perp \end{bmatrix}. \quad (2.11)$$

Using these notations, (2.10) can be rewritten as

$$\underline{b}_{21} + \Lambda_{\perp} \underline{\mathbf{p}} + B_{22} \underline{\mathbf{p}} - \underline{\mathbf{p}} \lambda_1 - \underline{\mathbf{p}} \underline{b}_{11} - \underline{\mathbf{p}} \underline{b}_{12} \underline{\mathbf{p}} = \underline{\mathbf{0}}_{N_T-1}, \quad (2.12)$$

with  $\Lambda_{\perp} = \text{diag}\{\underline{\lambda}_{\perp}\}$ . Neglecting the second-order terms ( $B_{22} \underline{\mathbf{p}}$ ,  $\underline{\mathbf{p}} \underline{b}_{11}$  and  $\underline{\mathbf{p}} \underline{b}_{12} \underline{\mathbf{p}}$ ) from (2.12), we get the first order perturbation equation

$$\Lambda_{\perp} \check{\underline{\mathbf{p}}} - \check{\underline{\mathbf{p}}} \lambda_1 = -\underline{b}_{21}, \quad (2.13)$$

where  $\check{\underline{\mathbf{p}}}$  is an approximation of  $\underline{\mathbf{p}}$ . Defining the linear operator  $\mathbf{T}$  as  $\mathbf{T}(\underline{\mathbf{p}}) = \Lambda_{\perp} \underline{\mathbf{p}} - \underline{\mathbf{p}} \lambda_1$ , eq. (2.12) becomes  $\underline{b}_{21} = -\mathbf{T}(\check{\underline{\mathbf{p}}})$ . Let us define

$$\delta = \inf_{\|\underline{\mathbf{p}}\|_F=1} \|\mathbf{T}(\underline{\mathbf{p}})\|_F, \quad (2.14)$$

where  $\|\cdot\|_F$  denotes the Frobenius norm. According to [52, Theorem 4.3],  $\delta$  is a function of the eigenvalues of  $\mathbf{A}$ :  $\delta = \min \{|\lambda_1 - \lambda_l| : \lambda_l \in \underline{\lambda}_{\perp}\}$ . The bound on the perturbation is a consequence of the definition of  $\delta$ :

$$\delta \|\check{\underline{\mathbf{p}}}\|_F \leq \|\mathbf{T}(\check{\underline{\mathbf{p}}})\|_F = \|\underline{b}_{21}\|_F. \quad (2.15)$$

### 2.2.1 Stochastic Bound

Since the above bound depends on  $\underline{b}_{21}$ , which is itself a function of the unknown noise realization  $\mathbf{E}$ , we propose a stochastic version of the bound. Let us recall the definition of the stochastic bound (again from [52]):

$$\|\mathbf{E}\|_S = \sqrt{\mathbb{E}[\|\mathbf{E}\|_F^2]}. \quad (2.16)$$

Let us examine in further detail the structure of  $\underline{b}_{21}$ : (2.11) yields

$$\underline{b}_{21} = \mathbf{W}_{\perp}^H \mathbf{B} \underline{\mathbf{w}}_1 = \mathbf{W}_{\perp}^H \mathbf{E}^H \mathbf{H} \underline{\mathbf{w}}_1 + \mathbf{W}_{\perp}^H \mathbf{H}^H \mathbf{E} \underline{\mathbf{w}}_1 + \mathbf{W}_{\perp}^H \mathbf{E}^H \mathbf{E} \underline{\mathbf{w}}_1. \quad (2.17)$$

Dropping the second order term  $\mathbf{W}_{\perp}^H \mathbf{E}^H \mathbf{E} \underline{\mathbf{w}}_1$  and writing the channel matrix  $\mathbf{H}$  according to its singular value decomposition  $\mathbf{H} = \mathbf{U} \mathbf{D}^{\frac{1}{2}} \mathbf{W}^H$  leads to

$$\underline{b}_{21} = \mathbf{W}_{\perp}^H \mathbf{E}^H \mathbf{U} \mathbf{D}^{\frac{1}{2}} \mathbf{W}^H \underline{\mathbf{w}}_1 + \mathbf{W}_{\perp}^H \mathbf{W} \mathbf{D}^{\frac{1}{2}} \mathbf{U}^H \mathbf{E} \underline{\mathbf{w}}_1 \quad (2.18)$$

$$= \mathbf{W}_{\perp}^H \mathbf{E}'^H \begin{bmatrix} \sqrt{\lambda_1}, 0, \dots, 0 \end{bmatrix}^H + \begin{bmatrix} 0 & \sqrt{\lambda_2} & \dots & 0 \\ \vdots & & \ddots & \\ 0 & 0 & \dots & \sqrt{\lambda_{N_T}} \end{bmatrix} \mathbf{E}' \underline{\mathbf{w}}_1, \quad (2.19)$$

where  $\mathbf{E}' = \mathbf{U}^H \mathbf{E}$  has the same Gaussian i.i.d. distribution as  $\mathbf{E}$  since  $\mathbf{U}$  is unitary. Note that the two terms in the above expression are statistically independent, since

the first depends only on the first row of  $\mathbf{E}'$ , and the second on the remaining rows. Therefore, their stochastic norms simply add up. Direct application of [52, Theorem 2.5] yields

$$\|\underline{b}_{21}\|_S^2 = \|\mathbf{W}_\perp^H\|_F^2 \lambda_1 \sigma_E^2 + \sum_{i=2}^{N_T} \lambda_i \|\underline{\mathbf{w}}_1\|_F^2 \sigma_E^2 = ((N_T - 1)\lambda_1 + \text{Tr}(\Lambda_\perp)) \sigma_E^2. \quad (2.20)$$

This yields the stochastic version of the bound (2.15):

$$\|\underline{\mathbf{p}}\|_S \leq \delta^{-1} \sqrt{(N_T - 1)\lambda_1 + \text{Tr}(\Lambda_\perp)} \sigma_E = \Delta. \quad (2.21)$$

### 2.2.2 Perturbation of the SINR

In the following we propose a stochastic SINR metric based on the knowledge of the measured channel  $\tilde{\mathbf{H}}$  and the variance  $\sigma_E^2$ . For tractability, we investigate here the use of  $\frac{P_{S,lb}}{I_{S,ub} + N_T/(\gamma_i \rho)}$  as the SINR metric, where  $P_{S,lb} \leq \mathbb{E}[\mathbf{v}_1^H \mathbf{H}^H \mathbf{H} \mathbf{v}_1]$  and  $I_{S,ub} \geq \mathbb{E}[\text{Tr}(\mathbf{V}_\perp^H \mathbf{H}^H \mathbf{H} \mathbf{V}_\perp)]$ . Those bounds are obtained by first bounding the power terms with functions of  $\|\underline{\mathbf{p}}\|_F$ , and then using the perturbation bound (2.21) since  $\mathbf{E}$  (and therefore  $\underline{\mathbf{p}}$ ) is not known deterministically.

In Appendix 2.4, we derive the (respectively lower and upper) bounds on the received signal and interference plus noise term, i.e.

$$P_{S,lb} = \lambda_1 |f_1|^2 - \gamma_1 \Delta + \sum_{l=1}^{N_T-1} |\underline{\mathbf{f}}_\perp(l)|^2 \underline{\lambda}_\perp(l), \quad (2.22)$$

$$I_{S,ub} = \lambda_1 \|\underline{\mathbf{g}}_1\|^2 + \gamma_2 \Delta + \sum_{l=1}^{N_T-1} \underline{\lambda}_\perp(l) \sum_{l'=1}^{N_T-1} |\mathbf{G}_\perp(l, l')|^2, \quad (2.23)$$

with  $\gamma_1 = 2|f_1| \sqrt{(\sum_l \xi_l) \max_l \xi_l}$ , where  $\xi_l = |\underline{\mathbf{f}}_\perp(l) (\lambda_1 - \underline{\lambda}_\perp(l))|$  and  $\gamma_2 = 2\sqrt{(\sum_l \zeta_l) \max_l \zeta_l}$  where  $\zeta_l = |\sum_{l'} \underline{\mathbf{g}}_1^*(l') \mathbf{G}_\perp(l, l') (\underline{\lambda}_\perp(l) - \lambda_1)|$ .

We finally obtain a conservative estimate of the SINR achieved over the real channel using (2.22) and (2.23) in  $\frac{P_{S,lb}}{I_{S,ub} + N_T/(\gamma_i \rho)}$ .

## 2.3 Simulation Results

In this section we compare the goodput and outage probability of the proposed feedback scheme to those achieved by other feedback metrics. The goodput is computed as  $\mathbb{E}[\sum_{l=1}^{N_T} \mathbb{I}[R_l \leq \log_2(1 + \text{SINR}_{\text{inst},l})] R_l]$  and the outage probability is denoted as  $p_{\text{out}} = \mathbb{P}(R_l > \log_2(1 + \text{SINR}_{\text{inst},l}))$ . We compare the following methods of SINR estimation:

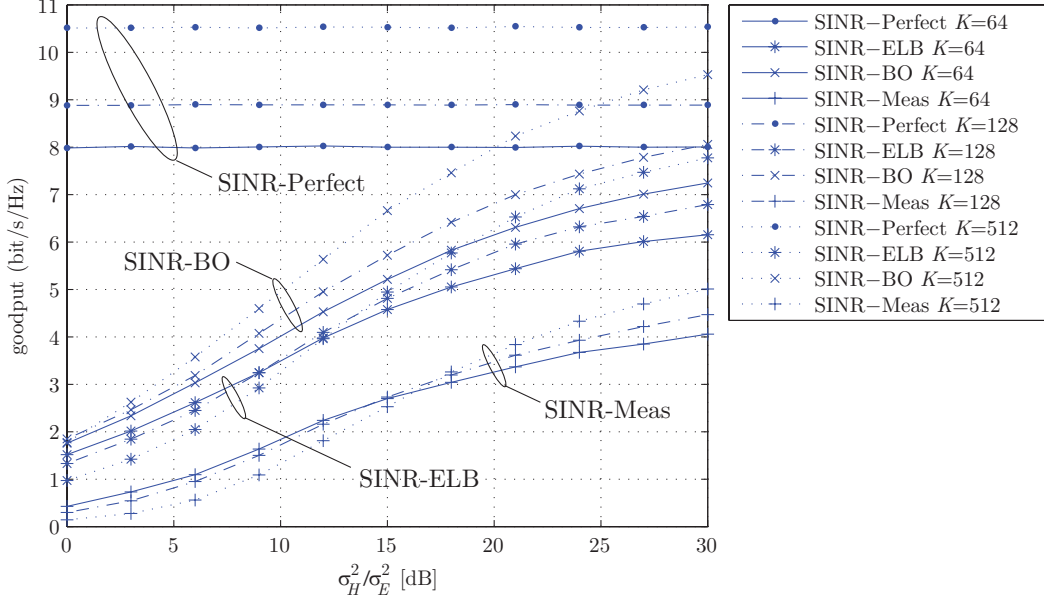


- the perfect SINR feedback, where  $\mathbf{H} = \tilde{\mathbf{H}}$ ,
- the measured SINR feedback (denoted by SINR-Meas), where the SINR is evaluated by directly plugging  $\tilde{\mathbf{H}}$  into the SINR formula (2.3),
- the SINR Expected Lower Bound (SINR-ELB) introduced in Section 2.2,
- the SINR back-off scheme (SINR-BO) [12] applied to the measured SINR. The optimal back-off coefficient is evaluated numerically for each value of  $\sigma_E^2$ .

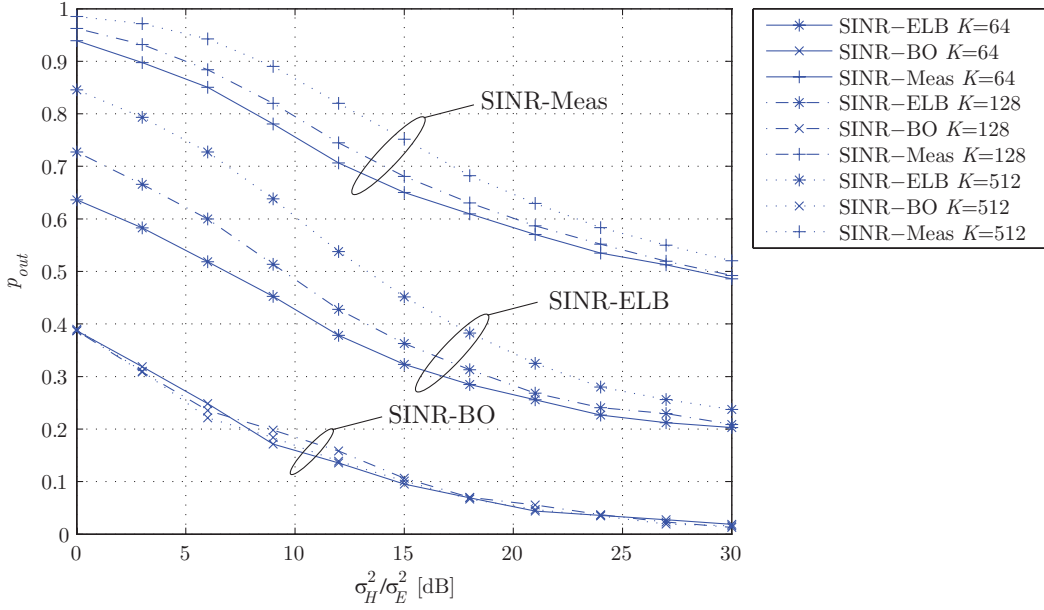
For all simulations, the signal-to-noise ratio is  $\rho = 20$  dB, the number of users is set to  $K = 64, 128, 512$ ,  $\gamma_i = 1 \forall i$  and  $\mathbf{H}$  is zero-mean Gaussian i.i.d. (Note however that the results in the previous section are derived for a deterministic  $\mathbf{H}$ ). The goodput and the outage probability  $p_{out}$  are plotted versus the relative channel measurement error denoted by  $\sigma_H^2/\sigma_E^2$ . Performance of a  $2 \times 2$  ( $N_T \times N_R$ ) antennas systems is depicted in Fig. 2.3, whereas Fig. 2.4 plots results for the  $4 \times 2$  antenna system.

For both the  $2 \times 2$  and  $4 \times 2$  antennas cases, the scheme that has perfect SINR information is clearly superior to the others. The achievable goodput increases with an increasing number of users in the network. The SINR-ELB performs better than the SINR-Meas feedback over the complete range of relative channel measurement error values, due to the high outage probability incurred by the latter. Conversely, the SINR-ELB metric ensures that the transmit data rate assigned to the scheduled users are estimated with a conservative bias, thereby reducing channel outages. In  $2 \times 2$  systems, the SINR-BO feedback method outperforms the SINR-ELB both in terms of goodput and in terms of outage probability. The SINR-BO method achieves low outage probabilities irrespective of the number of users, whereas the SINR-ELB and SINR-Meas feedback suffers from increased outage probabilities when the number of users increases. However, in  $4 \times 2$  antennas systems, the SINR-ELB metric provides a noticeable improvement in terms of outage probability, while approaching the performance of the SINR-BO for  $\sigma_H^2/\sigma_E^2 > 20\text{dB}, 15\text{dB}, 5\text{dB}$  if  $K=64, 128, 512$ , respectively. Clearly for high  $\sigma_H^2/\sigma_E^2$  values all the schemes perform equally.

Therefore, the newly introduced SINR-ELB metric is successful in reducing the outage probability with a marginal loss in the goodput in the case of  $4 \times 2$  systems. However, for  $2 \times 2$  antennas systems, the simpler SINR-BO scheme is superior.

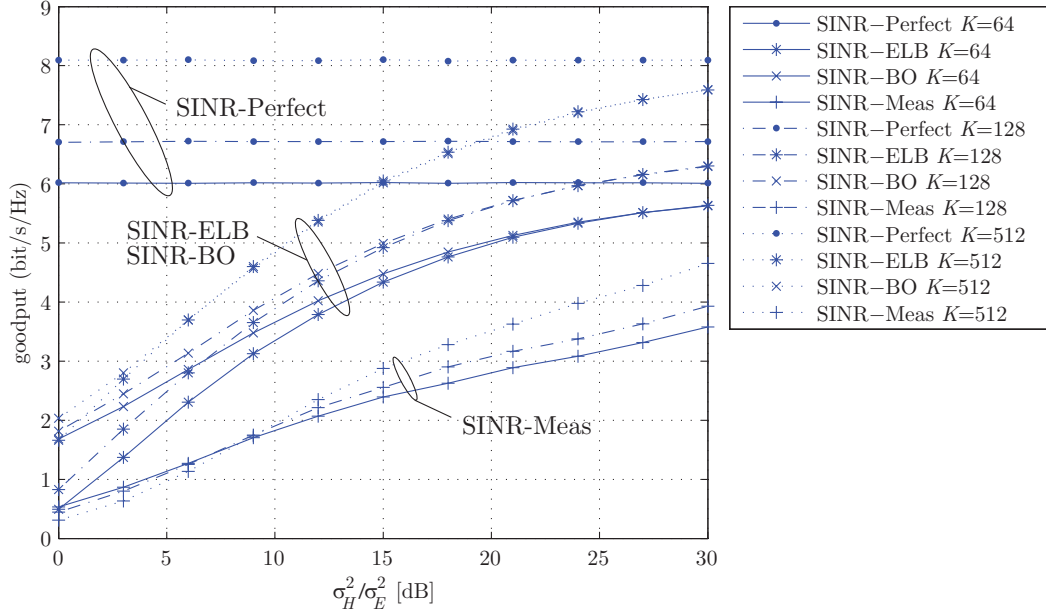


(a) Goodput versus relative channel measurement error.

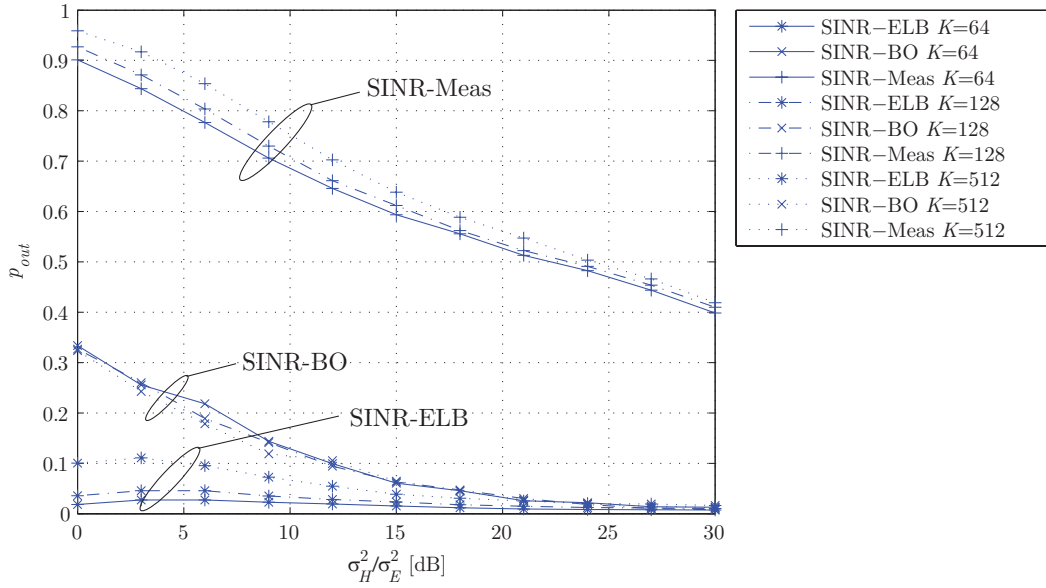


(b) Outage probability versus relative channel measurement error.

Figure 2.3: Performance of SINR metric over  $2 \times 2$  ( $N_T \times N_R$ ) antenna BC with different number of users.



(a) Goodput versus relative channel measurement error.



(b) Outage probability versus relative channel measurement error.

 Figure 2.4: Performance of SINR metric over  $4 \times 2$  ( $N_T \times N_R$ ) antenna BC channels with different number of users.

## 2.4 Appendix: Stochastic SINR Metric

In this appendix, we derive (lower and upper) bounds on the received signal and interference plus noise terms using the stochastic bound on the perturbation of the Hermitian matrix  $\mathbf{A}$ .

Let us consider the numerator of the SINR expressed in (2.5). Using the fact that the subspace estimation error denoted by the term  $\chi_2$  in (2.5) can be written as

$$\mathbf{W}^H \tilde{\mathbf{W}} = \begin{bmatrix} 1 & -\underline{\mathbf{p}}^H \\ \underline{\mathbf{p}} & \mathbf{I}_{N_T-1} \end{bmatrix}, \quad (2.24)$$

we obtain the following expression for the received signal power

$$P = \underline{\mathbf{v}}_1^H \mathbf{A} \underline{\mathbf{v}}_1 = \lambda_1 |f_1 - \underline{\mathbf{p}}^H \underline{\mathbf{f}}_\perp|^2 + (\underline{\mathbf{p}} f_1 + \underline{\mathbf{f}}_\perp)^H \Lambda_\perp (\underline{\mathbf{p}} f_1 + \underline{\mathbf{f}}_\perp) \quad (2.25)$$

$$\begin{aligned} &= \lambda_1 |f_1|^2 - \sum_{l=1}^{N_T-1} 2\Re\{f_1^* p_l^* \underline{\mathbf{f}}_\perp(l) (\lambda_1 - \underline{\lambda}_\perp(l))\} + \lambda_1 \left| \sum_{l=1}^{N_T-1} \underline{\mathbf{f}}_\perp^*(l) p_l \right|^2 \\ &\quad + |f_1|^2 \sum_{l=1}^{N_T-1} |p_l|^2 \underline{\lambda}_\perp(l) + \sum_{l=1}^{N_T-1} |\underline{\mathbf{f}}_\perp(l)|^2 \underline{\lambda}_\perp(l), \end{aligned} \quad (2.26)$$

with  $p_l$  and  $\underline{\mathbf{f}}_\perp(l)$  the  $l$ -th component of  $\underline{\mathbf{p}}$  and  $\underline{\mathbf{f}}_\perp$  respectively,  $\underline{\lambda}_\perp(l) = \lambda_{l+1}$ .

A lower bound on  $P$  is obtained from upper bounding the summation over the real part in (2.25), i.e.

$$\begin{aligned} \sum_{l=1}^{N_T-1} 2\Re\{f_1^* p_l^* \underline{\mathbf{f}}_\perp(l) (\lambda_1 - \underline{\lambda}_\perp(l))\} &\leq \sum_{l=1}^{N_T-1} 2|\Re\{f_1^* p_l^* \underline{\mathbf{f}}_\perp(l) (\lambda_1 - \underline{\lambda}_\perp(l))\}| \\ &\leq \sum_{l=1}^{N_T-1} 2|f_1| |p_l| |\underline{\mathbf{f}}_\perp(l) (\lambda_1 - \underline{\lambda}_\perp(l))|, \end{aligned}$$

where we obtained the last equality from

$$|\Re\{f_1^* p_l^* \underline{\mathbf{f}}_\perp(l) (\lambda_1 - \underline{\lambda}_\perp(l))\}| \leq |f_1| |p_l| |\underline{\mathbf{f}}_\perp(l) (\lambda_1 - \underline{\lambda}_\perp(l))|.$$

Then, applying the Jensen's inequality (with  $\xi_l = |\underline{\mathbf{f}}_\perp(l) (\lambda_1 - \underline{\lambda}_\perp(l))|$ ) we obtain

$$\left( \frac{\sum_l |p_l| \xi_l}{\sum_l \xi_l} \right)^2 \leq \frac{\sum_l \xi_l |p_l|^2}{\sum_l \xi_l} \leq \frac{\max_l \xi_l \sum_l |p_l|^2}{\sum_l \xi_l}. \quad (2.27)$$

This yields  $\sum_l 2\Re\{f_1^* p_l^* \underline{\mathbf{f}}_\perp(l) (\lambda_1 - \underline{\lambda}_\perp(l))\} \leq \gamma_1 \|\underline{\mathbf{p}}\|_F$ , where  $\gamma_1 = 2|f_1| \sqrt{(\sum_l \xi_l) \max_l \xi_l}$ , and therefore

$$P \geq \lambda_1 |f_1|^2 - \gamma_1 \|\underline{\mathbf{p}}\|_F + \sum_{l=1}^{N_T-1} |\underline{\mathbf{f}}_\perp(l)|^2 \underline{\lambda}_\perp(l). \quad (2.28)$$

Taking the expectation (over  $\mathbf{E}$ ) on both sides of this inequality yields

$$\mathbb{E}[P] \geq P_{S,lb} = \lambda_1 |f_1|^2 - \gamma_1 \Delta + \sum_{l=1}^{N_T-1} |\underline{\mathbf{f}}_{\perp}(l)|^2 \underline{\lambda}_{\perp}(l). \quad (2.29)$$

We proceed similarly for the interference power term. With (2.7) and (2.24) we obtain the following expression for the interference power (2.6)

$$\begin{aligned} I &= \text{Tr} \left[ \begin{bmatrix} \underline{\mathbf{g}}_1 \\ \underline{\mathbf{G}}_{\perp} \end{bmatrix}^H \begin{bmatrix} 1 & \underline{\mathbf{p}}^H \\ -\underline{\mathbf{p}} & \mathbf{I}_{N_T-1} \end{bmatrix} \mathbf{D} \begin{bmatrix} 1 & -\underline{\mathbf{p}}^H \\ \underline{\mathbf{p}} & \mathbf{I}_{N_T-1} \end{bmatrix} \begin{bmatrix} \underline{\mathbf{g}}_1 \\ \underline{\mathbf{G}}_{\perp} \end{bmatrix} \right] \\ &= \text{Tr} \left[ \lambda_1 \left( \underline{\mathbf{g}}_1^H \underline{\mathbf{g}}_1 - \underline{\mathbf{g}}_1^H \underline{\mathbf{p}}^H \underline{\mathbf{G}}_{\perp} - \underline{\mathbf{G}}_{\perp}^H \underline{\mathbf{p}} \underline{\mathbf{g}}_1 + \underline{\mathbf{G}}_{\perp}^H \underline{\mathbf{p}} \underline{\mathbf{p}}^H \underline{\mathbf{G}}_{\perp} \right) + \underline{\mathbf{g}}_1^H \underline{\mathbf{p}}^H \underline{\Lambda}_{\perp} \underline{\mathbf{p}} \underline{\mathbf{g}}_1 \right. \\ &\quad \left. + \underline{\mathbf{g}}_1^H \underline{\mathbf{p}}^H \underline{\Lambda}_{\perp} \underline{\mathbf{G}}_{\perp} + \underline{\mathbf{G}}_{\perp}^H \underline{\Lambda}_{\perp} \underline{\mathbf{p}} \underline{\mathbf{g}}_1 + \underline{\mathbf{G}}_{\perp}^H \underline{\Lambda}_{\perp} \underline{\mathbf{G}}_{\perp} \right]. \end{aligned} \quad (2.30)$$

If we drop the second order terms ( $\underline{\mathbf{G}}_{\perp}^H \underline{\mathbf{p}} \underline{\mathbf{p}}^H \underline{\mathbf{G}}_{\perp}$  and  $\underline{\mathbf{g}}_1^H \underline{\mathbf{p}}^H \underline{\Lambda}_{\perp} \underline{\mathbf{p}} \underline{\mathbf{g}}_1$ ) from (2.30), we obtain the following expression

$$\begin{aligned} I &= \lambda_1 \|\underline{\mathbf{g}}_1\|^2 + \sum_{l=1}^{N_T-1} 2\Re \left\{ \underline{\mathbf{p}}_l^* \sum_{l'=1}^{N_T-1} \underline{\mathbf{g}}_1^*(l') \underline{\mathbf{G}}_{\perp}(l, l') (\underline{\lambda}_{\perp}(l) - \lambda_1) \right\} \\ &\quad + \sum_{l=1}^{N_T-1} \underline{\lambda}_{\perp}(l) \sum_{l'=1}^{N_T-1} |\underline{\mathbf{G}}_{\perp}(l, l')|^2. \end{aligned} \quad (2.31)$$

Again, we upper bound the summation over the real part in (2.31) by

$$\begin{aligned} &\sum_{l=1}^{N_T-1} 2\Re \left\{ \underline{\mathbf{p}}_l^* \sum_{l'=1}^{N_T-1} \underline{\mathbf{g}}_1^*(l') \underline{\mathbf{G}}_{\perp}(l, l') (\underline{\lambda}_{\perp}(l) - \lambda_1) \right\} \\ &\leq \sum_{l=1}^{N_T-1} 2 \left| \Re \left\{ \underline{\mathbf{p}}_l^* \sum_{l'=1}^{N_T-1} \underline{\mathbf{g}}_1^*(l') \underline{\mathbf{G}}_{\perp}(l, l') (\underline{\lambda}_{\perp}(l) - \lambda_1) \right\} \right| \\ &\leq 2 \sqrt{\left( \sum_l \zeta_l \right) \max_l \zeta_l \|\underline{\mathbf{p}}\|_F} = \gamma_2 \|\underline{\mathbf{p}}\|_F, \end{aligned} \quad (2.32)$$

with  $\zeta_l = |\sum_{l'} \underline{\mathbf{g}}_1^*(l') \underline{\mathbf{G}}_{\perp}(l, l') (\underline{\lambda}_{\perp}(l) - \lambda_1)|$  and  $\gamma_2 = 2\sqrt{(\sum_l \zeta_l) \max_l \zeta_l}$ . Thus, we get the upper bound on the interference power

$$I \leq \lambda_1 \|\underline{\mathbf{g}}_1\|^2 + \gamma_2 \|\underline{\mathbf{p}}\|_F + \sum_{l=1}^{N_T-1} \underline{\lambda}_{\perp}(l) \sum_{l'=1}^{N_T-1} |\underline{\mathbf{G}}_{\perp}(l, l')|^2. \quad (2.33)$$

Taking the expectation (over  $\mathbf{E}$ ) on both sides of this inequality yields

$$\mathbb{E}[I] \leq I_{S,ub} = \lambda_1 \|\underline{\mathbf{g}}_1\|^2 + \gamma_2 \Delta + \sum_{l=1}^{N_T-1} \underline{\lambda}_\perp(l) \sum_{l'=1}^{N_T-1} |\mathbf{G}_\perp(l, l')|^2. \quad (2.34)$$

## **Part II**

# **MIMO Interference Alignment: Feasibility, Algorithms and Large System Analysis**





## 3 Introduction to Interference Alignment

In Part II of this thesis, we focus on interference between  $K$  transmitter-receiver pairs which we will call *links* in the following. Over these links users in different cells of a wireless access network or nodes in mobile ad hoc networks, aim to exchange independent messages. This setting is referred to as a  $K$ -user *interference channel* (IC). In the literature, the interference channel (IC) denotes a network solely comprised of two transmitter-receiver pairs, i.e. the 2-user interference channel.

In this chapter, we introduce the assumptions on cooperation, signaling and channel state information under which we want to study reliable wireless communication over a  $K$ -user IC. We introduce the number of degrees of freedom of a communication channel and discuss their ramification in interference networks. Furthermore, we outline the state of the art of interference alignment and emphasize the linear algebra foundations of the scheme. Finally, we derive the interference alignment conditions and illustrate them by two examples.

### 3.1 K-user Interference Channel

A  $K$ -user IC is a network comprised of  $K$  links, as shown in Fig. 3.1. The network is bipartite, i.e. all communication links originate from a set of transmitters and lead to a set of receivers. There are no multi-hop links between any source and destination. A  $K$ -user IC is an information theoretic model for the competition among  $K$  users accessing the same limited resources of a wireless network. Source nodes and destination nodes are non-cooperative and joint processing is excluded at either side as opposed to the broadcast or multiple access channel. Independent messages  $[W_i]_{i=1,\dots,K}$  are exchanged between transmitter-receiver pairs, i.e. transmitter  $i$  aims at conveying a message exclusively to receiver  $i$ . Receiver  $i$  suffers from co-channel interference (CCI) caused by  $K - 1$  aggregated signals carrying  $[W_j]_{j \neq i}$ .

The lack of cooperation and joint signal processing at transmitter and receiver side is the central challenge for reliable communication over a  $K$ -user IC. The distributed

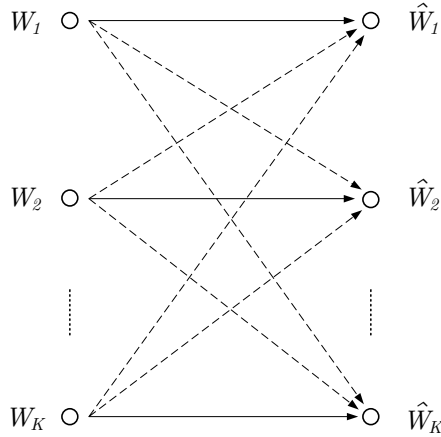


Figure 3.1: The  $K$ -user IC where each transmitter desires to communicate a message to its intended receiver, in the presence of interference from other user pairs.

nature of the network reveals itself through a performance loss compared to systems with node cooperation or  $K$  isolated *point-to-point* (P2P) systems.

Information theorists have pursued capacity characterization of the  $K$ -user IC for decades, see [17, Section I] and references therein. The *sum-capacity* of a communication network, denoted as  $C_\Sigma$ , is the supremum of all achievable sum-rates for which the probability of error for all messages  $[W_i]_{i=1,\dots,K}$  can be simultaneously made arbitrarily small. For the (2-user) IC,  $C_\Sigma$  has been characterized within one bit [58]. In the analysis of [58], achievability has been shown using a special case of the Han-Kobayashi scheme [59]. The *degrees of freedom* (DoF) characterization yields a first order approximation of the sum-capacity and therefore a structured approach towards finding  $C_\Sigma$  in a  $K$ -user IC at high SNR. Using this method, different operational regimes have been identified in the 2-user IC [58].

For more than two users, i.e the  $K > 2$  IC, the exact capacity characterization is unknown. However, the DoF characterization was derived in the seminal work of Cadambe and Jafar [17]. They showed that in a  $K$ -user SISO IC a sum-rate multiplexing gain of  $K/2$  per time or frequency dimension can be achieved almost surely. The achievability of this result is based on *interference alignment* (IA), a technique that reveals its strength in situations where the nuisance originates from multiple sources, i.e the  $K > 2$  IC. This significant contribution leveraged a novel branch of work on interference channel characterization.

Before being applied to interference channels, the idea of alignment has crystallized over a number of related works in other network settings. Interference alignment was considered in [60] as a coding technique for the two-user MIMO X channel, where it was shown to achieve multiplexing gains strictly higher than that of the em-

bedded MIMO interference channel, multiple-access channel, and broadcast channel taken separately. The X channel is a multi-user network where each transmitter  $i$  has independent messages  $[W_{ji}]_{j=1,\dots,K}$  for every receiver. In this setting, the signals of unintended received messages  $[W_{ji}]_{i \neq j}$  are aligned in the receive signal space of receiver  $j$ . The DoF region for the X channel was analyzed in [19] for an arbitrary number of antennas per user.

### 3.1.1 Interference Alignment

In the following, we focus on an achievable scheme for finding the maximum sum-rate multiplexing gain in the  $K$ -user IC. In [17], the idea of IA was introduced to the  $K$ -user IC. A shift of paradigm in the way interference is treated in this large network enables new insights into optimal interference management techniques and capacity scaling at high SNR that we summarize in this subsection.

Conventional interference management approaches such as interference cancellation, single-user encoding/decoding and interference avoidance (using orthogonal resource sharing) are used in many practical systems and are well understood from an information theoretic perspective. In particular, decoding of the interfering signal along with the desired signal is optimal if the interference is very strong and originates from a single source, i.e. in the context of the 2-user IC. Treating the interference as noise is optimal whenever the interference power is small compared to the signal of interest. Here, the number of interference sources can be arbitrary and single-user encoding/decoding suffices. Orthogonal channel access is optimal in the (2-user) IC when the power of the desired and interfering signals are of comparable strength. However, generalizing above findings to the  $K$ -user IC where the receive power of all desired and interfering signals are of comparable strength are not straightforward in general.

On a coarse level, the performance of aforementioned interference management strategies in a  $K$ -user IC can be illustrated as follows. Fig. 3.2 shows the sum-rate that we aim to maximize as a function of the SNR in the network. Numerical simulations show that at low SNR, an egoistic single-user encoding/decoding strategy performs well. In this regime, maximizing the signal of interest regardless of the interference that a transmitter-receiver pair is causing to the other users is sufficient since the noise level is high. However, the sum-rate saturates at high SNR and increasing the transmission power in the network leads to a diminishing increase of the sum-rate. Orthogonal schemes outperforms the egoistic strategy at medium and high SNR. In this regime, interference avoidance through orthogonal resource sharing lead to a linear scaling of the sum-rate as a function of the SNR. However,

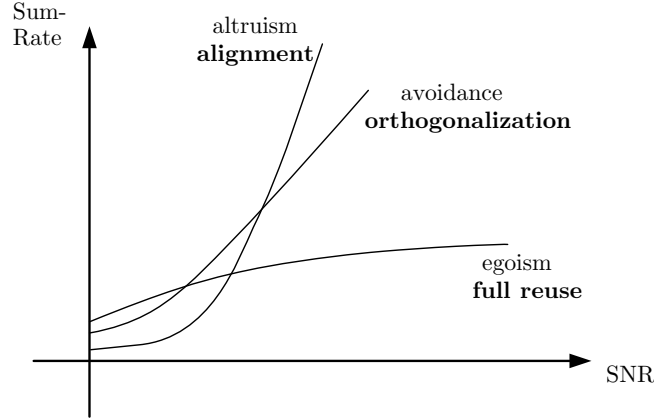


Figure 3.2: The sum-rate performance as a function of the SNR in dB of different resource sharing strategies in a  $K$ -user IC.

the linear scaling is limited by the fact that  $K$ -users have to share the resource and get only a fraction of the resource. At high SNR, an altruistic interference management strategy based on alignment outperforms orthogonal medium access. This novel strategy tackles interference at its source and steers it in such a way that it causes minimal damage at each unintended receiver. Conceptually, alignment reveals its potential merit in networks where a receiver gets impaired by nuisance from at least two sources  $K > 2$ . It was shown in [17] using an outerbound on the DoF that the maximum sum-rate multiplexing gain in the  $K$ -user IC, i.e. the maximum slope of the curve in Fig. 3.2, can be achieved using IA. It is impossible to achieve a higher slope of the sum-rate curve regardless of any sophisticated signal processing and therefore minimizing the interference that is caused to other receivers is optimal in the high SNR regime.

Seeking to be optimal at any SNR, precoding design at each transmitter must have the aim of striking a compromise between beamforming gain at the intended receiver (egoism) and the mitigation of interference created towards other receivers (altruism) [61], illustrated by Fig. 3.2. Combining egoistic and altruistic beamforming has been shown previously to be instrumental to optimizing the rates in a Multiple-Input-Single-Output (MISO) IC, i.e. where receivers have no interference canceling capability [62], [63].

Throughout this thesis, we will focus on alignment in signal space dimensions. Therefore, alignment is achieved by beamforming of signals in the observed signal space. The challenge is to steer the beams in such a way that the signals cast overlapping shadows at unintended receivers, while simultaneously remaining distin-

guishable at the intended receivers [22]. In other words, the key idea of interference alignment is to design the spatial properties of the emitted signals at the transmitter side such that the overlap between the signal spaces of all interference signals is maximized. An alignment-based interference management approach is taking care of spatial directions rather than the actual power of the receive signals inside of the subspaces. Therefore, in general it cannot be optimal at any SNR as visualized in Fig. 3.2. Particularly, as will be outlined in Chapter 4, the beamformers of user  $i$  are independent of the direct link between transmitter  $i$  and receiver  $i$ .

Global channel knowledge is a prerequisite for *constructive procedures* that find solutions of the alignment problem. All constructive methods that could be found so far [17], [64], [27] indicate that the solution to the alignment problem, i.e. the low rank precoder for a particular user is a function of the channel gains of all co-channel links (all diagonal arrows in Fig. 3.1). On the other hand, *iterative algorithms* based on channel reciprocity were proposed in [22] and [25] to find precoders in a distributed fashion, relaxing the requirement on CSI. Here, alternating optimization (introduced in [65]) of an interference leakage metric is necessary to account for the coupled nature of the alignment problem.

Two fundamentally different interference channel settings are analyzed in [17]. The  $K$ -user SISO interference channel with varying channel coefficients (also referred to as extended channel) and the  $K$ -user MIMO-IC, where the channel gains are drawn once and kept constant for the duration of transmission, denoted as  $K$ -user MIMO-IC with constant channel coefficients.

Let us introduce the notation for several  $K$ -user IC configurations and associated coding scheme definitions that we will use throughout Part II of this thesis. Let  $(N_S : [d_i]_{i=1,\dots,K})$  denote the  $K$ -user SISO-IC over the  $N_S$  dimensional extended channel with multiplexing gain allocation  $d_i$  for user  $i$ . Accordingly, let  $[(N_T \times N_R, d_i)]_{i=1,\dots,K}$  denote the  $K$ -user MIMO IC, where transmitters and receivers is equipped with  $N_T$  and  $N_R$  antennas, respectively and user  $i$  wishes to achieve a multiplexing gain  $d_i$ . Hence,  $d_i$  streams per transmitter are spatially pre-coded at transmitter  $i$ . For instance, the  $(3 : (2/3)(1/3)^2)$  is the three-user SISO-IC over the three-dimensional extended channel where user one aims for multiplexing gain  $2/3$  and user two and three for multiplexing gain  $1/3$ . The  $(5 \times 3, 2)(2 \times 3, 1)^2$  is the three-user MIMO-IC where one user aiming for multiplexing gain 2 is equipped with 3 transmit and receive antennas, and two users aiming for multiplexing gain 1 are equipped with 2 transmit and 3 receive antennas, respectively.

## 3.2 Degrees of Freedom of the SISO $K$ -user IC

In the following, we will define the number of *degrees of freedom* (DoF) of a wireless communication network and illustrate its significance as the number of interference-free signaling dimensions in the network. In this section, we focus on single-antenna transmitters and receivers whereas multi-antenna communication is treated in the next section.

If we assume a single active link in the network, see Fig. 3.3, then single-user communication can utilize the whole available resource. This resource may be transmission time or system bandwidth, associated with a cake in Fig. 3.3. In a Gaussian



Figure 3.3: Single-user communication system where the transmission can use the whole available resource.

SISO channel, the input/output relation at a given time is  $y = hx + n$ , with  $h$  the channel gain that is assumed constant for the duration of transmission and known at transmitter and receiver side and  $n \sim \mathcal{CN}(0, 1)$  is additive white Gaussian noise (AWGN) with unit variance. It reflects the frequency-flat model introduced in Chapter 1.3, i.e. narrowband transmission or OFDM modulation on one subcarrier. The SNR is defined as  $\rho$ , i.e. the transmit power while the noise power is normalized to unity [17]. The capacity of this channel is  $C = \log_2(1 + \rho|h|^2)$  bits/channel use [66].

**Definition 1.** The number of *degrees of freedom of the channel* (sometimes referred to as *capacity pre-log factor*) is defined as the asymptotically available multiplexing gain, i.e. the number of signaling dimensions per channel use at high SNR

$$d = \lim_{\rho \rightarrow \infty} \frac{C(\rho)}{\log_2(\rho)}, \quad (3.1)$$

with  $C$  being the capacity of the link.

For the single-user Gaussian SISO channel

$$d = \lim_{\rho \rightarrow \infty} \frac{\log_2(1 + \rho|h|^2)}{\log_2(\rho)} = \lim_{\rho \rightarrow \infty} \frac{\log_2(\rho) + \log_2(|h|^2)}{\log_2(\rho)} = 1, \quad (3.2)$$

where we used the fact that  $\log_2(1 + x) \approx \log_2(x)$  when  $x \gg 1$ . Hence, with  $W$  in Fig. 3.3 we can reliably communicate approximately  $\log_2(\rho)$  bits per channel-use in the high SNR regime. The capacity pre-log factor or the number of DoF for the

1-user Gaussian SISO channel is therefore  $d = 1$ . The capacity  $C$  as a function of the SNR is asymptotically

$$C(\rho) = \log_2(\rho) + o(\log_2(\rho)) \text{ bits/channel use.} \quad (3.3)$$

Let us now generalize the above line of thought and consider a network with  $K$  links, as shown in Fig. 3.4(a). For the  $K$ -user SISO-IC, the input/output relation is

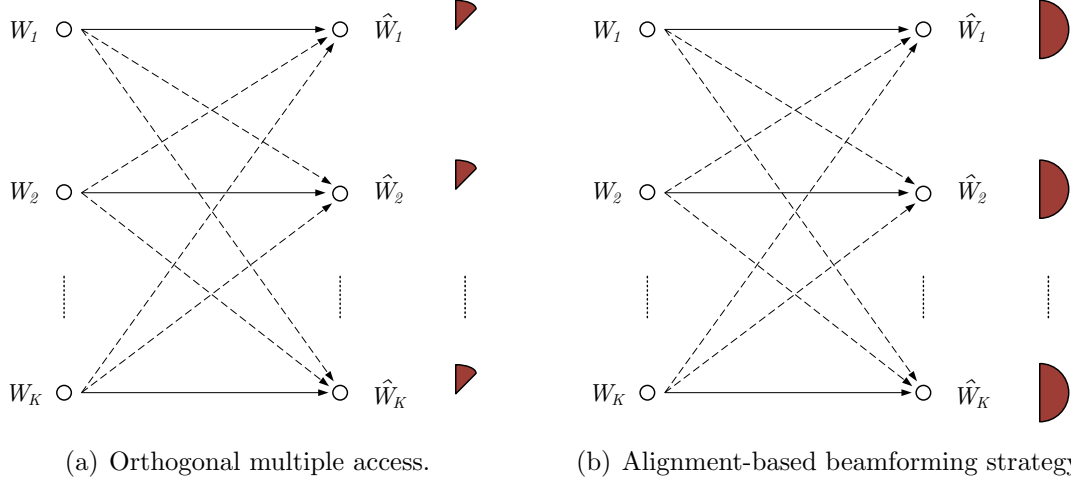


Figure 3.4: Strategies for communication over the  $K$ -user IC and their qualitative share of the common resource with respect to single-user communication.

$$\begin{aligned} y_1 &= h_{11}x_1 + h_{12}x_2 + \dots + h_{1K}x_K + n_1 \\ y_2 &= h_{21}x_1 + h_{22}x_2 + \dots + h_{2K}x_K + n_2 \\ &\vdots \\ y_K &= h_{K1}x_1 + h_{K2}x_2 + \dots + h_{KK}x_K + n_K \end{aligned} \quad (3.4)$$

with  $h_{ij}$  the channel gain from transmitter  $j$  to receiver  $i$ , and  $n_i$  is AWGN with unit variance, i.e.  $\mathbb{E}[n_i n_{i'}^*] = \delta[i - i']$ . We assume global CSI. The SNR is defined as  $\rho$  the total transmit power of all nodes while the local noise power at each node is normalized to unity [17]. Similar to Definition 1, we define the DoF for the network as follows:

**Definition 2.** The number of *degrees of freedom of the  $K$ -user IC* (the capacity pre-log factor) is defined as the asymptotically available multiplexing gain, i.e. the number of signaling dimensions per channel use

$$d_{\mathbf{H}} = \lim_{\rho \rightarrow \infty} \frac{C_{\Sigma}(\rho)}{\log_2(\rho)}, \quad (3.5)$$

with  $C_\Sigma(\rho)$  the sum-capacity of the network.

Let us now choose an orthogonal resource sharing approach and calculate the sum-rate multiplexing gain. Prevalent techniques such as allocation of users on different time slots (via Time Division Multiple Access (TDMA)) or frequency bands (via frequency division multiple access (FDMA)) follow this strategy. Obviously, the drawback of this approach is the diminishing access to the resource when the number of users grows. The multiplexing gain in the  $K$ -user SISO-IC can be calculated as follows

$$\begin{aligned} d_{\text{orth}} &= \lim_{\rho \rightarrow \infty} \frac{R_\Sigma(\rho)}{\log_2(\rho)} = \lim_{\rho \rightarrow \infty} \frac{\sum_{i=1}^K \frac{1}{K} \log_2(1 + K\rho|h|^2)}{\log_2(\rho)} \\ &= \lim_{\rho \rightarrow \infty} \frac{\log_2(\rho) + \sum_{i=1}^K \frac{1}{K} \log_2(K|h|^2)}{\log_2(\rho)} = 1, \end{aligned} \quad (3.6)$$

with  $R_\Sigma(\rho)$  the sum-rate in the network. The factor  $1/K$  in the expression for the sum-rate reflects the fact that the available resource is shared among  $K$  users. As a consequence, the power per user is increased by a factor of  $K$  in (3.6). It was conjectured [18] that the achievable DoF in a  $K$ -user SISO-IC is  $d_{\mathbf{H}} = 1$ , yielding every user  $d_i = 1/K$  DoF. This conjecture is inspired by the conventional wisdom that the available resource has to be divided among the users for interference-free communication, as symbolized by the slices in Fig. 3.4(a).

The intriguing result of Cadambe and Jafar [17] is that independent of the number of users, it is possible for each transmitter-receiver pair to communicate interference free for half the time or using half the system bandwidth. Accordingly, in a  $K$ -user SISO IC (3.4) the sum-capacity as a function of  $\rho$  can be characterized almost surely as

$$C_\Sigma(\rho) = \frac{K}{2} \log_2(\rho) + o(\log_2(\rho)) \text{ bit/channel use.} \quad (3.7)$$

The sum-capacity pre-log factor in (3.7) grows linearly with the number of users and the DoF per user are  $d_i = 1/2$  and hence all users get half the communication resources, illustrated by 3.4(b). The achievability of the above result (3.7) has been proved using interference alignment, a linear beamforming scheme. Hence, the maximum multiplexing gain in a  $K$ -user SISO-IC can be achieved almost surely with linear signal processing at the transmitter and receiver, and point-to-point channel codes. The sum-capacity characterization (3.7) is tight in the high SNR regime where the term  $o(\log_2(\rho_i))$  becomes negligible.

For the  $(N_S : [(d_i)]_{i=1,\dots,K})$  IC configuration, interference alignment is achieved by linear beamforming over the  $N_S$ -dimensional extended channel [17]. The channel



coefficients of the extended channel, i.e.  $h_{ij}[1], h_{ij}[1], \dots, h_{ij}[N_S]$  for the link between transmitter  $i$  and  $j$ , are drawn from a continuous distribution. Cadambe and Jafar refer to channel extensions in the time domain or frequency domain, however with varying channel coefficients as the important assumption. So called supersymbols  $\underline{\mathbf{x}}_i \in \mathbb{C}^{N_S \times 1}$  are transmitted over  $N_S$  channel accesses [17]. The linear beamforming in the observed signal space is

$$\underline{\mathbf{x}}_i = \sum_{l=1}^{d_i N_S} \underline{\mathbf{v}}_l s_{il} = \mathbf{V}_i \underline{\mathbf{s}}_i, \quad (3.8)$$

with independent symbol streams  $[s_{il}]_{l=1, \dots, d_i N_S}$  and their associated beamforming vectors  $[\underline{\mathbf{v}}_l]_{l=1, \dots, d_i N_S}$ ,  $\underline{\mathbf{s}}_i = [s_{i1}, \dots, s_{i[d_i N_S]}]$  and  $\mathbf{V}_i = [\underline{\mathbf{v}}_{i1}, \dots, \underline{\mathbf{v}}_{i[d_i N_S]}]$ . (3.8) can be interpreted as low rank precoding of  $d_i N_S$  symbol streams  $\underline{\mathbf{s}}_i$  over  $N_S$  signal space dimensions. The channel matrices, i.e. the linear transformation, linking input to output (neglecting the receiver noise) are diagonal and non-degenerate, i.e.  $H_{ij} = \text{diag}\{[h_{ij}[0], h_{ij}[1], \dots, h_{ij}[N_S]]\}$ .

The minimum network configuration allowing an alignment solution consists of  $K = 3$  users and beamforming across three consecutive channel accesses, i.e.  $(3 : (2/3)(1/3)^2)$ . In this setting, there exist constructive solutions for the alignment problem [17]. We observe that this minimal feasible network configuration leads to a sum-rate multiplexing gain  $\sum_i d_i = 4/3$ . This is far away from the DoF of the 3-user SISO IC, i.e.  $d_{\mathbf{H}} = 3/2$ . Long symbol extensions are necessary, i.e. precoding over many channel accesses ( $N_S$  large), to approach the DoF of the channel. The alignment problem is solved for  $(2\kappa + 1 : (\frac{\kappa+1}{2\kappa+1})(\frac{\kappa}{2\kappa+1})^2)$  for any integer  $\kappa$ , leading to  $\sum_i d_i = \frac{3\kappa+1}{2\kappa+1}$ . Hence, a sufficiently large symbol extension ( $\kappa$  large) is necessary to asymptotically achieve  $d_{\mathbf{H}} = 3/2$ .

The generalization to  $K \geq 3$  is discussed in [17]. For  $K \geq 3$ , the minimum  $N_S$  allowing for a constructive alignment solution is  $N_S = (\kappa + 1)^{(K-1)(K-2)-1} + \kappa^{(K-1)(K-2)-1}$  in the  $(N_S : (\frac{(\kappa+1)^{(K-1)(K-2)-1}}{N_S})(\frac{\kappa^{(K-1)(K-2)-1}}{N_S})^{(K-1)})$  network. Hence,  $N_S$  is scaling exponentially with the number of users  $K$ . Assuming  $\kappa = 1$ , symbol extensions of  $N_S = 3, 33, 2049, 524289, \dots$  for  $K = 3, 4, 5, 6, \dots$  are necessary, prohibiting a real time application. Again,  $\kappa$  must be taken asymptotically large in order to converge to the DoF of the  $K$ -user IC, i.e.  $d_{\mathbf{H}} = K/2$ .

An improved interference alignment scheme that achieves a higher multiplexing gain at any given number of channel realization in comparison with the above scheme is proposed in [67]. For  $K \geq 3$ , the minimum  $N_S$  allowing for a constructive alignment solution is  $N_S = \binom{\kappa+(K-1)(K-2)-1}{(K-1)(K-2)-1} + \binom{\kappa+(K-1)(K-2)}{(K-1)(K-2)-1}$  in the network with the following configuration  $(N_S : ((\binom{\kappa+(K-1)(K-2)-1}{(K-1)(K-2)-1})/N_S)((\binom{\kappa+(K-1)(K-2)}{(K-1)(K-2)-1})/N_S)^{(K-1)})$ . Assuming  $\kappa =$

1, symbol extensions of  $N_S = 5, 27, 90, 230, \dots$  for  $K = 3, 4, 5, 6, \dots$  are necessary. The improved scheme achieves the optimal multiplexing gain asymptotically when  $\kappa$  and as a consequence  $N_S$  grow.

Interference alignment in single-antenna networks with limited feedback is considered in [68] over a frequency-selective channel with  $L_h$  taps. Perfect channel state information at all receivers is assumed, whereas the feedback link is modeled as an error-free non-interfering broadcast channel with limited rate. It is shown that the interference alignment solutions derived in [17] based on quantized channel feedback according to the vector quantization scheme proposed in [69] achieves the maximum multiplexing gain, given that the number of feedback bits is at least  $KL_h \log_2(\rho)$ .

### 3.3 Degrees of Freedom of the MIMO $K$ -user IC

In this subsection, we consider communication from transmitters and receivers equipped with  $N_T$  transmit and  $N_R$  receive antennas, respectively.

Let us begin with the single-user case. The wireless link in Fig. 3.3 is a Gaussian vector channel. The input/output relation in vector notation writes  $\underline{\mathbf{y}} = \mathbf{H}\underline{\mathbf{x}} + \underline{\mathbf{n}}$ , with the  $N_R \times N_T$  MIMO matrix  $\mathbf{H}$ , known at transmitter and receiver side and spatially white additive Gaussian noise  $\underline{\mathbf{n}} \sim \mathcal{CN}(0, \mathbf{I}_{N_R})$ , with unit variance. The SNR is defined as  $\rho$ , i.e. the transmit power  $\mathbb{E}[\text{Tr}(\underline{\mathbf{x}}\underline{\mathbf{x}}^H)]$  while the noise power at each receive antenna is normalized to unity [17]. We assume that the channel is not rank-deficient, which happens w.p. one if the entries of the channel matrix  $\mathbf{H}$  are drawn i.i.d. from any continuous distribution and kept constant for the duration of transmission.

Let us now recall the architecture that enables spatial multiplexing. The MIMO matrix has a *singular value decomposition* (SVD)

$$\mathbf{H} = \mathbf{U}\mathbf{\Sigma}\mathbf{V}^H, \quad (3.9)$$

where  $\mathbf{U} \in \mathbb{C}^{N_R \times N_R}$  and  $\mathbf{V} \in \mathbb{C}^{N_T \times N_T}$  are unitary matrices and  $\mathbf{\Sigma} \in \mathbb{R}^{N_R \times N_T}$  is a rectangular matrix whose diagonal elements are non-negative real numbers and whose off-diagonal elements are zero. The diagonal elements  $\sigma_1 \geq \sigma_2 \geq \dots \geq \sigma_{N^{\min}}$  are the  $N^{\min} = \min\{N_T, N_R\}$  *singular values* of the matrix  $\mathbf{H}$ . Hence, we can achieve a multiplexing gain  $N^{\min}$  with signals  $\underline{\mathbf{x}} \in \mathbb{C}^{N_T \times 1}$  according to

$$\underline{\mathbf{x}} = \mathbf{V}\underline{\mathbf{s}}, \quad (3.10)$$

precoding symbols  $\underline{\mathbf{s}} = [s_1, \dots, s_{N^{\min}}]^T$  along the *eigenmodes* of the MIMO channel with  $\mathbf{V} = [\underline{\mathbf{v}}_1, \dots, \underline{\mathbf{v}}_{N^{\min}}]$  the stacked right singular vectors (columns of  $\mathbf{V}$ )

corresponding to the  $N^{\min}$  singular values, i.e.  $\mathbf{V} \in \mathbb{C}^{N_T \times N^{\min}}$ . Similarly let  $\mathbf{U} = [\mathbf{u}_1, \dots, \mathbf{u}_{N^{\min}}]$  denote the stacked left singular vectors (columns of  $\mathbf{U}$ ) corresponding to the  $N^{\min}$  singular values, i.e.  $\mathbf{U} \in \mathbb{C}^{N_R \times N^{\min}}$ .

Defining  $\bar{\mathbf{y}} = \mathbf{U}^H \mathbf{y}^1$  and  $\bar{\mathbf{n}} = \mathbf{U}^H \mathbf{n}$ , we can rewrite the single-user MIMO channel as  $\bar{\mathbf{y}} = \text{diag}([\sigma_1, \sigma_2, \dots, \sigma_{N^{\min}}]) \bar{\mathbf{s}} + \bar{\mathbf{n}}$  with  $\bar{\mathbf{n}} \sim \mathcal{CN}(0, \mathbf{I}_{N^{\min}})$  and  $\|\bar{\mathbf{x}}\|^2 = \|\bar{\mathbf{s}}\|^2$ . Hence, we found an equivalent representation of the MIMO channel comprised of parallel Gaussian channels whose capacity writes [66]

$$C = \sum_{l=1}^{N^{\min}} \log_2 (1 + \tilde{\rho}_l \sigma_l^2), \quad (3.11)$$

where  $\tilde{\rho}_1, \dots, \tilde{\rho}_{N^{\min}}$  are the *waterfilling* power allocations  $\tilde{\rho}_l = (\mu - (1/\sigma_l^2))^+$  with  $\mu$  chosen such that  $\sum_{l=1}^{N^{\min}} \tilde{\rho}_l = \rho$ . The multiplexing gain is therefore

$$\begin{aligned} d &= \lim_{\rho \rightarrow \infty} \frac{C}{\log_2(\rho)} = \lim_{\rho \rightarrow \infty} \frac{\sum_{l=1}^{N^{\min}} \log_2 (1 + \frac{\rho}{N^{\min}} \sigma_l^2)}{\log_2(\rho)} \\ &= \lim_{\rho \rightarrow \infty} \frac{N^{\min} \log_2(\rho) + \sum_{l=1}^{N^{\min}} \log_2 \left( \frac{\sigma_l^2}{N^{\min}} \right)}{\log_2(\rho)} = N^{\min}, \end{aligned} \quad (3.12)$$

where for the second equality we used the fact that for  $\rho \rightarrow \infty$  allocating uniform power on all eigenmodes is optimal and for the third equality the fact that  $\log_2(1+x) \approx \log_2(x)$  when  $x \gg 1$ . Hence, with  $W$  in Fig. 3.3 we can reliably communicate approximately  $\min\{N_T, N_R\} \log_2(1+\rho)$  bits per channel-use in the high SNR regime. The DoF or the capacity pre-log is the equal to the rank of the MIMO matrix  $d = N^{\min} = \text{rank}(\mathbf{H}) = \min\{N_T, N_R\}$  signaling dimensions per channel use w.p. one. The capacity can be characterized as [51]

$$C(\rho) = \min\{N_T, N_R\} \log_2(1 + \rho) + o(\log_2(\rho)) \text{ bit/channel use}. \quad (3.13)$$

Let us now consider the multi-user MIMO-IC. The input/output relation for user  $i$  ((1.1) introduced in Section 1.3) writes  $\mathbf{y}_i = \mathbf{H}_{ii} \mathbf{x}_i + \sum_{j \neq i} \mathbf{H}_{ij} \mathbf{x}_j + \mathbf{n}_i$ .  $\mathbf{H}_{ii}, \mathbf{H}_{ij} \in \mathbb{C}^{N_R \times N_T}$  are matrices representing the MIMO channels of the link between intended communication pairs and the interfering link between transmitter  $j$  and unintended receiver  $i$ , respectively, experienced by user  $i$ . The entries of the MIMO matrices are kept constant for the duration of transmission.  $\mathbf{n}_i$  is AWGN satisfying  $\mathbb{E}[\mathbf{n}_i \mathbf{n}_i^H] = \mathbf{I}_{N_R} \delta[i - i']$ . The SNR  $\rho$  is defined as the total power across all transmitters, while the local noise power at each node per antenna is normalized to unity [17]. The

<sup>1</sup>Throughout this thesis  $\bar{\mathbf{v}}$  denotes the projection of a signal  $\mathbf{v}$  onto a subspace of the received signal space.

multiplexing gain in the  $K$ -user MIMO-IC using orthogonal resource sharing can be calculated as follows

$$\begin{aligned}
 d_{\text{orth}} &= \lim_{\rho \rightarrow \infty} \frac{R_{\Sigma}(\rho)}{\log_2(\rho)} = \lim_{\rho \rightarrow \infty} \frac{\sum_{i=1}^K \frac{1}{K} \sum_{l=1}^{N^{\min}} \log_2 \left( 1 + \frac{\rho}{N^{\min}} \sigma_{il}^2 \right)}{\log_2(\rho)} \\
 &= \lim_{\rho \rightarrow \infty} \frac{\frac{1}{K} \sum_{i=1}^K N^{\min} \log_2(\rho) + \frac{1}{K} \sum_{i=1}^K \sum_{l=1}^{N^{\min}} \log_2 \left( \frac{\sigma_{il}^2}{N^{\min}} \right)}{\log_2(\rho)} \\
 &= \frac{1}{K} \sum_{i=1}^K N^{\min} = N^{\min}, \tag{3.14}
 \end{aligned}$$

with  $\sigma_{il}^2$  the strength the  $l$ -th eigenmode of  $\mathbf{H}_{ii}$  and  $R_{\Sigma}(\rho)$  the sum-rate in the network. Here, waterfilling is performed independently in non-interfering channels isolated in the time or frequency domain with uniform power on all eigenmodes and total power  $\rho$  per user. For the 3-user IC over a constant  $M \times M$  MIMO channel ( $N_T = N_R = M$ ) it is shown in [17] that the sum-capacity can be written as

$$C_{\Sigma}(\rho) = \frac{3M}{2} \log_2(1 + \rho) + o(\log_2(\rho)) \text{ bit/channel-use.} \tag{3.15}$$

Hence,  $d_{\mathbf{H}} = 3M/2 > d_{\text{orth}} = M$  and every user gets  $d_i = M/2$  interference-free signaling dimensions per channel use, i.e. half the number of degrees of freedom of the corresponding isolated MIMO channel. Achievability of above result is based on MIMO IA. The considered signal space for alignment is comprised of the spatial dimensions between multiple transmit and receive antennas. Furthermore, a constructive method for finding the precoders is presented in [17].

In the case of multiple antennas, the transmitted  $N_T \times 1$  symbols  $[\underline{\mathbf{x}}_i]_{i=1,\dots,K}$  over the constant MIMO channel can be written as

$$\underline{\mathbf{x}}_i = \sum_{l=1}^{d_i} \underline{\mathbf{v}}_l s_{il} = \mathbf{V}_i \underline{\mathbf{s}}_i, \tag{3.16}$$

with independent symbol streams  $[s_{il}]_{l=1,\dots,d_i}$  and their associated beamforming vectors  $[\underline{\mathbf{v}}_{il}]_{l=1,\dots,d_i}$ ,  $\underline{\mathbf{s}}_i = [s_{i1}, \dots, s_{id_i}]$  and  $\mathbf{V}_i = [\underline{\mathbf{v}}_{i1}, \dots, \underline{\mathbf{v}}_{id_i}]$ . (3.16) can be interpreted as low rank precoding of  $d_i$  symbol streams  $\underline{\mathbf{s}}_i$  over  $N_T^{[i]}$  signal space dimensions. The MIMO channel matrices, i.e. the linear transformation, linking input to output (neglecting the receiver noise) are fully populated.

The MIMO setting reveals a different behavior with respect to minimum dimension for finding an alignment solution compared to the SISO case. Alignment is achieved without symbol extensions. The maximum achievable multiplexing gain per

user in the absence of interference is  $\min\{N_T, N_R\}$ , see (3.13). *Feasibility conditions* derived in [27], [64] and [31] determine whether it is possible to find an alignment solution almost surely for a  $[(N_T \times N_R, d_i)]_{i=1,\dots,K}$  network under mild conditions on the distribution of the fading process. For feasible network settings, an iterative algorithm [22, Algorithm 1] was introduced to find numerically the precoding matrices achieving interference alignment. At every iteration, the algorithm from [22] involves the computation of  $K$  eigenvalue problems. Depending on the interference channel setting the convergence speed can vary significantly. An alignment algorithm based on alternating optimization of a similar interference leakage metric was introduced in [25]. In [26], the optimization metrics of iterative algorithms are modified in order to account for colored noise at the receivers or to jointly optimize transmit precoders and specified receive spatial filters, e.g. joint MMSE design. A distributed algorithm for adjusting beamformers in MIMO networks with single-stream transmission per user is developed in [24]. It is shown that at high SNR the algorithm achieves alignment whereas at medium and low SNR the algorithm outperforms alignment-based precoding.

In general, explicit solutions are not known in many cases even when interference alignment solutions are known to be feasible. For certain  $K$ -user MIMO-IC settings, constructive methods could be found. For the  $(M \times M, M/2)^3$  IC configuration, with  $N_T = N_R = M$ , a closed-form solution for the alignment problem is presented in [17] as well as for the  $(4 \times 8, 3)(4 \times 8, 2)^3$  IC [30], the  $(2 \times 3, 1)^2(3 \times 2, 1)^2$  and the  $(2 \times 3, 1)^4$  IC in [28].

MIMO channels with time-varying channel coefficients are considered in [30], an inner bound and an outer bound on the total number of degrees of freedom for the MIMO case are presented. Extending alignment-based interference suppression schemes to larger networks, [45] applies interference alignment to large scale Gaussian interference networks and derives bound on the sum-capacity. However, fading effects were omitted from the analysis in [45].

The evaluation of the sum-rate (or of the mutual information) achieved by IA using measured channels is performed in [70]. The experimental study shows that IA achieves the sum-rate scaling linearly with the number of users in a variety of indoor and outdoor measurement scenarios. The interference alignment solutions are calculated off-line using the measured MIMO-OFDM channels.

### 3.4 Linear Algebra Background

The basis of interference alignment in signal space dimensions is *linear algebra*. In the following, we review a selection of linear algebra concepts in order to illustrate

subspace-based interference alignment.

Let us consider a generic input/output relation without incorporating receiver noise, i.e. we focus on receiver  $i$  in Fig. 3.1 and observe  $N_e$  signal space dimension that are the result of a transmission of  $N_v$  input symbols  $s_1, s_2, \dots, s_{N_v}$  over a channel that is represented by a linear transformation. The receive signal writes

$$\underline{\mathbf{y}}_i = \underline{\mathbf{v}}_1 s_1 + \underline{\mathbf{v}}_2 s_2 + \dots + \underline{\mathbf{v}}_{N_v} s_{N_v}. \quad (3.17)$$

The observation  $\underline{\mathbf{y}} = [y_1, y_2, \dots, y_{N_e}]^T$  is a linear combination of the  $N_v$  vectors  $\underline{\mathbf{v}}_1, \underline{\mathbf{v}}_2, \dots, \underline{\mathbf{v}}_{N_v} \in \mathbb{C}^{N_e}$  in the observed signal space. The vectors are *linearly independent* if and only if for  $\mu_l \in \mathbb{C}$

$$\sum_{l=1}^{N_v} \mu_l \underline{\mathbf{v}}_l = \underline{\mathbf{0}} \Rightarrow \mu_l = 0, l \in \{1, \dots, N_v\}. \quad (3.18)$$

The vectors  $\underline{\mathbf{v}}_1, \underline{\mathbf{v}}_2, \dots, \underline{\mathbf{v}}_{N_v}$  span a *vector-subspace*, i.e.

$$\mathcal{S}(\underline{\mathbf{v}}_1, \underline{\mathbf{v}}_2, \dots, \underline{\mathbf{v}}_{N_v}) = \left\{ \underline{\mathbf{v}} \text{ s. t. } \underline{\mathbf{v}} = \sum_{l=1}^{N_v} \mu_l \underline{\mathbf{v}}_l \text{ and } \mu_l \in \mathbb{C} \right\}. \quad (3.19)$$

The *dimension* of  $\mathcal{S}(\underline{\mathbf{v}}_1, \underline{\mathbf{v}}_2, \dots, \underline{\mathbf{v}}_{N_v})$  is the minimum number of independent vectors required to span the vector-subspace or the maximum number of linearly independent vectors in  $\{\underline{\mathbf{v}}_1, \underline{\mathbf{v}}_2, \dots, \underline{\mathbf{v}}_{N_v}\}$ .

We revisit the input/output relation (3.17) with the aim to recover *all* the symbols  $s_1, s_2, \dots, s_{N_v}$  from the observations. Clearly, if  $N_e < N_v$  then we cannot solve the system of linear equations for all variables, i.e. the system is over-determined. On the other hand, if  $N_e \geq N_v$  then (in general) it is possible to retrieve the transmitted symbols.

Let us now focus our attention on the case where we have more symbols than observations, i.e.  $N_e < N_v$  as we will encounter in the  $K$ -user IC. We have argued that all symbols cannot be recovered from the observations. Interestingly, our chances of success change if we try to recover only a *subset* of symbols from the observations. Henceforth, we denote as  $S = \{1, \dots, N_v\}$  the set of indices of the symbols and the subset  $S_i \subset S$  containing the indices of the symbols of interest for user  $i$ . The subsets  $[S_i]_{i=1, \dots, K}$  partition the set of indices, i.e.  $\bigcup S_i = S$ . The linear transformation (3.17) can be written in vector notation as

$$\begin{aligned} \underline{\mathbf{y}}_i &= \underline{\mathbf{v}}_1 s_1 + \underline{\mathbf{v}}_2 s_2 + \dots + \underline{\mathbf{v}}_{N_v} s_{N_v} \\ &= \sum_{l \in S_i} \underline{\mathbf{v}}_l s_l + \sum_{l' \in (S \setminus S_i)} \underline{\mathbf{v}}_{l'} s_{l'}, \end{aligned} \quad (3.20)$$

where  $\underline{\mathbf{v}}_l$  can be interpreted as the *receive direction* over which the symbol  $s_l$  is observed. The second line in (3.20) partitions the signal of interest for user  $i$  and the unintended signals, i.e. the interference.

*Theorem 1.* The *interference alignment condition* for a particular user in a multi-user IC reads as follows. Given the input/output relation (3.17) with  $N_e < N_v$ , a user  $i$  can retrieve symbols with indices  $S_i$  out of  $N_v$  transmitted symbols observed over  $N_e$  signal space dimensions if and only if

$$\begin{aligned} & [\underline{\mathbf{v}}_l]_{l \in S_i} \notin \mathcal{S}([\underline{\mathbf{v}}_{l'}]_{l' \in (S \setminus S_i)}) \\ \dim(\mathcal{S}([\underline{\mathbf{v}}_l]_{l \in S_i})) &= |S_i|, \end{aligned} \quad (3.21)$$

with  $|S_i|$  the dimension of the space spanned by the intended signal.

*Proof.* Let us denote  $D_I = \dim(\mathcal{S}([\underline{\mathbf{v}}_{l'}]_{l' \in (S \setminus S_i)}))$  the dimension of the subspace spanned by the interference and  $[\underline{\mathbf{v}}'_j]_{j=1, \dots, D_I}$  a basis of this subspace. The linear transformation (3.20) can be written as

$$\begin{aligned} \underline{\mathbf{y}}_i &= \sum_{l \in S_i} \underline{\mathbf{v}}_l s_l + \sum_{j'=1}^{D_I} \underline{\mathbf{v}}'_j s'_{j'}, = \underbrace{[[\underline{\mathbf{v}}_l]_{l \in S_i}, [\underline{\mathbf{v}}'_j]_{j=1, \dots, D_I}]}_{\Upsilon} \underbrace{[[s_l]_{l \in S_i}, [s'_{j'}]_{j=1, \dots, D_I}]}_{\mathbf{s}}^T \\ &= \Upsilon \mathbf{s}. \end{aligned} \quad (3.22)$$

with dummy interference symbols  $[s'_{j'}]_{j=1, \dots, D_I}$ .  $[s_l]_{l \in S_i}$  are the first  $|S_i|$  symbols of  $\Upsilon^{-1} \underline{\mathbf{y}}_i$ .  $\square$

The dimension of the subspace spanned by the unintended signals fulfills

$$\dim(\mathcal{S}([\underline{\mathbf{v}}_{l'}]_{l' \in (S \setminus S_i)})) \leq N_v - |S_i|. \quad (3.23)$$

For example, user 1 can retrieve symbol  $s_1$  ( $S_1 = \{1\}$ ) if and only if

$$\underline{\mathbf{v}}_1 \notin \mathcal{S}(\underline{\mathbf{v}}_2, \underline{\mathbf{v}}_3, \dots, \underline{\mathbf{v}}_{N_v}). \quad (3.24)$$

The dimension of the space spanned by the interference fulfills  $\dim(\mathcal{S}(\underline{\mathbf{v}}_2, \underline{\mathbf{v}}_3, \dots, \underline{\mathbf{v}}_{N_v})) \leq N_e - 1$ . If  $N_e = 2$  then the  $N_v - 1$  unintended signals must align along a one dimensional subspace. Given condition (3.24), we can solve (3.20) for a scaled version of  $s_1$  by projecting  $\underline{\mathbf{y}}_1$  into the *null space* of  $\mathcal{S}(\underline{\mathbf{v}}_2, \underline{\mathbf{v}}_3, \dots, \underline{\mathbf{v}}_{N_v})$ . Note that any independent choice of the  $\underline{\mathbf{v}}_i$ 's spans the whole signal space, i.e.  $\dim(\mathcal{S}(\underline{\mathbf{v}}_2, \underline{\mathbf{v}}_3, \dots, \underline{\mathbf{v}}_{N_v})) = N_e$ .

### 3.4.1 SISO and MIMO Interference Alignment Conditions

The generic input/output relation (3.17) for users  $i = 1, \dots, K$  can represent the  $K$ -user SISO- and the MIMO-IC case. The alignment condition (3.21) can be particularized to both cases. Henceforth, we group the symbols associated with users as follows. A vector  $\underline{\mathbf{s}}_i = [s_{i1}, s_{i2}, \dots, s_{ib_i}]^T$  indicates that user  $i$  transmits  $b_i$  symbols, whereas a scalar  $s_i$  indicates that user  $i$  is transmitting only one symbol. Hence, the set of indices for user  $i$  is  $S_i = \{i1, \dots, ib_i\}$  or  $S_i = \{i\}$ . Every symbol is precoded with a corresponding precoding vector, i.e. along a *transmit beamforming direction*. A matrix  $\mathbf{V}_i = [\underline{\mathbf{v}}_{i1}, \underline{\mathbf{v}}_{i2}, \dots, \underline{\mathbf{v}}_{ib_i}]$  includes precoding vectors for  $b_i$  symbols, whereas  $\underline{\mathbf{v}}_i = \underline{\mathbf{v}}_{i1}$  denotes the precoder for one symbol  $s_i$ . The receive signal of user  $i$  observed over  $N_e$  signal space dimensions (3.17) and (3.20) can be written as

$$\underline{\mathbf{y}}_i = \sum_{l \in S_i} \underbrace{\mathbf{H}_{il} \underline{\mathbf{v}}_l}_{\underline{\mathbf{v}}_l} s_l + \sum_{j \neq i} \sum_{l' \in S_j} \underbrace{\mathbf{H}_{ij} \underline{\mathbf{v}}_{l'}}_{\underline{\mathbf{v}}_{l'}} s_{l'}, \quad (3.25)$$

where for the  $K$ -user SISO-IC  $N_e = N_S$ ,  $\underline{\mathbf{y}}_i = [y_i[1], \dots, y_i[N_S]]^T$  and  $|S| = |\bigcup S_i| = N_v = \sum_i d_i N_S$ , with  $\sum_i d_i$  the sum multiplexing gain of the network. Furthermore,  $\mathbf{H}_{ij} = \text{diag}\{h_{ij}[1], h_{ij}[2], \dots, h_{ij}[N_S]\}$  is the extended channel with  $h_{ij}[\cdot]$  the time/frequency-varying channel coefficients from transmitter  $j$  to receiver  $i$ .  $\underline{\mathbf{v}}_l$  is the  $N_S \times 1$  precoding vector. For the  $K$ -user MIMO-IC in (3.25)  $N_e = N_R$ ,  $\underline{\mathbf{y}}_i = [y_{i1}, \dots, y_{iN_R}]^T$  and  $|S| = |\bigcup S_i| = N_v = \sum_i d_i$ .  $\mathbf{H}_{ij}$  is the  $N_R \times N_T$  MIMO matrix with  $[\mathbf{H}_{ij}]_{(n_r, n_t)} = h_{ij}(n_r, n_t)$  the channel gain from transmit antenna  $n_t$  of user  $j$  to receive antenna  $n_r$  of user  $i$ .  $\underline{\mathbf{v}}_l$  is the  $N_T \times 1$  precoding vector. Note that the *receive direction*  $\underline{\mathbf{v}}_l$  (3.25) of symbol  $s_l$  is determined by the channel matrix in conjunction with the precoder. Table 3.1 summarizes the parameters of a SISO and MIMO  $K$ -user IC.

|                       | $N_v$ (3.17)     | $N_e$ (3.17) | $\dim(\mathbf{H}_{ij})$ | $\dim(\underline{\mathbf{v}}_l)$ | $b_i$     |
|-----------------------|------------------|--------------|-------------------------|----------------------------------|-----------|
| Extended SISO channel | $\sum_i d_i N_S$ | $N_S$        | $N_S \times N_S$        | $N_S \times 1$                   | $d_i N_S$ |
| Constant MIMO channel | $\sum_i d_i$     | $N_R$        | $N_R \times N_T$        | $N_T \times 1$                   | $d_i$     |

Table 3.1: Parameter set of the SISO and MIMO  $K$ -user IC.

The interference alignment condition (3.21) has to be fulfilled for all users  $i = 1, \dots, K$  simultaneously. The coupled nature of the alignment problem reveals itself from the fact that the precoder  $\underline{\mathbf{v}}_l$  of symbol  $s_l$  at transmitter  $j$  determines receive directions  $[\underline{\mathbf{v}}_i]_{i=1, \dots, K} = [\mathbf{H}_{ij} \underline{\mathbf{v}}_l]_{i=1, \dots, K}$  for this symbol at all receivers. Hence,  $b_i$  symbols per transmitter receiver pair can be recovered without interference in a



$K$ -user SISO- or MIMO-IC if and only if for all users  $i = 1, \dots, K$

$$\begin{aligned} [\mathbf{H}_{ii}\mathbf{v}_l]_{l \in S_i} &\notin \mathcal{S}([\mathbf{H}_{ij}\mathbf{v}_{l'}]_{j \neq i, l' \in S_j}) \\ \dim(\mathcal{S}([\mathbf{H}_{ii}\mathbf{v}_l]_{l \in S_i})) &= |S_i| = b_i, \end{aligned} \quad (3.26)$$

with  $b_i$  the dimension of the subspace spanned by the intended signal. The dimensions of the subspaces spanned by the unintended signal fulfill

$$\dim(\mathcal{S}([\mathbf{H}_{ij}\mathbf{v}_{l'}]_{j \neq i, l' \in S_j})) \leq N_e - b_i. \quad (3.27)$$

The receive directions of symbols over a shared signal space are chosen, such that a subset of all transmitted symbols can be retrieved at those receivers where they are desired. Accordingly, a coupled system of linear equations (3.17) for  $i = 1, \dots, K$  is structured though alignment such that  $N_v$  symbols can be simultaneously decoded at the intended receivers without joint signal processing. The solution to the interference alignment problem is non-unique. In general, there exist multiple sets of precoders  $[\mathbf{v}_l]_{l=1, \dots, N_v}$  for which the alignment condition (3.26) can be fulfilled, as will be outlined in Section 4.3. The following two examples illustrate interference alignment.

**Example 1:** Let us consider the  $K = 3$  user SISO-IC over the  $N_e = N_s = 3$  dimensional extended channel (without receiver noise), see Fig. 3.5. In order to find an alignment solution  $\sum_i d_i = N_v/N_s = 4/3$  with  $d_1 = 2/N_s = 2/3$  and  $d_2 = d_3 = 1/N_s = 1/3$ . The users transmit  $N_v = 4$  symbols  $s_{11}, s_{12}, s_2$  and  $s_3$ , i.e. the indices set is  $S = \{11, 12, 2, 3\}$ . The input/output relation (3.25) is

$$\underline{\mathbf{y}}_i = \mathbf{H}_{i1}\mathbf{V}_1\underline{\mathbf{s}}_1 + \mathbf{H}_{i2}\mathbf{v}_2s_2 + \mathbf{H}_{i3}\mathbf{v}_3s_3, \quad (3.28)$$

with  $\mathbf{V}_1 = [\mathbf{v}_{11}, \mathbf{v}_{12}]$  and  $\underline{\mathbf{s}}_1 = [s_{11}, s_{12}]^T$ . The interference alignment conditions are

$$\begin{aligned} \text{for user 1: } &\mathbf{H}_{11}\mathbf{v}_{11}, \mathbf{H}_{11}\mathbf{v}_{12} \notin \mathcal{S}(\mathbf{H}_{12}\mathbf{v}_2, \mathbf{H}_{13}\mathbf{v}_3) \\ &\dim(\mathcal{S}(\mathbf{H}_{11}\mathbf{v}_{11}, \mathbf{H}_{11}\mathbf{v}_{12})) = 2 \\ \text{for user 2: } &\mathbf{H}_{22}\mathbf{v}_2 \notin \mathcal{S}(\mathbf{H}_{21}\mathbf{v}_{11}, \mathbf{H}_{21}\mathbf{v}_{12}, \mathbf{H}_{23}\mathbf{v}_3) \\ &\dim(\mathcal{S}(\mathbf{H}_{22}\mathbf{v}_2)) = 1 \\ \text{for user 3: } &\mathbf{H}_{33}\mathbf{v}_3 \notin \mathcal{S}(\mathbf{H}_{31}\mathbf{v}_{11}, \mathbf{H}_{31}\mathbf{v}_{12}, \mathbf{H}_{32}\mathbf{v}_2) \\ &\dim(\mathcal{S}(\mathbf{H}_{33}\mathbf{v}_3)) = 1. \end{aligned} \quad (3.29)$$

Fig. 3.5 shows an alignment solution for the  $(3 : (2/3)(1/3)^2)$  network. The figure shows beamforming of encoded symbols in the transmit signal space

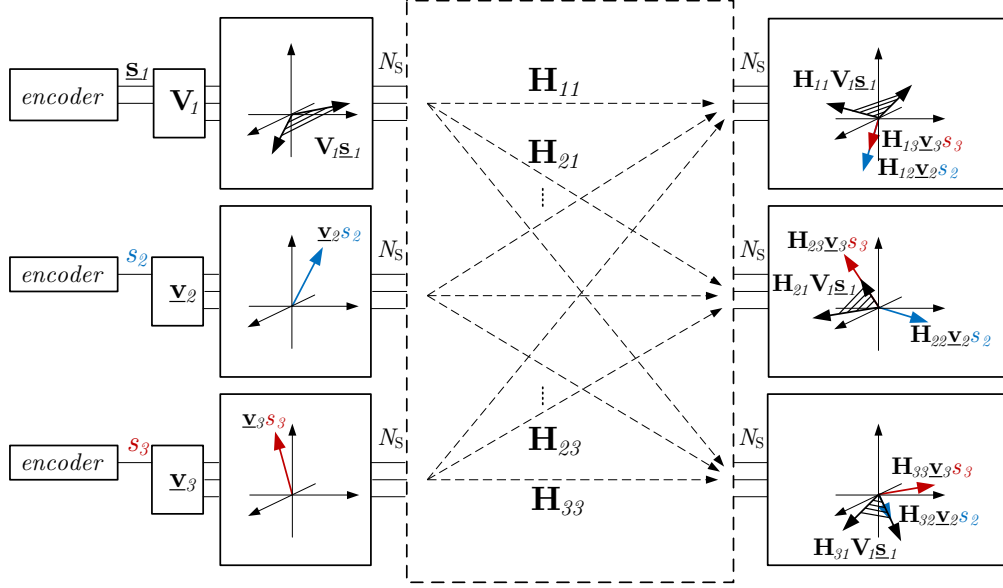


Figure 3.5: Interference alignment solution for the  $K = 3$ -user SISO-IC with  $(d_1, d_2, d_3) = (2/3, 1/3, 1/3)$ .

on the left-hand side (LHS) and the receive signal space on the right-hand side (RHS) depicting all involved signals as arrows. The interfering signals  $\mathbf{H}_{12}\mathbf{v}_2s_2$ ,  $\mathbf{H}_{13}\mathbf{v}_3s_3$  at receiver 1 are aligned along a one dimensional subspace of the receive signal space (depicted by the red and blue arrows in Fig. 3.5). The intended symbols  $\mathbf{s}_1$  span a 2-dimensional subspace and can be retrieved according to Theorem 1 as follows:

$$\mathbf{s}_1 = [(\mathbf{H}_{11}\mathbf{V}_1, \mathbf{H}_{12}\mathbf{v}_2)^{-1}\mathbf{y}_1]_{(1:2,1)}. \quad (3.30)$$

The interfering signals  $\mathbf{H}_{i1}\mathbf{V}_1\mathbf{s}_1$ ,  $\mathbf{H}_{ij}\mathbf{v}_js_j$  at receiver  $i = 2, 3$  and  $j \neq i \in \{2, 3\}$  are aligned along a two dimensional subspace of the receive signal space (depicted by the black and red arrows at receiver 2 and the black and blue at receiver 3, respectively, in Fig. 3.5). The intended symbol  $s_i$  can be retrieved as follows

$$s_i = [(\mathbf{H}_{ii}\mathbf{v}_i, \mathbf{H}_{i1}\mathbf{V}_1)^{-1}\mathbf{y}_i]_{(1,1)}. \quad (3.31)$$

**Example 2:** The  $K = 3$  user ( $N_A = N_T = N_R$ )  $2 \times 2$  MIMO-IC (without receiver noise) is depicted in Fig. 3.6. The DoF are  $d_{\mathbf{H}} = N_v = 3$  leading to  $d_1 = d_2 = d_3 = 1$ . Hence, the users transmit  $N_v = 3$  symbols  $s_1, s_2$  and  $s_3$ , i.e. the indices

set is  $S = \{1, 2, 3\}$ . The input/output relation (3.25) writes

$$\underline{\mathbf{y}}_i = \mathbf{H}_{i1}\underline{\mathbf{v}}_1s_1 + \mathbf{H}_{i2}\underline{\mathbf{v}}_2s_2 + \mathbf{H}_{i3}\underline{\mathbf{v}}_3s_3. \quad (3.32)$$

The interference alignment conditions are

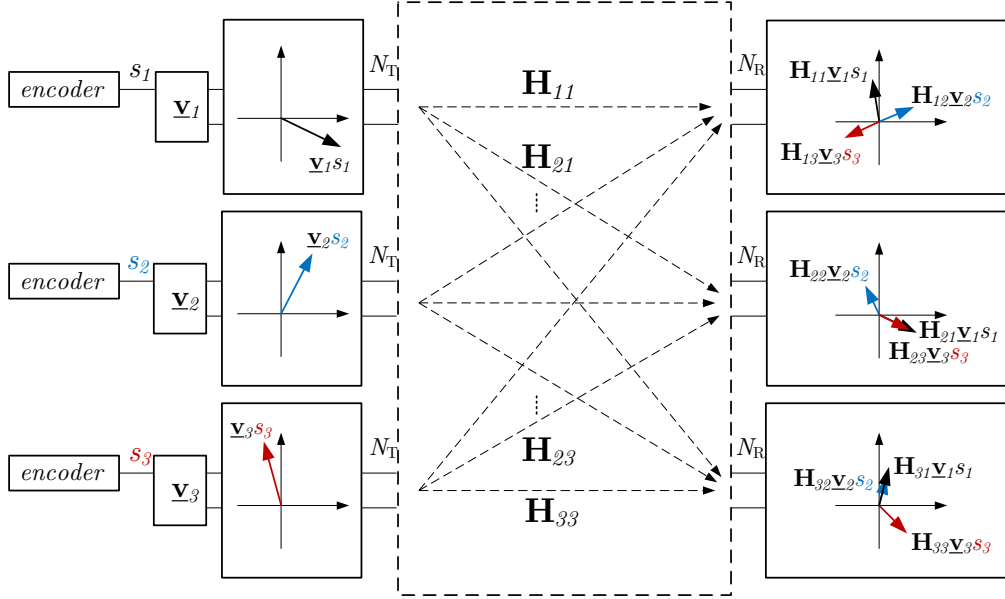


Figure 3.6: Interference alignment solution for the  $K = 3$  user  $2 \times 2$  MIMO-IC with  $(d_1, d_2, d_3) = (1, 1, 1)$ .

$$\begin{aligned} \text{for } i = 1, 2, 3: \mathbf{H}_{ii}\underline{\mathbf{v}}_i &\notin \mathcal{S}([\mathbf{H}_{ij}\underline{\mathbf{v}}_j]_{j \neq i}) \\ \dim(\mathcal{S}(\mathbf{H}_{ii}\underline{\mathbf{v}}_i)) &= 1. \end{aligned} \quad (3.33)$$

Fig. 3.6 shows an alignment solution for the  $(2 \times 2, 1)^3$  network. The interfering signals  $[\mathbf{H}_{ij}\underline{\mathbf{v}}_j]_{j \neq i}$  are aligned along a one dimensional subspace of the  $i$ th receive signal space (visualized by the arrows that are collinear, in Fig. 3.6). The intended symbol  $s_i$  can be retrieved as follows

$$s_i = [[\mathbf{H}_{ii}\underline{\mathbf{v}}_i, \mathbf{H}_{ij}\underline{\mathbf{v}}_j]^{-1}\underline{\mathbf{y}}_i]_{(1,1)}. \quad (3.34)$$



## 4 MIMO Interference Alignment

This chapter discusses interference alignment (IA) for the  $K$ -user constant MIMO-IC. Henceforth, we study alignment in the spatial domain between multiple transmit and receive antennas in order to avoid long symbol extensions required in networks with single-antenna terminals. In SISO networks, the reduced symbol rate or sub-carrier spacing if IA is applied in the time or frequency domain prohibits real time implementation in practical systems. We recall the conditions for MIMO-IA from Subsection 3.4.1 and rewrite them as a system of bilinear equations. Interference network settings, where an interference alignment solution is feasible, are characterized in the following. We outline alignment procedures subdivided into iterative and constructive methods. Furthermore, we derive expressions for the achievable ergodic rates with perfect and imperfect channel state information and illustrate them by simulation results.

Results presented in this chapter were first published in [64] and [71].

### 4.1 MIMO Interference Channel

Let us consider the MIMO-IC (see Fig. 4.1) is comprised of  $K$  multiple antenna transmitter-receiver pairs, aiming for conveying independent messages  $[W_i]_{i=1,\dots,K}$  exclusively to their counterpart, i.e. transmitter  $i$  to receiver  $i$ . Transmitter and receiver  $i = 1, \dots, K$  are equipped with  $N_T$  and  $N_R$  antennas, respectively. We assume that the MIMO channel is frequency flat, according to (1.1) introduced in Chapter 1.3. The channel fading coefficients are drawn once and kept constant for the duration of transmission, denoted as *constant MIMO channel* [23]. Throughout this chapter, the pathloss factor in (1.1) is set to  $\gamma_{ij} = 1 \forall i, j$ . We assume that channel knowledge is causal and globally available, i.e. each node knows all coefficients.

In single-user wireless communication, multiple antennas can provide several gains. *Diversity gain* can be achieved which increases the reliability and reduces the error rate of the wireless link. Moreover, *power gain* (also denoted as *array gain*) can be achieved which leads to an increased energy efficiency. Furthermore, an additional spatial dimension between multiple transmit and receive antennas yields *degree-of-freedom gain* (also denoted as *multiplexing gain*, see (3.13)). These

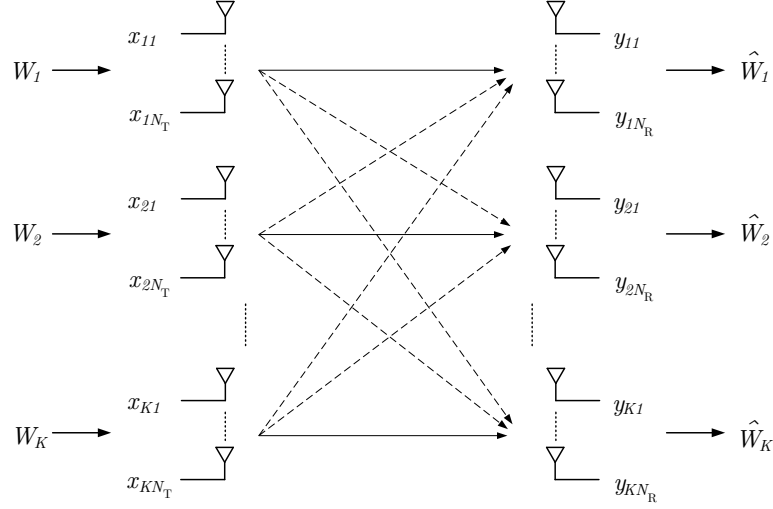


Figure 4.1: The  $K$ -user MIMO-IC where transmitters and receivers are equipped with  $N_T$  and  $N_R$  antennas, respectively.

additional DoF can be exploited by spatially multiplexing several data streams onto the MIMO channel which lead to an increased spectral efficiency. Multi-user wireless communication over a  $K$ -user MIMO-IC yields another advantage. It allows to mitigate interference in the spatial domain, i.e. several data streams from different users can be multiplexed over the  $K$ -user MIMO-IC using interference alignment introduced in Chapter 3.

The fundamental difference between single-user MIMO systems and the MIMO-IC is that the spatial dimensions between multiple transmit and receive antennas have to be shared among the users. Let us focus on the  $i^{\text{th}}$  receiver, which receives interference from other transmitters  $j \neq i$  in addition to its intended signal. The receive signal  $\underline{\mathbf{y}}_i = [y_{i1}, y_{i1}, \dots, y_{iN_R}]^T$  observed over  $N_R$  signal space dimensions (see Fig. 4.1) writes (expression (3.25) plus AWGN)

$$\underline{\mathbf{y}}_i = \mathbf{H}_{ii}\underline{\mathbf{x}}_i + \sum_{j \neq i} \mathbf{H}_{ij}\underline{\mathbf{x}}_j + \underline{\mathbf{n}}_i = \sum_{l \in S_i} \mathbf{H}_{il}\underline{\mathbf{v}}_l s_l + \sum_{j \neq i} \sum_{l' \in S_j} \mathbf{H}_{ij}\underline{\mathbf{v}}_{l'} s_{l'} + \underline{\mathbf{n}}_i, \quad (4.1)$$

where  $\underline{\mathbf{x}}_i = [x_{i1}, x_{i2}, \dots, x_{iN_T}]^T$  is the transmitted signal from user  $i$  with  $\mathbb{E}[\text{Tr}(\underline{\mathbf{x}}_i \underline{\mathbf{x}}_i^H)] \leq \rho_i$ . We use linear beamforming at each transmitter as indicated by the second equality of (4.1).  $s_l \in \mathbb{C}$  is the transmit symbol of stream  $l$  from transmitter  $i$ .  $l \in S_i$  with  $S_i$  the set of indices of the spatial streams of transmitter  $i$ . The multiplexing gain  $d_i$  of user  $i$  is the cardinality of the index set, i.e.  $d_i = |S_i|^1$ .

<sup>1</sup>If all users transmit the same number of streams, we omit the index and refer to  $d = |S_i| \forall i$

$\mathbf{v}_l \in \mathbb{C}^{N_T} \times 1$  is the precoding vector of the  $l^{\text{th}}$  stream.  $\mathbf{n}_i$  is circularly symmetric complex AWGN satisfying  $\mathbb{E}[\mathbf{n}_i \mathbf{n}_i^H] = \mathbf{I}_{N_R} \delta[i - i']$ .

### 4.1.1 Opportunistic Beamforming

Let us consider a  $K$ -user MIMO-IC with  $M = N_T = N_R$  antennas. Allowing all users to exploit the maximum multiplexing gain  $N^{\min}$  of the MIMO link  $\mathbf{H}_{ii}$  using spatial multiplexing outlined in Section 3.3 leads to an over-determined problem at all receivers, i.e. the number of variables  $N_v = KM$  is greater than the number of equations  $N_e = M$ . Due to the lack of cooperation at transmitter and receiver side, single-user decoding performs poorly at high SNR since there exist no linear filter that can suppress the interference and recover the symbols of interest  $S_i$  from the receive signal  $\mathbf{y}_i$ .

Independent transmission of a single stream per user over the *dominant eigenmodes* (EM) of the MIMO links  $[\mathbf{H}_{ii}]_{i=1,\dots,K}$  maximizes the intended signal power at each receiver and achieves array gain [49]. For  $\mathbf{x}_i = \mathbf{v}_i s_i \forall i$ , i.e. beamforming is done with the right singular vector  $\mathbf{v}_i$  corresponding to the strongest singular value of  $\mathbf{H}_{ii}$ . However, if  $K > M$  or equivalently  $N_v > N_e$ , the interfering signals span the whole signal space at each receiver and single-user decoding performs poorly at high SNR.

The multiplexing gain in the  $K$ -user MIMO IC using orthogonal resource sharing has been calculated in Section 3.3. The sum-rate multiplexing gain at high SNR according to (3.14) is  $d_{\text{orth}} = N^{\min} = \min\{N_T, N_R\}$ .

## 4.2 Alignment-Based Interference Management

The aforementioned precoding schemes that exploit multiplexing gain and array gain independently per user as well as orthogonal resource sharing achieve network multiplexing gains that do not scale with the number of users  $K$  in the network. We now introduce an alignment-based (altruistic) precoding scheme. In the following, we recall the criteria for achieving a multiplexing gain in a  $K$ -user MIMO-IC introduced in Subsection 3.4.1, i.e. the conditions for data transmission along "parallel pipes" in the spatial domain of the  $K$ -user MIMO-IC. We extend the criteria of IA enabling *receive diversity* inside the interference-free subspace, especially beneficial when the SNR is not asymptotically high.

Let us consider a generic  $K$ -user  $N_T \times N_R$  MIMO-IC. We build on the condition (3.26) for interference alignment and specify them for the  $K$ -user MIMO-IC. Hence, a network multiplexing gain  $d_{\mathbf{H}} = \sum_i d_i$  can be achieved, i.e.  $\mathbf{s}_i = [s_{i1}, \dots, s_{id_i}]^T$  spatial

streams per user can be transmitted over the IC, if and only if for all  $i = 1, \dots, K$ ,

$$\begin{aligned} [\mathbf{H}_{ii}\mathbf{v}_l]_{l \in S_i} &\notin \mathcal{S}([\mathbf{H}_{ij}\mathbf{v}_{l'}]_{j \neq i, l' \in S_j}), \\ \dim(\mathcal{S}([\mathbf{H}_{ii}\mathbf{v}_l]_{l \in S_i})) &= d_i. \end{aligned} \quad (4.2)$$

With interference alignment, the dimension of the subspace spanned by the interfering signals fulfills

$$\dim(\mathcal{S}([\mathbf{H}_{ij}\mathbf{v}_{l'}]_{j \neq i, l' \in S_j})) \leq N_R - d_i. \quad (4.3)$$

In the following we rewrite the condition (4.2) as a system of bilinear equations, following [22]. Thereby, we distinguish two cases. Firstly, the general case where the receiver exploits spatial diversity (diversity gain) inside the interference-free subspace created by IA, i.e. the codimension of the interference subspace at receiver  $i$  is larger than  $d_i$  and (4.3) is fulfilled with inequality. Secondly, the case where the codimension of the interference space at the receive is equal to the multiplexing gain per user, i.e. (4.3) is fulfilled with equality.

Interference alignment in a MIMO-IC is achieved with multiplexing gain allocation  $(d_1, \dots, d_K)$  if and only if there exists  $N_T \times d_i$  truncated unitary matrices (precoding matrices)  $\mathbf{V}_i = [\mathbf{v}_{i1}, \dots, \mathbf{v}_{id_i}]$  and  $N_R \times d'_i$  truncated unitary matrices (interference suppression matrices)  $\mathbf{U}_i = [\mathbf{u}_{i1}, \dots, \mathbf{u}_{id'_i}]$  such that, for  $i = 1, \dots, K$ ,

$$\mathbf{U}_i^H \mathbf{H}_{ij} \mathbf{V}_j = \mathbf{O}_{d'_i \times d_j}, \forall j \neq i, \quad \text{and} \quad (4.4)$$

$$\text{rank}(\mathbf{U}_i^H \mathbf{H}_{ii} \mathbf{V}_i) = d_i. \quad (4.5)$$

Criteria (4.4) accounts for the alignment of all interference in a subspace of codimension  $d'_i$  at receiver  $i$ , whereas criteria (4.5) accounts for an interference-free subspace of rank  $d_i$  for the intended transmission. Note that the precoders are independent of the direct links between transmitter-receiver pairs, since  $[\mathbf{H}_{ii}]_{i=1, \dots, K}$  are not part of the condition (4.4). This fact reveals the altruistic nature of IA.

If  $d_i \neq d'_i$ , we specify this case as the  $[(N_T \times N_R, d_i, d'_i)]_{i=1, \dots, K}$ -IC permitting for extra receive diversity, where criterion (4.3) is fulfilled with inequality. The interference-free equivalent channel in (4.5) is  $\mathbf{U}_i^H \mathbf{H}_{ii} \mathbf{V}_i \in \mathbb{C}^{d'_i \times d_i}$  is tall and permits to increase the available receive diversity. Henceforth, the  $[(N_T \times N_R, d_i)]_{i=1, \dots, K}$ -IC indicates the network configuration where we pursue exclusively DoF gains at the receivers, i.e.  $d'_i = d_i$ . Here, criterion (4.3) is fulfilled with equality and the interference-free equivalent channel  $\mathbf{U}_i^H \mathbf{H}_{ii} \mathbf{V}_i \in \mathbb{C}^{d_i \times d_i}$  is square. Clearly, both the  $\mathbf{U}_i$ 's and  $\mathbf{V}_i$ 's are unknowns in the IA criteria (4.4) and (4.5). Therefore, the problem of finding an IA solution is non-linear.



### 4.2.1 Feasibility Conditions

In this subsection, we introduce feasibility conditions that specify the existence of a IA solution in a  $(N_T \times N_R, d, d')^K$ -IC. All users have uniform multiplexing and diversity gain allocation. The feasibility conditions are derived by comparing the total number of equations  $N_e$  to the overall number of variables  $N_v$  in the MIMO-IC. In [64], we derived a conjecture on the feasibility of IA over the  $(N_T \times N_R, 1)^K$ -IC, which was generalized in [27] for a network with arbitrary (non-uniform) multiplexing gain allocation. For clarity, we restrict to the case of uniform multiplexing/diversity gain allocations that are henceforth used in this manuscript. In [31], the feasibility conditions were extended to account for receive diversity.

*Theorem 2* (Feasibility conditions). IA with uniform multiplexing/diversity gain allocation per user over the MIMO-IC whose channel coefficients are drawn i.i.d. from a continuous distribution is *feasible* if and only if  $N_v \geq N_e$  which is equivalent to

$$d(N_T - d) + d'(N_R - d') - dd'(K - 1) \geq 0, \quad (4.6)$$

for a network configuration with receive diversity  $(N_T \times N_R, d, d')^K$  and  $N_v \geq N_e$  is equivalent to

$$N_T + N_R - (K + 1)d \geq 0, \quad (4.7)$$







for a network setting aiming exclusively for multiplexing gains at each receiver  $(N_T \times N_R, d)^K$ .

*Proof.* The proof can be found in [27, 28, 31]. The authors introduce the notion of a proper system and argue that proper systems admit a solution to the IA problem almost surely, albeit providing a formal proof of the claim only for single-beam transmission. Nevertheless, this criterion has been found experimentally to be reliable for the multi-beam case as well, and we will therefore rely on it in the sequel.  $\square$

It was noted in [31] that the feasibility condition (4.6) establishes a multi-user *diversity-multiplexing tradeoff* (DMT) applicable to the interference channel, in a way reminiscent of the result in [72]. If IA is feasible, the users enjoy multiplexing gain  $d$  and receive diversity  $d' - d + 1$ . (4.6) governs how the channel DoF can be traded-off between diversity, multiplexing and between users.

In Table 4.1, examples of  $K$ -user MIMO-IC configurations with feasible IA solutions are given. The achievable multiplexing gain per user with respect to the corresponding isolated single-user channel is depicted in the last column. Furthermore, the existence of a non-iterative constructive method for the IA precoders is

listed in the fourth column. Those methods will be discussed in Subsection 4.3.2. The first example is the  $(3 \times 3, 1)^4$ -IC. The corresponding feasibility condition (4.7) is fulfilled with inequality, hence a better scaling of the sum multiplexing gain is possible with a different gain allocation. However, for this configuration a closed form IA solution is given in [64] and will be outlined in Subsection 4.3.2. The second example is the  $(4 \times 4, 2)^3$ -IC, for which the condition (4.7) is fulfilled with equality and a closed form IA solution is given in [17]. Every user in this IC achieves half the multiplexing gain as in the corresponding single-user channel visualized by half the cake. The third row lists the  $(4 \times 2, 1)^5$ -IC, which fulfills condition (4.7) with equality and every user gets half the cake. A closed-form IA solution for this network is yet an open problem.

|     | $K$ | $N_T$ | $N_R$ | $d$ | $d'$ | feasibility condition | constructive method     | mux gain per user   |
|-----|-----|-------|-------|-----|------|-----------------------|-------------------------|---|
| (♣) | 4   | 3     | 3     | 1   | 1    | (4.7)✓                | [64] $K = M + 1, d = 1$ |    |
| (♣) | 3   | 4     | 4     | 2   | 2    | (4.7)✓                | [17] $K = 3, d = M/2$   |    |
|     | 5   | 4     | 2     | 1   | 1    | (4.7)✓                | not known               |    |
|     | 3   | 5     | 3     | 2   | 2    | (4.7)✓                | not known               |  |
| (♠) | 4   | 5     | 3     | 1   | 2    | (4.6)✓                | not known               |  |
|     | 7   | 5     | 3     | 1   | 1    | (4.7)✓                | not known               |  |

(♣) symmetric MIMO  $N_T = N_R = M$

(♠) receive diversity  $d' - d + 1$


  $N^{\min} = \min\{N_T, N_R\}$

Table 4.1: A selection of  $K$ -user MIMO-ICs with feasible IA solutions along with the existence of a constructive method for finding a IA solution.

The multi-user DMT is illustrated in last three rows of Table 4.1 and illustrated in Fig. 4.2 for a network with  $N_T = 5$  and  $N_R = 3$  antennas. Depending on the multiplexing/diversity gain allocation, a different number of users can be accommodated in the network according to feasibility condition (4.6). The cases are listed in Table 4.1. For all settings, (4.6) is fulfilled with equality. Figure 4.2(a) shows the signal space of receiver  $i$  of the  $(5 \times 3, 1, 2)^4$ -IC. The interference from  $K - 1 = 3$  transmitters is aligned along a one-dimensional subspace. The signal of interest is not collinear to the interference. Figure 4.2(b) shows the signal space of receiver  $i$  of the  $(5 \times 3, 1)^7$ -IC. The interference from  $K - 1 = 6$  transmitters is aligned in a two-dimensional subspace. The signal of interest is not collinear to the interference subspace.

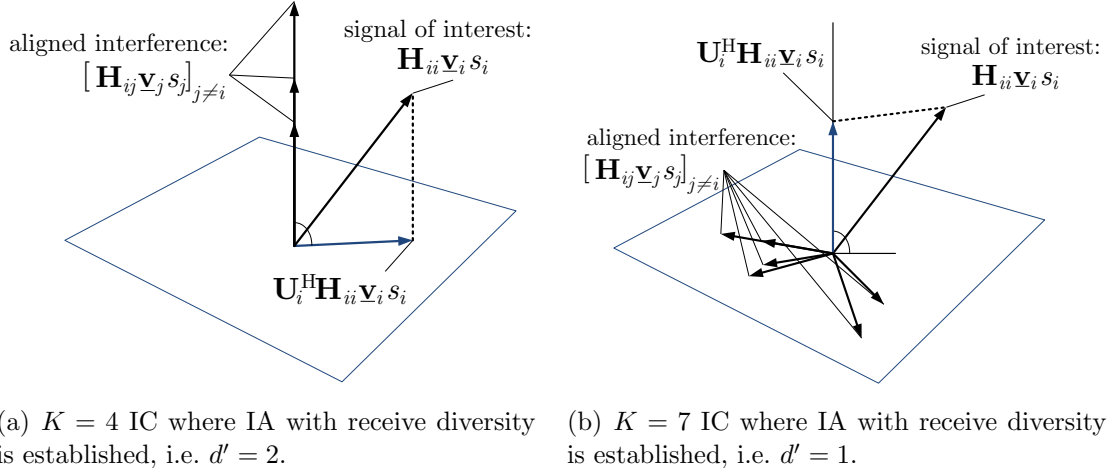


Figure 4.2: Receive signal space of MIMO-IC with receive diversity (LHS,  $K=4$ ) and without receive diversity (RHS,  $K=7$ ) for a fixed antenna configuration, i.e.  $N_T = 5$  and  $N_R = 3$ .

### 4.2.2 Projection Receiver

Let us now assume a  $(N_T \times N_R, d, d')$ -IC where IA is feasible, i.e. there exist precoding matrices  $\mathbf{V}_i$ 's and interference suppression matrices  $\mathbf{U}_i$ 's that fulfill the IA criteria (4.4) and (4.5).

We define the projection receiver as the projection of the receive signal  $\mathbf{y}_i$  onto the subspace orthogonal to the one spanned by the aligned interference  $[\mathbf{H}_{ij} \mathbf{V}_j \mathbf{s}_j]_{j \neq i}$ , i.e.  $\mathcal{S}([\mathbf{u}_{il}]_{l \in S_i})$ .  $\mathbf{U}_i^H \mathbf{y}_i$  should be interpreted as the projection of  $\mathbf{y}_i$  onto  $\mathcal{S}([\mathbf{u}_{il}]_{l \in S_i})$  but expressed in terms of the coordinates defined by the basis of  $\mathcal{S}([\mathbf{u}_{il}]_{l \in S_i})$ . The projection is visualized along the dashed lines in Fig. 4.2. In Fig. 4.2(a), the projected signal of interest  $\mathbf{U}_i^H \mathbf{H}_{ii} \mathbf{V}_i \mathbf{s}_i$  is spanning a one dimensional subspace in the two-dimensional interference-free subspace enabled through the receive diversity. The projected signal of interest in Fig. 4.2(b) is lying in the one-dimensional interference-free subspace.

The receive signal of user  $i$  after the projection yields

$$\bar{\mathbf{y}}_i = \mathbf{U}_i^H \mathbf{y}_i = \mathbf{U}_i^H \mathbf{H}_{ii} \mathbf{V}_i \mathbf{s}_i + \sum_{j \neq i} \mathbf{U}_i^H \mathbf{H}_{ij} \mathbf{V}_j \mathbf{s}_j + \mathbf{U}_i^H \mathbf{n}_i = \mathbf{U}_i^H \mathbf{H}_{ii} \mathbf{V}_i \mathbf{s}_i + \bar{\mathbf{n}}_i, \quad (4.8)$$

where we used the fact that the interference term in (4.8) is perfectly suppressed, due to (4.4). We define the *effective channel*  $\bar{\mathbf{H}}_{ii} = \mathbf{U}_i^H \mathbf{H}_{ii} \mathbf{V}_i$  as the interference-free and dimension reduced equivalent channel as seen by receiver  $i$ .  $\bar{\mathbf{H}}_{ii} \in \mathbb{C}^{d' \times d}$  is tall for the receiver exploiting receive diversity, as opposed to the symmetric effective channel  $\bar{\mathbf{H}}_{ii} \in \mathbb{C}^{d \times d}$  of a user focusing on multiplexing gains. The residual noise  $\bar{\mathbf{n}}_i$  is

circularly symmetric Gaussian  $\mathcal{CN}(0, \sigma_n^2 \mathbf{I}_{d'})$ . Note that the energy of the signal part that lies in the interference subspace is lost, depicted by the dashed lines in Fig. 4.2 which is the part of the arrow representing  $\mathbf{H}_{ii}\mathbf{v}_i s_i$  that lies perpendicular to the interference subspace. Fig. 4.3 shows the  $(3 \times 3, 1, 2)^3$ -IC on the left-hand side (LHS)

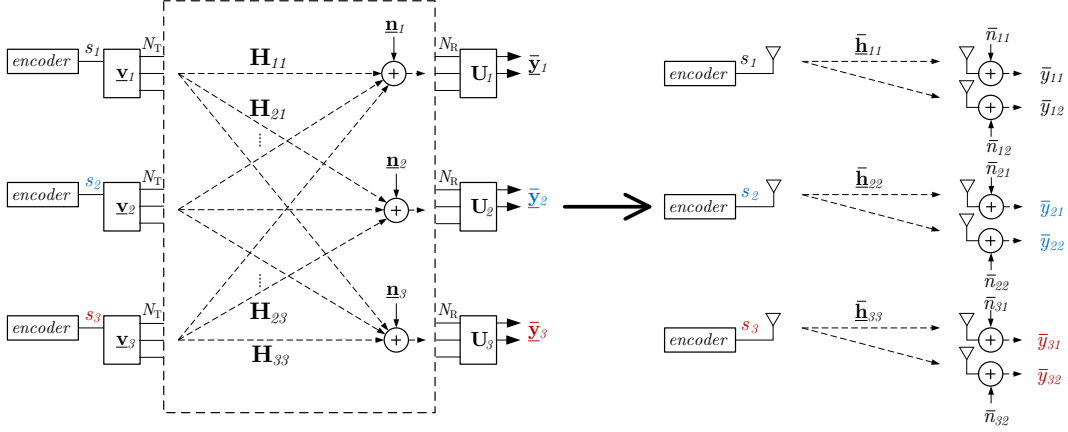


Figure 4.3: Alignment in the  $(3 \times 3, 1, 2)^3$ -IC leading to a dimension-reduced interference-free effective channel.

and its  $2 \times 1$  effective channel  $\bar{\mathbf{h}}_{ii}$  after interference suppression on the right-hand side (RHS). The effective channel can be interpreted as an equivalent  $1 \times 2$  single-input multiple-output (SIMO) system with corresponding AWGN. Hence, each user enjoys a diversity gain  $d' = 2$ .

## 4.3 Alignment Procedures

In this section, we introduce procedures to solve the alignment problem in a  $K$ -user MIMO-IC that will be used throughout this thesis. We distinguish between an iterative method and constructive methods that express closed-form IA solutions. Numerical simulations have shown that if a network configuration is feasible, then iterative methods reliably find a set of precoding matrices that fulfill the interference alignment conditions. The solution to the alignment problem is *non-unique* and depends on the initial conditions of the iterative algorithm.

### 4.3.1 Iterative Alignment Procedure

The iterative algorithm [22, Algorithm 1], finds the precoding matrices  $\mathbf{V}_i$ 's and interference suppression matrices  $\mathbf{U}_i$ 's and numerically verifies the achievability of

IA in  $K$ -user MIMO-IC settings. The algorithm is based on the minimization of an interference leakage metric (zero leakage is equivalent to the system of equations in (4.4) and (4.5)). The metric reads

$$I_w = \sum_{i=1}^K \sum_{\substack{j=1 \\ j \neq i}}^K \frac{\rho_i}{d} \frac{\rho_j}{d} \|\mathbf{U}_i^H \mathbf{H}_{ij} \mathbf{V}_j\|_F^2. \quad (4.9)$$

At every iteration, the algorithm solves  $K$  eigenvalue problems. In particular, every receiver  $i$  computes its interference covariance matrix and identifies the receive signal subspace that contains the least interference. The  $d$  eigenvectors corresponding to this subspace are used for precoding over the *reciprocal network* where the role of the transmitters and receivers are interchanged. In the reciprocal network,  $\overleftarrow{\mathbf{H}}_{ij} = \mathbf{H}_{ji}$  is the  $N_R \times N_T$  matrix of channel coefficients between transmitter  $j$  and receiver  $i$ . The identification of the subspace containing the least interference and adjustment of the precoders over the reciprocal network is repeated until all  $K$  interference covariances are rank-deficient, hence the interference-free subspaces have been isolated. It is proven that the algorithm converges, however due to the non-convex nature of the interference minimization problem, convergence to a global minimum is not guaranteed. Depending on the interference channel setting the convergence speed can vary significantly.

### 4.3.2 Constructive Alignment Procedures

In this subsection, we focus on constructive methods to find solutions to the alignment problem, i.e. the low rank precoding matrices. We find solutions for the symmetric network case where the number of transmit antennas equals the number of receive antenna ( $N_T = N_R = M$ ), the number of transmitter-receiver pairs  $K = M+1$ , and single-stream precoding  $d = 1$  is used. We describe a novel alignment method that provides a solution to the IA conditions (4.4) and (4.5) by reformulating (4.4) as an eigenvalue problem. The extension to cases where the antenna deployment is non-uniform and multi-beam transmission is not straightforward in general.

*Theorem 3.* For the symmetric  $(M \times M, 1)^{M+1}$  IC configuration ( $M = N_T = N_R$ ) with channel coefficients drawn independently from a continuous distribution, a constructive solution to the IA problem, i.e. the precoding vectors  $[\mathbf{v}_1]_{i=1,\dots,K}$  stacked in  $\underline{\mathbf{v}} = [\mathbf{v}_1^T \ \mathbf{v}_2^T \ \dots \ \mathbf{v}_K^T]^T$ , can be found almost surely by the eigenvector  $\underline{\mathbf{v}}$  corresponding to any nonzero eigenvalue of

$$\left( \hat{\mathbf{H}} - \lambda \mathbf{I}_{KM} \right) \underline{\mathbf{v}} = \underline{\mathbf{0}}_{KM}, \quad (4.10)$$

where the matrix  $\widehat{\mathbf{H}}$  has the structure according to (4.21) with coefficients  $\nu_{ij}$ 's in (4.21) chosen non-zero.

*Proof.* Let us consider the  $M$ -dimensional receive signal spaces. Each  $\mathbf{u}_i$  in the IA condition (4.4) defines a subspace of codimension one. Furthermore, (4.4) is equivalent to requiring that the interfering signals  $\mathbf{H}_{ij}\mathbf{v}_j \forall j \neq i$  at each receiver lie in subspaces of dimension at most  $M - 1$ , according to the alignment condition (4.3). Thus, since  $K = M + 1$ , this is equivalent to linear dependency (3.18) of the  $K - 1 = M$  interfering signals at each receiver. That is, there exist  $\mu_{ij}$ 's,  $j \neq i$ , where at least one of the  $\mu_{ij}$ 's is nonzero, such that  $\forall i$

$$\sum_{j=1, j \neq i}^K \mu_{ij} \mathbf{H}_{ij} \mathbf{v}_j = \mathbf{0}_M, \quad (4.11)$$

with  $\mathbf{0}_M$  the  $M \times 1$  all zero vector.

From now on, we tackle (4.4) simultaneously for all receivers  $i$ . Therefore, we use the stacked precoding vectors  $\mathbf{v} = [\mathbf{v}_1^T \mathbf{v}_2^T \dots \mathbf{v}_K^T]^T$  and define

$$\mathbf{H} = \begin{bmatrix} \mathbf{O}_M & \mu_{12}\mathbf{H}_{12} & \dots & \mu_{1K}\mathbf{H}_{1K} \\ \mu_{21}\mathbf{H}_{21} & \mathbf{O}_M & \dots & \vdots \\ \vdots & \ddots & \dots & \mu_{(K-1)K}\mathbf{H}_{(K-1)K} \\ \mu_{K1}\mathbf{H}_{K1} & \dots & \dots & \mathbf{O}_M \end{bmatrix}, \quad (4.12)$$

where  $\mathbf{O}_M$  is the  $M \times M$  all zero matrix.  $\mathbf{H}$  incorporates the channel matrices of all interfering links in the interference channel. Using this notation, (4.4) is equivalent to

$$\mathbf{H}\mathbf{v} = \mathbf{0}_{KM}, \quad (4.13)$$

for any given  $\mu_{ij}$ 's defined by (4.11), with  $\mathbf{0}_{KM}$  the  $KM \times 1$  all zero vector. Equation (4.13) is invariant under left multiplication with a matrix  $\mathbf{P}$  that shifts rows, i.e.

$$\mathbf{H}\mathbf{v} = \mathbf{0}_{KM} \Leftrightarrow \mathbf{P}\mathbf{H}\mathbf{v} = \mathbf{0}_{KM}. \quad (4.14)$$

We get a nonzero block diagonal  $\mathbf{B} = \text{diag}\{\mu_{K1} \mathbf{H}_{K1} \dots \mu_{(K-1)K} \mathbf{H}_{(K-1)K}\}$  in  $\mathbf{P}\mathbf{H}$ , using the following permutation matrix

$$\mathbf{P} = \begin{bmatrix} \mathbf{O}_M & \dots & \mathbf{O}_M & \mathbf{I}_M \\ \mathbf{I}_M & \mathbf{O}_M & \ddots & \mathbf{O}_M \\ \vdots & \ddots & \ddots & \vdots \\ \mathbf{O}_M & \dots & \mathbf{I}_M & \mathbf{O}_M \end{bmatrix}. \quad (4.15)$$

Permutation matrices are orthonormal, nonsingular and there exists unique inverse of  $\mathbf{P}^{-1} = \mathbf{P}^H$ , i.e.  $\mathbf{P}^H \mathbf{P} = \mathbf{I}_M$  [73]. Furthermore, since all channel matrices are of rank  $M$  w.p. one and if we assume that  $(\mu_{K1}, \dots, \mu_{(K-1)K}) \neq 0$ , we can pre-multiply the permuted matrix  $\mathbf{P}\mathbf{H}$  with  $\mathbf{B}^{-1}$ . The null space of a matrix is invariant under pre-multiplication with a full rank matrix. Thus, we find an equivalent condition for (4.13), i.e.

$$\mathbf{P}\mathbf{H}\underline{\mathbf{v}} = \underline{\mathbf{0}}_{KM} \Leftrightarrow \mathbf{B}^{-1}\mathbf{P}\mathbf{H}\underline{\mathbf{v}} = \underline{\mathbf{0}}_{KM}. \quad (4.16)$$

Now, we define the matrix

$$\hat{\mathbf{H}} = -\lambda(\mathbf{B}^{-1}\mathbf{P}\mathbf{H} - \mathbf{I}_{KM}), \quad (4.17)$$

with the free parameter  $\lambda \neq 0$ . We can solve  $\hat{\mathbf{H}}$  for  $\mathbf{H}$  along the following steps

$$\begin{aligned} (-1/\lambda)\hat{\mathbf{H}} &= \mathbf{B}^{-1}\mathbf{P}\mathbf{H} - \mathbf{I}_{KM} \\ (-1/\lambda)\mathbf{P}^H\mathbf{B}\hat{\mathbf{H}} &= \mathbf{H} - \mathbf{P}^H\mathbf{B} \\ (-1/\lambda)\mathbf{P}^H\mathbf{B}\hat{\mathbf{H}} + \mathbf{P}^H\mathbf{B} &= \mathbf{H}, \end{aligned} \quad (4.18)$$

where for the first equality we used the fact that  $\mathbf{B}$  is invertible and  $\mathbf{P}^H\mathbf{P} = \mathbf{I}_M$ . Inserting (4.18) into (4.16) leads to

$$(-1/\lambda)\mathbf{B}^{-1}\mathbf{P}\mathbf{P}^H\mathbf{B}\hat{\mathbf{H}}\underline{\mathbf{v}} + \mathbf{B}^{-1}\mathbf{P}\mathbf{P}^H\mathbf{B}\underline{\mathbf{v}} = \underline{\mathbf{0}}_{KM}, \quad (4.19)$$

which turns (4.13) into the standard eigenvalue equation

$$(\hat{\mathbf{H}} - \lambda\mathbf{I}_{KM})\underline{\mathbf{v}} = \underline{\mathbf{0}}_{KM}. \quad (4.20)$$

The matrix  $\hat{\mathbf{H}}$  has the following structure

$$\begin{bmatrix} \mathbf{O}_M & \nu_{12}\mathbf{H}_{K1}^{-1}\mathbf{H}_{K2} & \dots & \mathbf{O}_M \\ \mathbf{O}_M & \mathbf{O}_M & \nu_{23}\mathbf{H}_{12}^{-1}\mathbf{H}_{13} & \dots & \nu_{K2}\mathbf{H}_{12}^{-1}\mathbf{H}_{1K} \\ \nu_{31}\mathbf{H}_{23}^{-1}\mathbf{H}_{21} & \mathbf{O}_M & \ddots & \dots & \vdots \\ \vdots & \ddots & \ddots & \dots & \vdots \\ \nu_{K1}\mathbf{H}_{(K-1)K}^{-1}\mathbf{H}_{(K-1)1} & \dots & \nu_{K(K-2)}\mathbf{H}_{(K-1)K}^{-1}\mathbf{H}_{(K-1)(K-2)} & \dots & \nu_{(K-1)K}\mathbf{H}_{(K-2)(K-1)}^{-1}\mathbf{H}_{(K-2)K} \\ & & & & \mathbf{O}_M \end{bmatrix}. \quad (4.21)$$

It is clear from (4.13)-(4.20) that any  $\underline{\mathbf{v}}$  associated to a nonzero eigenvalue of  $\hat{\mathbf{H}}$  fulfills (4.13), for a given choice of the  $(\mu_{K1}, \dots, \mu_{(K-1)K})$  for which  $\mathbf{B}$  is not singular. That is, if we denote  $\nu_{ij} = -(\mu_{lj}/\mu_{li})\lambda$  with  $l = \text{mod}(i-2, K) + 1$ , it is sufficient to choose the  $\nu_{ij}$ 's such that  $\hat{\mathbf{H}}$  has at least one non-zero eigenvalue, to solve the interference alignment problem. Note that due to the structure of  $\hat{\mathbf{H}}$  (4.21), choosing e.g.  $\nu_{ij} = 1, \forall(i, j)$  guarantees that this happens w.p. one when the channel coefficients are drawn independently from a continuous distribution.  $\square$

Hence, with the above constructive method it is possible to achieve a sum multiplexing gain  $K$  in the symmetric  $(M \times M, 1)^{M+1}$  IC almost surely. Finally, in order to provide the complete solution to (4.4), the vectors  $\mathbf{v}_1, \mathbf{v}_2, \dots, \mathbf{v}_K$  must be normalized, and the  $\mathbf{u}_i$  can be determined by finding any unit norm vector in the orthogonal complement of the subspace (of dimension at most  $M - 1$ ) spanned by interfering signals  $\mathbf{H}_{ij}\mathbf{v}_j \forall j \neq i$  at each receiver  $i$ . The IA solution is non-unique since any eigenvector corresponding to a non-zero eigenvalue in (4.20) provides a set of precoders fulfilling the IA criteria. Furthermore, the precoders for the MIMO-IC cannot be inherited in the SISO case since the second IA criteria (4.5) is not fulfilled w.p. one. Theorem 3 leads to alignment solutions but the effective channel  $\bar{\mathbf{H}}_{ii} = \mathbf{u}_i^H \mathbf{H}_{ii} \mathbf{v}_i$  might be rank deficient.

Note that for the square channels ( $N_T = N_R = M$ ) considered above, our constructive method only provides solutions for the case  $K = M + 1$  ( $\checkmark^*$  in Table 4.2), while (4.7) suggests that a better scaling of the method is possible, since solutions can be found numerically if and only if  $K \leq 2M - 1$ .

| $M \backslash K$ | 3              | 4              | 5              | 6            | 7            | 8 |
|------------------|----------------|----------------|----------------|--------------|--------------|---|
| 2                | $\checkmark^*$ |                |                |              |              |   |
| 3                | $\checkmark$   | $\checkmark^*$ | $\checkmark$   |              |              |   |
| 4                | $\checkmark$   | $\checkmark$   | $\checkmark^*$ | $\checkmark$ | $\checkmark$ |   |
| $\vdots$         |                |                |                |              |              |   |

Table 4.2: Feasibility of IA ( $\checkmark$  =yes) for different  $(M \times M, 1)^K$ -IC settings, where for the particular cases  $\checkmark^*$  Theorem 3 finds closed-form IA solutions.

## 4.4 Ergodic Performance

In this section, we characterize the ergodic sum-rate of the  $K$ -user MIMO-IC using alignment-based precoding and the projection receiver introduced in Subsection 4.2.1. The case of perfect global CSI is discussed first and then extended to the case of imperfect CSI. Henceforth, we assume that  $\mathbf{H}_{ij}$  is Rayleigh fading, introduced in Section 1.3, i.e. the  $h_{ij}(n_r, n_t)$ 's are complex Gaussian i.i.d. random variables, with zero mean and unit variance.

Let us further analyze the effective channel  $\bar{\mathbf{H}}_{ii} = \mathbf{U}_i^H \mathbf{H}_{ii} \mathbf{V}_i$  introduced in (4.8). Since  $\mathbf{U}_i$  and  $\mathbf{V}_i$  are truncated unitary matrices,  $\bar{\mathbf{H}}_{ii} = \mathbf{U}_i^H \mathbf{H}_{ii} \mathbf{V}_i$  has Gaussian



i.i.d. coefficients of the same variance as  $\mathbf{H}_{ii}$ , and the noise term  $\bar{\mathbf{n}}_i = \mathbf{U}_i^H \mathbf{n}_i$  in (4.8) has Gaussian i.i.d. coefficients with unit variance. We define the SNR  $\rho_i = \mathbb{E}[\text{Tr}(\mathbf{x}_i \mathbf{x}_i^H)]$ . According to (3.16)  $\rho_i = \text{Tr}(\mathbf{V}_i \mathbf{Q}_{\mathbf{s}_i \mathbf{s}_i} \mathbf{V}_i^H) = \text{Tr}(\mathbf{Q}_{\mathbf{s}_i \mathbf{s}_i})$ , with  $\mathbf{Q}_{\mathbf{s}_i \mathbf{s}_i} = \mathbb{E}_{\mathbf{s}_i}[\mathbf{s}_i \mathbf{s}_i^H]$  the signal covariance. Therefore, (4.8) describes the transmission over a Rayleigh-fading channel of dimensions  $d' \times d$ , over which the mutual information has been characterized in [74]

$$R_i = I(\mathbf{s}_i; \bar{\mathbf{y}}_i | \mathbf{H}) = \mathbb{E}_{\mathbf{H}} [\log_2 \det (\mathbf{I}_d + \bar{\mathbf{H}}_{ii} \mathbf{Q}_{\mathbf{s}_i \mathbf{s}_i} \bar{\mathbf{H}}_{ii}^H)] . \quad (4.22)$$

Under the assumption of a spatially white transmit signal inside the subspace defined by  $\mathbf{V}_i$  ( $\mathbf{Q}_{\mathbf{s}_i \mathbf{s}_i} = \frac{\rho_i}{d} \mathbf{I}_d$ ), we have from [74] that

$$\mathbb{E}_{\mathbf{H}_{ii}} \left[ \log_2 \det \left( \mathbf{I}_d + \frac{\rho_i}{d} \bar{\mathbf{H}}_{ii} \bar{\mathbf{H}}_{ii}^H \right) \right] = C(d, d', \frac{\rho_i}{d}). \quad (4.23)$$

where

$$C(d, d', \rho') = e^{\frac{1}{\rho'}} \log_2(e) \sum_{k=0}^{d-1} \sum_{l=0}^k \sum_{m=0}^{2l} \left\{ \frac{(-1)^m (2l)! (d' - d + m)! (2k - 2l)!}{2^{2k-m} l! m! (d' - d + m)!} \binom{2k - 2l}{k - l} \right\} \quad (4.24)$$

$$\left( \binom{2l + 2d' - 2d}{2l - m} \sum_{p=1}^{d' - d + m + 1} E_p \left( \frac{1}{\rho'} \right) \right\}, \quad (4.25)$$

and where  $E_p(\cdot)$  denotes the exponential integral function of order  $p$ , i.e.

$$E_p(z) = \int_1^\infty e^{-zx} x^{-p} dx \quad \text{Re}\{z\} > 0. \quad (4.26)$$

#### 4.4.1 Noisy Channel State Information

We focus now on the impact of noisy channel state information (CSI) on the performance of IA. Here, we focus on the case where  $d = d'$ . Let  $\tilde{\mathbf{H}}_{ii}$  and  $\tilde{\mathbf{H}}_{ij}$  denote the MIMO channels estimated by user  $i$  and let us assume that the IA is done based on these noisy estimates. In general,  $\tilde{\mathbf{H}} \neq \mathbf{H}$ , due to both estimation noise and time variation of the channel. Let  $\mathbf{E} = \tilde{\mathbf{H}} - \mathbf{H}$  denote the channel measurement error, and assume that it is a complex Gaussian circularly-symmetric random matrix with i.i.d. components of zero-mean and variance  $\sigma_E^2$ .

In this setting, IA is based on the estimated channels, i.e.,  $\tilde{\mathbf{U}}_i^H \tilde{\mathbf{H}}_{ij} \tilde{\mathbf{V}}_j = 0$  is fulfilled for all  $j \neq i$ . This leads to a mismatch with the channel conditions during the time of transmission  $\tilde{\mathbf{U}}_i^H \mathbf{H}_{ij} \tilde{\mathbf{V}}_j \neq 0 \forall j \neq i$ . The receive signal of user  $i$  after interference suppression with  $\tilde{\mathbf{U}}$  and  $\tilde{\mathbf{V}}$  computed from  $\tilde{\mathbf{H}}$  yields

$$\bar{\mathbf{y}}_i = \tilde{\mathbf{U}}_i^H \mathbf{H}_{ii} \tilde{\mathbf{V}}_i \mathbf{s}_i + \sum_{j \neq i} \tilde{\mathbf{U}}_i^H \mathbf{H}_{ij} \tilde{\mathbf{V}}_j \mathbf{s}_j + \bar{\mathbf{n}}_i. \quad (4.27)$$

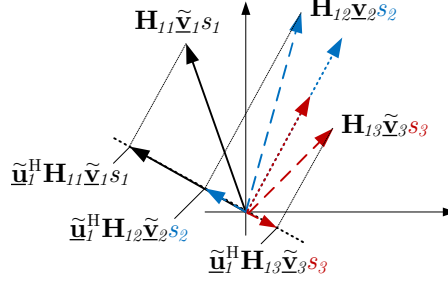


Figure 4.4: Interference leakage at receiver one in the  $(2 \times 2, 1)^3$ -IC where IA based on imperfect CSI.

Note that we project  $\mathbf{y}_i$  (by the product with  $\tilde{\mathbf{U}}_i^H$ ) onto the orthogonal subspace of the assumed interference, and that an interference term remains (second term in the RHS of (4.27), non-zero interference leakage), due to the fact that the IA condition is fulfilled for the noisy estimated channels. Fig. 4.4 shows IA in the  $(2 \times 2, 1)^3$ -IC with imperfect CSI. Interference suppression is performed at receiver one with the linear projector  $\tilde{\mathbf{u}}_1$  that is based on the noisy channel estimates  $\tilde{\mathbf{H}}$ . Now, the interference from transmitter two and three spans the full signal space of receiver one and it is not possible to suppress it completely. The assumed interference  $[\tilde{\mathbf{H}}_{ij} \tilde{\mathbf{v}}_j s_j]_{j=2,3}$ , would align as indicated by the dotted arrows in Fig. 4.4.

The equivalent channel (4.27), assumed known at receiver  $i$  leads to the following achievable ergodic rate for user  $i$

$$R_i = I(\underline{\mathbf{s}}_i; \underline{\mathbf{y}}_i | \mathbf{H}) = \mathbb{E}_{\mathbf{H}, \mathbf{E}} \left[ \log_2 \det \left( \mathbf{I}_d + \bar{\mathbf{H}}_{ii} \mathbf{Q}_{\underline{\mathbf{s}}_i \underline{\mathbf{s}}_i} \bar{\mathbf{H}}_{ii}^H \left( \sum_{j \neq i} \bar{\mathbf{H}}_{ij} \mathbf{Q}_{\underline{\mathbf{s}}_j \underline{\mathbf{s}}_j} \bar{\mathbf{H}}_{ij}^H + \mathbf{I}_d \right)^{-1} \right) \right], \quad (4.28)$$

with the transmit signal covariance  $\mathbf{Q}_{\underline{\mathbf{s}}_j \underline{\mathbf{s}}_j} = \mathbb{E}_{\underline{\mathbf{s}}_j} [\underline{\mathbf{s}}_j \underline{\mathbf{s}}_j^H]$  and  $\bar{\mathbf{H}}_{ij}$  must be redefined as  $\bar{\mathbf{H}}_{ij} = \tilde{\mathbf{U}}_i^H \mathbf{H}_{ij} \tilde{\mathbf{V}}_j \forall (i, j)$ . Furthermore we used the fact that all  $\underline{\mathbf{s}}_i$ 's are independent.

#### 4.4.2 Bounds of Ergodic Rate with Imperfect CSI

In this subsection, we focus on the case where the channels are not re-estimated for data transmission, i.e., the equivalent channels  $[\tilde{\mathbf{U}}_i^H \mathbf{H}_{ij} \tilde{\mathbf{V}}_j]_{j=1, \dots, K}$  are not perfectly known at receiver  $i$ . We want to derive bounds on the performance of IA for this setting, without focusing on optimizing the signal transmit covariances  $\mathbf{Q}_{\underline{\mathbf{s}}_i \underline{\mathbf{s}}_i}$ .

Inserting channel estimates used for the IA in (4.27) yields

$$\begin{aligned}\bar{\mathbf{y}}_i &= \tilde{\mathbf{U}}_i^H (\tilde{\mathbf{H}}_{ii} - \mathbf{E}_{ii}) \tilde{\mathbf{V}}_i \mathbf{s}_i + \sum_{j \neq i} \tilde{\mathbf{U}}_i^H (\tilde{\mathbf{H}}_{ij} - \mathbf{E}_{ij}) \tilde{\mathbf{V}}_j \mathbf{s}_j + \bar{\mathbf{n}}_i \\ &= \tilde{\mathbf{U}}_i^H (\tilde{\mathbf{H}}_{ii} - \mathbf{E}_{ii}) \tilde{\mathbf{V}}_i \mathbf{s}_i - \sum_{j \neq i} \tilde{\mathbf{U}}_i^H \mathbf{E}_{ij} \tilde{\mathbf{V}}_j \mathbf{s}_j + \bar{\mathbf{n}}_i,\end{aligned}\quad (4.29)$$

where the second equality comes from the IA condition  $\tilde{\mathbf{U}}_i^H \tilde{\mathbf{H}}_{ij} \tilde{\mathbf{V}}_j = 0 \forall j \neq i$ . Let us examine in further detail the structure of the interference terms in (4.29). Since  $\tilde{\mathbf{U}}_i^H \tilde{\mathbf{U}}_i = \mathbf{I}_d$  and  $\tilde{\mathbf{V}}_j^H \tilde{\mathbf{V}}_j = \mathbf{I}_d$ ,  $\tilde{\mathbf{U}}_i^H \mathbf{E}_{ij} \tilde{\mathbf{V}}_j = \bar{\mathbf{E}}_{ij}$  has  $d \times d$  Gaussian i.i.d. coefficients with variance  $\sigma_E^2$ . We denote  $\bar{\mathbf{E}}_{ij}$  as the  $d \times d$  effective error matrix.

Extending the above derivation for the signal term  $\tilde{\mathbf{U}}_i^H \mathbf{E}_{ii} \tilde{\mathbf{V}}_i$  turns (4.29) into

$$\bar{\mathbf{y}}_i = \underbrace{(\tilde{\mathbf{U}}_i^H \tilde{\mathbf{H}}_{ii} \tilde{\mathbf{V}}_i + \bar{\mathbf{E}}_{ii})}_{\tilde{\tilde{\mathbf{H}}}_{ii}} \mathbf{s}_i + \sum_{j \neq i} \bar{\mathbf{E}}_{ij} \mathbf{s}_j + \bar{\mathbf{n}}_i, \quad (4.30)$$

where  $\bar{\mathbf{E}}_{ii}$  is the  $d \times d$  effective error matrix of the channel between transmitter  $i$  and receiver  $i$  and  $\tilde{\tilde{\mathbf{H}}}_{ii}$  denotes the  $d \times d$  effective estimated channel matrix.

*Theorem 4.* The ergodic mutual information of user  $i$  in an  $K$ -user MIMO interference channel with multiplexing gain allocation  $d = d'$  where IA solutions are based on noisy CSI and the channels are not re-estimated for data transmission is lower bounded as

$$I(\mathbf{s}_i; \bar{\mathbf{y}}_i | \tilde{\mathbf{H}}) \geq \mathbb{E}_{\tilde{\mathbf{H}}} \left[ \log_2 \det \left( \frac{1}{\sigma_E^2 d \rho_i + 1} \left( \rho_i \tilde{\tilde{\mathbf{H}}}_{ii} \tilde{\tilde{\mathbf{H}}}_{ii}^H + \left( \sigma_E^2 \rho_i + \sum_{j \neq i} \sigma_E^2 \rho_j + 1 \right) \mathbf{I}_d \right) \right) \right], \quad (4.31)$$

under the assumption of a spatially white transmit signal  $\mathbf{Q}_{\mathbf{s}_i \mathbf{s}_i} = (\rho_i/d) \mathbf{I}_d \forall i$ , and upper bounded as

$$\begin{aligned}I(\mathbf{s}_i; \bar{\mathbf{y}}_i | \tilde{\mathbf{H}}) &\leq \pi e \det \left( \frac{\rho_i}{d} \tilde{\tilde{\mathbf{H}}}_{ii} \tilde{\tilde{\mathbf{H}}}_{ii}^H + (K \sigma_E^2 + 1) \mathbf{I}_d \right) - \\ &\quad \det \left( d \log_2(\pi e) + d \exp \left( \frac{d}{\sigma_E^2 \rho_i} \right) \log_2(e) \sum_{p=1}^n E_p \left( \frac{d}{\sigma_E^2 \rho_i} \right) \right),\end{aligned}\quad (4.32)$$

if all  $\rho_i$  are equal.

*Proof.* The proof is outlined in Appendix 4.6. □

## 4.5 Simulation Results

In this section, we present simulation results for the ergodic rates over the  $K$ -user MIMO IC and discuss the derived analytical formulas. We begin with a comparison of the performance curves of opportunistic beamforming, orthogonal resource sharing described in Subsection 4.1.1 and alignment-based strategies described in Section 4.2 under the assumption of perfect CSI at transmitter and receiver side. Thereafter, the multi-user diversity-multiplexing tradeoff established in Section 4.2.1 is illustrated. Furthermore, the ergodic achievable rates using IA based on imperfect CSI are plotted and compared to the sensitivity of a selfish strategy that exploits CSI about the direct link of each user independently.

The SNR  $\rho_i = \mathbb{E}[\text{Tr}(\mathbf{x}_i \mathbf{x}_i^H)]$  is assumed identical for all  $K$  users. The rates are averaged over different realizations of the channel fading. All channels are assumed Gaussian i.i.d., with unit variance elements. The iterative IA algorithm [22, Algorithm 1], with random unit vectors  $[v_i^{\text{init}}]_{i=1,\dots,K}$  according to an isotropic distribution for the initialization, was used for the Monte-Carlo simulations. For all network configurations used in this section an IA solution is feasible and the iterative IA algorithm always converges to zero interference leakage. The Monte-Carlo simulation results are compared to the analytical formula derived in Section 4.4 for IA with projection receiver. The ergodic sum-rate  $\sum_i R_i$  achieved by IA with projection receiver obtained by Monte-Carlo simulation of the LHS of (4.23) are compared with the RHS of (4.23). IA with the optimum receiver evaluates the sum mutual information  $\sum_i I(\underline{\mathbf{s}}_i; \underline{\mathbf{y}}_i | \mathbf{H})$  with

$$I(\underline{\mathbf{s}}_i; \underline{\mathbf{y}}_i | \mathbf{H}) = \mathbb{E}_{\mathbf{H}} \left[ \log_2 \det \left( \mathbf{I}_{N_R} + \mathbf{H}_{ii} \mathbf{Q}_{\mathbf{x}_i \mathbf{x}_i} \mathbf{H}_{ii}^H \left( \sum_{j \neq i} \mathbf{H}_{ij} \mathbf{Q}_{\mathbf{x}_j \mathbf{x}_j} \mathbf{H}_{ij}^H + \mathbf{I}_{N_R} \right)^{-1} \right) \right], \quad (4.33)$$

where for all  $i$   $\mathbf{Q}_{\mathbf{x}_i \mathbf{x}_i} = \frac{\rho_i}{d} \mathbf{V}_i \mathbf{V}_i^H$ , i.e. the users split the transmit power evenly among  $d$  uncorrelated transmit directions. The performance of orthogonal resource sharing based on waterfilling independently in non-interfering channels isolated in time or frequency domain is evaluated as follows. The ergodic sum-rate writes  $R_{\Sigma} = \sum_i R_{i, \mathbf{WF}}$  with

$$R_{i, \mathbf{WF}} = \mathbb{E}_{\mathbf{H}} \left[ \frac{1}{K} \log_2 \det \left( \mathbf{I}_{N_R} + \mathbf{H}_{ii} \mathbf{Q}_{\mathbf{WF}, i} \mathbf{H}_{ii}^H \left( \sum_{j \neq i} \mathbf{H}_{ij} \mathbf{Q}_{\mathbf{WF}, j} \mathbf{H}_{ij}^H \right)^{-1} \right) \right], \quad (4.34)$$

where  $\mathbf{Q}_{\mathbf{WF}, i} = \mathbf{V}_i \text{diag} \{[\tilde{\rho}_{i1}, \dots, \tilde{\rho}_{iN^{\min}}]\} \mathbf{V}_i^H$ , with  $N^{\min} = \min\{N_T, N_R\}$ ,  $\mathbf{V}_i$  according to (3.10) and the waterfilling power allocation introduced in (3.11). The power

budget per user is increased by  $K$  since each user accesses only a fraction of the shared resource, i.e.  $\text{Tr}[\mathbf{Q}_{\text{WF},i}] = K\rho_i$ . The achievable sum-rate of dominant eigenmode and multi-stream transmission with full resource sharing is  $\sum_i I(\underline{\mathbf{s}}_i; \underline{\mathbf{y}}_i | \mathbf{H})$  with  $I(\underline{\mathbf{s}}_i; \underline{\mathbf{y}}_i | \mathbf{H})$  according to (4.33). For dominant eigenmode the transmit covariance for user  $i$  writes  $\mathbf{Q}_{\underline{\mathbf{x}}_i \underline{\mathbf{x}}_i} = \rho_i \underline{\mathbf{v}}_i \underline{\mathbf{v}}_i^H$  with  $\underline{\mathbf{v}}_i$  the right singular vector corresponding to the largest singular value in (3.10) whereas for multi-stream transmission  $\mathbf{Q}_{\underline{\mathbf{x}}_i \underline{\mathbf{x}}_i} = (\rho_i/N^{\min}) \mathbf{V}_i \mathbf{V}_i^H$  with  $\mathbf{V}_i$  according to (3.10).

### 4.5.1 Beamforming with Perfect Channel State Information

Fig. 4.5 depicts the simulated achievable ergodic rates for the 3-user  $2 \times 2$  ( $N_T \times N_R$ ) MIMO IC for a range of SNR. Interference alignment with uniform multiplexing gain

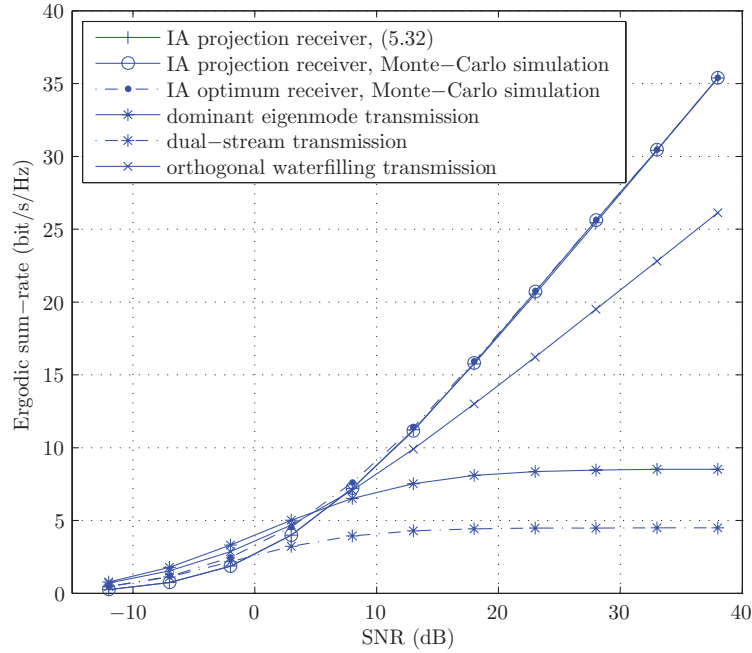


Figure 4.5: Ergodic sum-rate achieved with various interference management approaches,  $K = 3$ ,  $N_T = 2$ ,  $N_R = 2$ , IA with  $d = 1$ ,  $d' = 1$ , as a function of the SNR.

allocation  $d = 1$  is used. This network configuration does not allow for diversity gain ( $d' = 1$ ) and the corresponding feasibility condition (4.7) is fulfilled with equality. A closed form solution for the IA precoders can be found with the constructive procedure introduced in Section 4.3.2. In Fig. 4.5, the Monte-Carlo simulation of the projection receiver shows an excellent agreement with the explicit formula of the

ergodic rate. IA with the optimum receiver slightly outperforms IA with projection receiver at low SNR. At high SNR, the advantage of the optimum receiver vanishes due to the severe strength of the accumulated interference power in the interference subspace. Both receivers perform equally well, achieving the maximum sum-rate multiplexing gain  $d_{\mathbf{H}} = KM/2 = 3$ . Orthogonal resource sharing outperforms IA at medium and low SNR, whereas at high SNR the orthogonality is limiting the performance and the scheme achieves a sum-rate multiplexing gain of  $d_{\text{orth}} = N^{\min} = 2$ . The performance curve for dual stream and dominant EM transmission saturates at high SNR due to the uncoordinated interference between user, however dominant EM transmission outperforms all other schemes at low SNR.

Fig. 4.6 depicts the simulated ergodic achievable rates for the symmetric 5-user  $4 \times 2$  ( $N_T \times N_R$ ) MIMO IC as a function of SNR. Interference alignment with

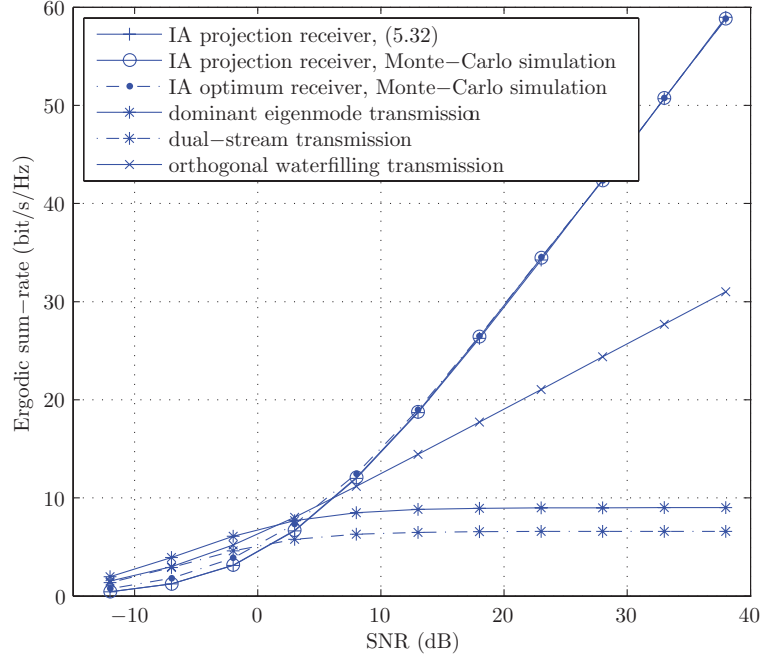


Figure 4.6: Ergodic sum-rate achieved with various interference management approaches,  $K = 5$ ,  $N_T = 4$ ,  $N_R = 2$ , IA with  $d = 1$ ,  $d' = 1$ , as a function of the SNR.

uniform multiplexing gain allocation  $d = 1$  is used. For each user, interference is alignment in a one-dimensional subspace of the  $N_R = 2$ -dimensional receive signal space. This network configuration does not allow for diversity gain ( $d' = 1$ ) and the corresponding feasibility condition (4.7) is fulfilled with equality. The development of a closed form constructive IA solution for this network is still an open problem.

The slope of the performance curves in Fig. 4.6 at high SNR shows that IA achieves the DoF  $d_{\mathbf{H}} = 5$ , whereas orthogonal resource sharing achieves a maximum sum-rate multiplexing gain  $d_{\text{orth}} = N^{\min} = 2$ . However, in the network configuration at hand, orthogonal waterfilling transmission outperforms all other schemes in the SNR interval of 2-4 dB. Again, dominant EM performs best at low SNR.

#### 4.5.2 Multiuser Diversity-Multiplexing Trade-off

Let us now evaluate the influence of the multi-user DMT on the achievable ergodic rates of IA and compare to independent beamforming per user. The results are presented in Fig. 4.7 for an interference network where all the transmitters are equipped with  $N_T = 5$  and all receivers with  $N_R = 3$  antennas, respectively.

The considered MIMO-IC settings were introduced in Table 4.1. Depending on  $d$  and  $d'$ , a different number of users can be accommodated. We consider the case of  $K = 3$  users with  $d = d' = 2$ ,  $K = 4$  users with  $d = 1$  and  $d' = 2$ , as well as the case  $K = 7$  where  $d = d' = 1$ . In all cases, the criterion (4.6) is fulfilled with equality.

In Fig. 4.7(a) it is noticeable that the receive diversity is beneficial to the ergodic rate per user if we compare  $d = d' = 1$  and  $d = 1, d' = 2$ . A horizontal shift of the curve can be observed. However, increasing the additional multiplexing gain and therefore an increased slope of the curve in the setting  $d = 2, d' = 2$  outperforms the per user rate of the other network configurations. Simultaneous access of only three users in the network, which is imposed by the feasibility condition (4.6), is the drawback. The slope of the curves corresponding to orthogonal resource sharing scales with  $N^{\min}/K$  and hence  $K = 3$  exhibits the steepest slope. Dominant eigenmode transmission performs poorly at high SNR for  $K=4,7$ . However, in the case of  $K = 3$  users, the interference spans only a two-dimensional subspace at each receiver and therefore the slope scales linearly at high SNR.

Considering the sum-rate (Fig. 4.7(b)), we observe that below 8 dB the IA configuration with  $d = 2$  performs worst and the configuration with  $d = d' = 1$  outperforms all other alignment-based schemes at any SNR due to the fact that  $K = 7$  users can be supported while still fulfilling the IA condition. Interestingly, for the range between 0 to 5 dB, comparing the rates for configuration  $d = d' = 1$  and  $d = 1, d' = 2$  in Fig. 4.7(a) indicates that it is possible to trade the number of users  $K$  for the per-user rate through the introduction of diversity in the interference-free subspace while the sum-rate (Fig. 4.7(b)) remain comparable. Orthogonal resource sharing achieves a network multiplexing gain  $d_{\text{orth}} = N^{\min}$  with a horizontal shift in the curves for increasing  $K$ . Dominant eigenmode transmission performs poorly at high SNR for  $K=4,7$  whereas  $K = 3$  achieves linear scaling of the ergodic sum-rate at

high SNR with slope  $N^{\min}$ . However the slope is not scaling linearly with  $K$ .

### 4.5.3 Imperfect Channel State Information

For the analysis of imperfect CSI, we choose the same  $(4 \times 2, 1)^5$ -IC configuration as previously considered. The transmit power per user is set to  $\text{Tr}(\mathbf{Q}_{\mathbf{s}_i \mathbf{s}_i}) = \rho_i = 18$  dB. Here, the variance of the elements of the interfering channels  $[\mathbf{H}_{ij}]_{i \neq j}$  have variance  $\beta$ . Therefore,  $\beta$  refers to the average path-loss of the interfering links.

We compare the following strategies with different levels of CSI for IA:

- IA with perfect CSI and projection receiver, as in eq. (4.22), denoted by IA  $\mathbf{U}^H \mathbf{H} \mathbf{V}$ ,
- IA with imperfect  $\tilde{\mathbf{U}}$  and  $\tilde{\mathbf{V}}$  but the receivers can track the equivalent channel perfectly (for example through re-estimation), as in eq.(4.28), denoted by IA  $\tilde{\mathbf{U}}^H \mathbf{H} \tilde{\mathbf{V}}$ ,
- Lower and upper bounds (eqs. (4.31) and (4.32)) introduced in Theorem 4 for IA with imperfect  $\tilde{\mathbf{U}}$  and  $\tilde{\mathbf{V}}$  and noisy CSI, denoted by Lower Bound IA  $\tilde{\mathbf{U}}^H \tilde{\mathbf{H}} \tilde{\mathbf{V}}$  and Upper Bound IA  $\tilde{\mathbf{U}}^H \tilde{\mathbf{H}} \tilde{\mathbf{V}}$  respectively,

and the following strategy that exploits CSI about the direct link of each user independently:

- Maximum EM transmission for each transmitter receiver pair individually. With perfect CSI,  $\mathbf{Q}_{\mathbf{x}_i \mathbf{x}_i} = \mathbf{v}_{i1} \rho_i \mathbf{v}_{i1}^H \forall i$  in (4.33), where  $\mathbf{v}_{i1}$  is the vector associated to the dominant EM of the channel, i.e. corresponding to the strongest singular value  $\sigma_{i1}$  in (3.9). With imperfect CSI,  $\tilde{\mathbf{v}}_{\text{EM}}$  is affected by the channel uncertainty, i.e.  $\mathbf{Q}_{\mathbf{x}_i \mathbf{x}_i} = \tilde{\mathbf{v}}_{i1} \rho_i \tilde{\mathbf{v}}_{i1}^H \forall i$  in (4.33) (denoted by max Eigenmode  $\mathbf{H} \mathbf{v}_{\text{EM}}$  and  $\mathbf{H} \tilde{\mathbf{v}}_{\text{EM}}$ ).

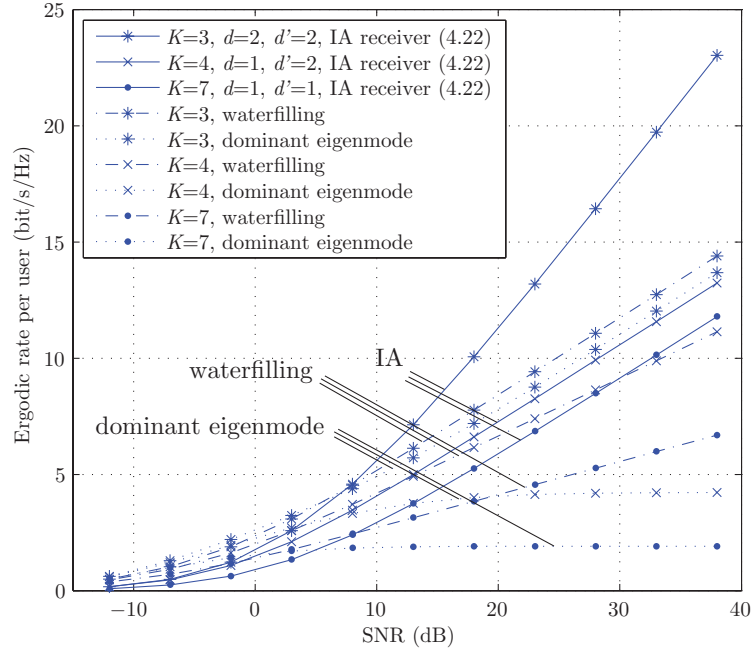
In Figures 4.8 and 4.9, the ergodic sum-rate per user is plotted versus the relative channel measurement error denoted by  $\sigma_H^2/\sigma_E^2$ , respectively for  $\beta = 1$  and  $\beta = 0.5$ .

For both values of  $\beta$ , the IA with perfect CSI clearly outperforms the other methods: IA with the projection receiver converts the interference network into five parallel links without interference from other transmit-receive pairs, and the loss in receive signal power is clearly compensated by the absence of interference. On the average, the signal power loss of IA caused by the interference suppression projections at the receivers has been measured in the simulation to be around 3dB. IA with imperfect  $\tilde{\mathbf{U}}$  and  $\tilde{\mathbf{V}}$  performs better than maximum EM transmission if the

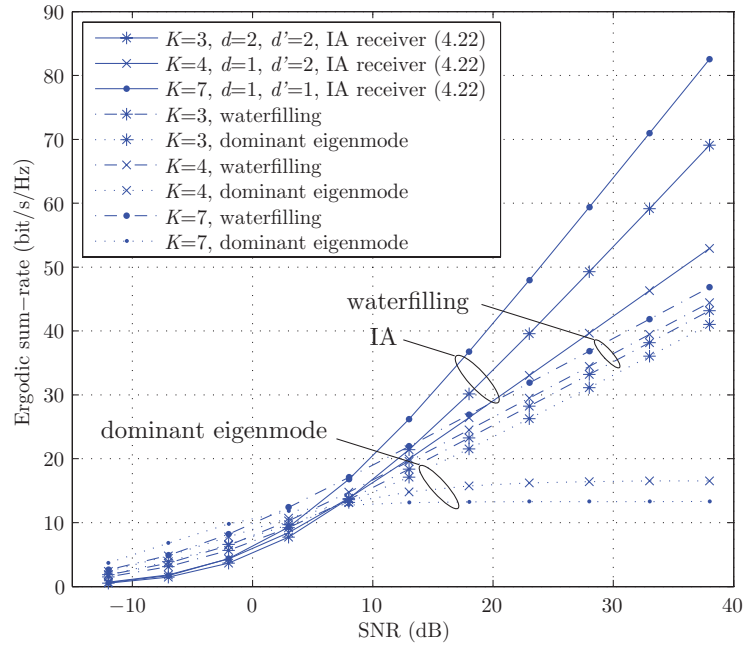


relative channel estimation error is above 16 dB. An improvement can be achieved by perfectly tracking the channel at each receiver.

Maximum EM transmission transmits one stream with full transmit power over the strongest EM of the MIMO channels corresponding to the direct links and therefore potentially creates a lot of uncoordinated interference for the other users. The effect of this interference leakage on the ergodic sum-rate per cell decreases for smaller values of  $\beta$ . The effect of imperfect  $\tilde{\mathbf{v}}_{\text{EM}}$  further decreases the sum-rate for  $\sigma_{\text{H}}^2/\sigma_{\text{E}}^2 < 15$  dB.



(a) Per user rate.



(b) Sum-rate.

Figure 4.7: DMT illustrated by the ergodic rates achieved by IA in a symmetric system with variable number of users and a fixed antenna configuration, i.e.  $N_T = 5$  and  $N_R = 3$ .

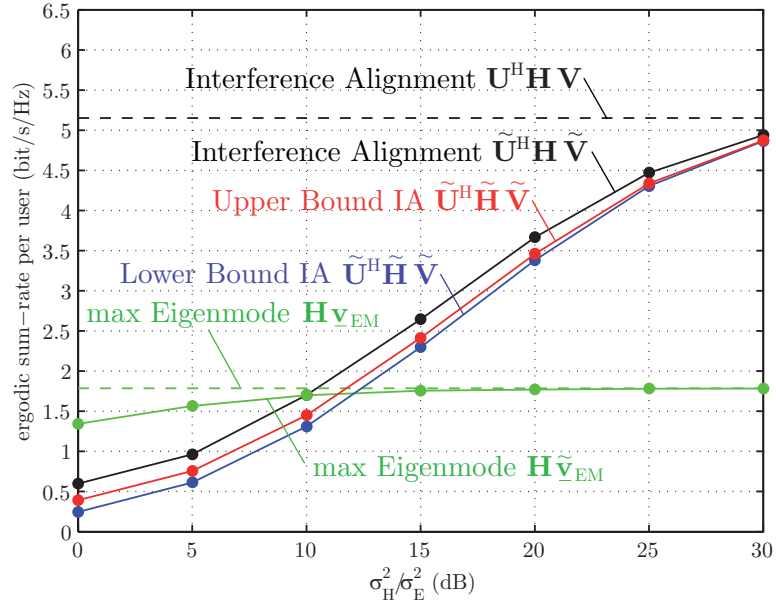


Figure 4.8: Ergodic rate per user for  $\beta = 1$  where IA is based on imperfect CSI along with bounds and comparison to opportunistic precoding.

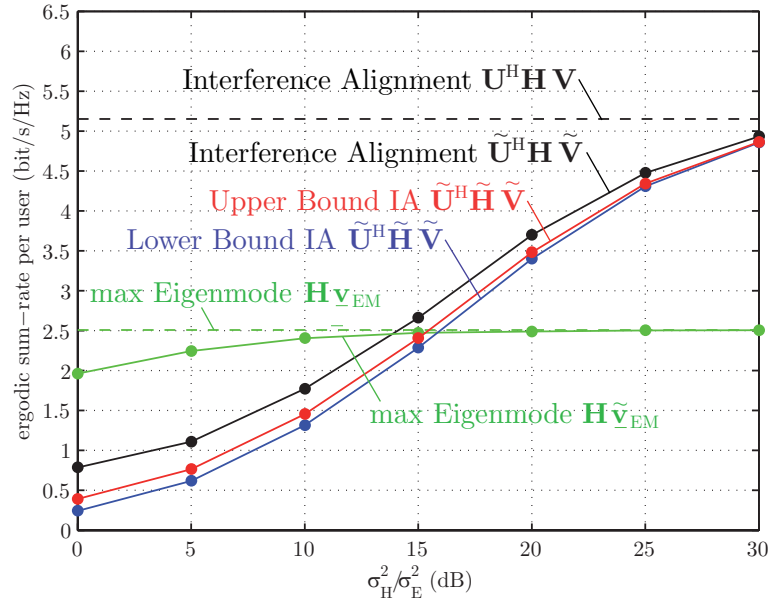


Figure 4.9: Ergodic rate per user for  $\beta = 0.5$  where IA is based on imperfect CSI along with bounds and comparison to opportunistic precoding.

## 4.6 Appendix: Proof of Theorem 4

The proof of Theorem 4 is outlined in the following subsections.

### 4.6.1 Lower Bound of the Ergodic Mutual Information

We focus on the mutual information  $I(\underline{\mathbf{s}}_i; \underline{\mathbf{y}}_i | \tilde{\mathbf{H}})$  given the estimated channels  $\tilde{\mathbf{H}}_{ii}$  and  $\tilde{\mathbf{H}}_{ij} \forall j \neq i$  at transmitter and receiver  $i$ . Expanding  $I(\underline{\mathbf{s}}_i; \underline{\mathbf{y}}_i | \tilde{\mathbf{H}} = \tilde{\mathbf{H}})$  into differential entropies yields

$$I(\underline{\mathbf{s}}_i; \underline{\mathbf{y}}_i | \tilde{\mathbf{H}} = \tilde{\mathbf{H}}) = h(\underline{\mathbf{s}}_i | \tilde{\mathbf{H}} = \tilde{\mathbf{H}}) - h(\underline{\mathbf{s}}_i | \underline{\mathbf{y}}_i, \tilde{\mathbf{H}} = \tilde{\mathbf{H}}). \quad (4.35)$$

We choose  $\underline{\mathbf{s}}_i$  given  $\tilde{\mathbf{H}}$  to be Gaussian, even though the Gaussian distribution may not be the one that maximizes the mutual information for the specific interference and noise distribution. Thus, we fix the value of  $h(\underline{\mathbf{s}}_i | \tilde{\mathbf{H}} = \tilde{\mathbf{H}}) = \log_2 \det(\pi e \mathbf{Q}_{\underline{\mathbf{s}}_i \underline{\mathbf{s}}_i})$  [51] and find an upper bound on  $h(\underline{\mathbf{s}}_i | \underline{\mathbf{y}}_i, \tilde{\mathbf{H}} = \tilde{\mathbf{H}})$  following [75]. The conditional distribution  $p(\underline{\mathbf{s}}_i | \underline{\mathbf{y}}_i, \tilde{\mathbf{H}})$  is not Gaussian. Using the fact that adding a constant does not change differential entropy, and that the entropy of a random variable with given variance is upper-bounded by the entropy of a Gaussian random variable with the same variance, we can derive an upper bound

$$h(\underline{\mathbf{s}}_i | \underline{\mathbf{y}}_i, \tilde{\mathbf{H}} = \tilde{\mathbf{H}}) \leq \log_2 \det(\pi e \mathbf{Q}_{\underline{\mathbf{g}} \underline{\mathbf{g}}}), \quad (4.36)$$

where  $\underline{\mathbf{g}} = \underline{\mathbf{s}}_i - \mathbf{A} \underline{\mathbf{y}}_i$  given  $\tilde{\mathbf{H}} = \tilde{\mathbf{H}}$ ,  $\mathbf{A}$  is any given matrix and  $\mathbf{Q}_{\underline{\mathbf{g}} \underline{\mathbf{g}}} = \mathbb{E}_{\underline{\mathbf{s}}_i, \underline{\mathbf{s}}_j, \tilde{\mathbf{E}}_{ii}, \tilde{\mathbf{E}}_{ij}, \tilde{\mathbf{n}}_i}[(\underline{\mathbf{s}}_i - \mathbf{A} \underline{\mathbf{y}}_i)(\underline{\mathbf{s}}_i - \mathbf{A} \underline{\mathbf{y}}_i)^H | \tilde{\mathbf{H}} = \tilde{\mathbf{H}}]$ . Since (4.36) holds for any  $\mathbf{A}$ , we may pick  $\mathbf{A}$  such that  $\mathbf{A} \underline{\mathbf{y}}_i$  is the linear minimum mean-square error (LMMSE) estimate of  $\underline{\mathbf{s}}_i$  in terms of  $\underline{\mathbf{y}}_i$  given  $\tilde{\mathbf{H}} = \tilde{\mathbf{H}}$ , in order to tighten the bound. Using the formula for the residual error of LMMSE estimation yields [76]

$$h(\underline{\mathbf{s}}_i | \underline{\mathbf{y}}_i, \tilde{\mathbf{H}} = \tilde{\mathbf{H}}) \leq \log_2 \det \left( \pi e \left( \mathbf{Q}_{\underline{\mathbf{s}}_i \underline{\mathbf{s}}_i} - \mathbf{Q}_{\underline{\mathbf{y}}_i \underline{\mathbf{s}}_i}^H \mathbf{Q}_{\underline{\mathbf{y}}_i \underline{\mathbf{y}}_i}^{-1} \mathbf{Q}_{\underline{\mathbf{y}}_i \underline{\mathbf{s}}_i} \right) \right), \quad (4.37)$$

with

$$\begin{aligned} \mathbf{Q}_{\underline{\mathbf{y}}_i \underline{\mathbf{s}}_i} &= \mathbb{E}_{\underline{\mathbf{s}}_i, \underline{\mathbf{s}}_j, \tilde{\mathbf{E}}_{ii}, \tilde{\mathbf{E}}_{ij}, \tilde{\mathbf{n}}_i}[\underline{\mathbf{y}}_i \underline{\mathbf{s}}_i^H | \tilde{\mathbf{H}} = \tilde{\mathbf{H}}] = \tilde{\mathbf{H}}_{ii} \mathbf{Q}_{\underline{\mathbf{s}}_i \underline{\mathbf{s}}_i}, \\ \mathbf{Q}_{\underline{\mathbf{y}}_i \underline{\mathbf{y}}_i} &= \mathbb{E}_{\underline{\mathbf{s}}_i, \underline{\mathbf{s}}_j, \tilde{\mathbf{E}}_{ii}, \tilde{\mathbf{E}}_{ij}, \tilde{\mathbf{n}}_i}[\underline{\mathbf{y}}_i \underline{\mathbf{y}}_i^H | \tilde{\mathbf{H}} = \tilde{\mathbf{H}}] = \tilde{\mathbf{H}}_{ii} \mathbf{Q}_{\underline{\mathbf{s}}_i \underline{\mathbf{s}}_i} \tilde{\mathbf{H}}_{ii}^H + \sigma_E^2 \text{Tr}(\mathbf{Q}_{\underline{\mathbf{s}}_i \underline{\mathbf{s}}_i}) \mathbf{I}_{d_i} + \\ &\quad \sum_{j \neq i} \sigma_E^2 \text{Tr}(\mathbf{Q}_{\underline{\mathbf{s}}_j \underline{\mathbf{s}}_j}) \mathbf{I}_{d_i} + \mathbf{I}_{d_i}. \end{aligned} \quad (4.38)$$

Hence a lower bound of the mutual information given  $\tilde{\mathbf{H}} = \tilde{\mathbf{H}}$  can be derived by inserting (4.37) into (5.3) which leads to

$$I(\mathbf{s}_i; \bar{\mathbf{y}}_i | \tilde{\mathbf{H}} = \tilde{\mathbf{H}}) \geq \log_2 \det \left( \mathbf{Q}_{\mathbf{s}_i \mathbf{s}_i} \left( \mathbf{Q}_{\mathbf{s}_i \mathbf{s}_i} - \mathbf{Q}_{\bar{\mathbf{y}}_i \mathbf{s}_i}^H \mathbf{Q}_{\bar{\mathbf{y}}_i \bar{\mathbf{y}}_i}^{-1} \mathbf{Q}_{\bar{\mathbf{y}}_i \mathbf{s}_i} \right)^{-1} \right). \quad (4.39)$$

If we assume that  $\mathbf{Q}_{\mathbf{s}_i \mathbf{s}_i} = (\rho_i/d_i) \mathbf{I}_{d_i} \forall i$ , we can further simplify (4.39) using the Woodbury identity, and derive the bound on the ergodic mutual information as follows

$$I(\mathbf{s}_i; \bar{\mathbf{y}}_i | \tilde{\mathbf{H}}) \geq \mathbb{E}_{\tilde{\mathbf{H}}} \left[ \log_2 \det \left( \frac{1}{\sigma_E^2 d_i \rho_i + 1} \left( \rho_i \tilde{\mathbf{H}}_{ii} \tilde{\mathbf{H}}_{ii}^H + \left( \sigma_E^2 \rho_i + \sum_{j \neq i} \sigma_E^2 \rho_j + 1 \right) \mathbf{I}_{d_i} \right) \right) \right]. \quad (4.40)$$

#### 4.6.2 Upper Bound of the Ergodic Mutual Information

Expanding  $I(\mathbf{s}_i; \bar{\mathbf{y}}_i | \tilde{\mathbf{H}} = \tilde{\mathbf{H}})$  into differential entropies yields

$$I(\mathbf{s}_i; \bar{\mathbf{y}}_i | \tilde{\mathbf{H}} = \tilde{\mathbf{H}}) = h(\bar{\mathbf{y}}_i | \tilde{\mathbf{H}} = \tilde{\mathbf{H}}) - h(\bar{\mathbf{y}}_i | \mathbf{s}_i, \tilde{\mathbf{H}} = \tilde{\mathbf{H}}). \quad (4.41)$$

We upper bound the first term of the right-hand side (RHS) of (5.4) by the differential entropy of a Gaussian random variable with the same variance as  $\bar{\mathbf{y}}_i$  given  $\tilde{\mathbf{H}} = \tilde{\mathbf{H}}$  [77], i.e.,

$$h(\bar{\mathbf{y}}_i | \tilde{\mathbf{H}} = \tilde{\mathbf{H}}) \leq \log_2 \det \left( \pi e \mathbf{Q}_{\bar{\mathbf{y}}_i \bar{\mathbf{y}}_i} \right), \quad (4.42)$$

with  $\mathbf{Q}_{\bar{\mathbf{y}}_i \bar{\mathbf{y}}_i} = \mathbb{E}_{\mathbf{s}_i, \mathbf{s}_j, \bar{\mathbf{E}}_{ii}, \bar{\mathbf{E}}_{ij}, \bar{\mathbf{n}}_i} [\bar{\mathbf{y}}_i \bar{\mathbf{y}}_i^H | \tilde{\mathbf{H}} = \tilde{\mathbf{H}}]$ . Using the fact that conditioning reduces entropy we lower bound  $h(\bar{\mathbf{y}}_i | \mathbf{s}_i, \tilde{\mathbf{H}})$  with  $h(\bar{\mathbf{y}}_i | \mathbf{s}_1, \dots, \mathbf{s}_K, \tilde{\mathbf{H}})$ . Since we have shown that  $\bar{\mathbf{E}}_{ij} \forall (i, j)$  is Gaussian,  $\bar{\mathbf{y}}_i$  given  $\mathbf{s}_1, \dots, \mathbf{s}_K, \tilde{\mathbf{H}}$  is a Gaussian random variable  $\bar{\mathbf{y}}'_i$  with mean  $\tilde{\mathbf{H}}_{ii} \mathbf{s}_i$  and covariance

$$\mathbf{Q}_{\bar{\mathbf{y}}'_i \bar{\mathbf{y}}'_i} = \mathbb{E}_{\bar{\mathbf{E}}_{ii}, \bar{\mathbf{E}}_{ij}, \bar{\mathbf{n}}_i} [\bar{\mathbf{y}}_i \bar{\mathbf{y}}_i^H | \mathbf{s}_1, \dots, \mathbf{s}_K, \tilde{\mathbf{H}}] = \left( \sigma_E^2 \left( \sum_{j=1}^K \|\mathbf{s}_j\|^2 \right) + 1 \right) \mathbf{I}_{d_i}, \quad (4.43)$$

where we used the fact that all  $\bar{\mathbf{E}}_{ij} \forall (i, j)$  and  $\bar{\mathbf{n}}_i$  are independent. Thus, using (4.42) and the definition of conditional entropy yields

$$I(\mathbf{s}_i; \bar{\mathbf{y}}_i | \tilde{\mathbf{H}}) \leq \mathbb{E}_{\tilde{\mathbf{H}}} \left[ \log_2 \det \left( \pi e \mathbf{Q}_{\bar{\mathbf{y}}_i \bar{\mathbf{y}}_i} \right) \right] - \mathbb{E}_{\mathbf{s}_1, \dots, \mathbf{s}_K} \left[ \log_2 \det \left( \pi e \mathbf{Q}_{\bar{\mathbf{y}}'_i \bar{\mathbf{y}}'_i} \right) \right], \quad (4.44)$$

where the second expectation can be further simplified to

$$\mathbb{E}_{\mathbf{s}_1, \dots, \mathbf{s}_K} \left[ \log_2 \det \left( \pi e \mathbf{Q}_{\bar{\mathbf{y}}'_i \bar{\mathbf{y}}'_i} \right) \right] = d_i \log_2 (\pi e) + d_i \left( \mathbb{E}_{\mathbf{s}_1, \dots, \mathbf{s}_K} \left[ \log_2 \left( \sigma_E^2 \left( \sum_{j=1}^K \|\mathbf{s}_j\|^2 \right) + 1 \right) \right] \right).$$

We can further derive a closed form expression for the second expectation of the RHS of (4.44) for the special case where all  $\rho_j$  and all  $d$  are equal. We then can sum up the chi-square random variables  $\|\mathbf{s}_j\|^2(d/\rho_j)$  with  $2d$  degrees of freedom in the RHS of (4.43), i.e.,  $\xi = \sum_j \|\mathbf{s}_j\|^2(d/\rho_j)$  which has a chi-square distribution with  $2n = K2d$  degrees of freedom. This yields

$$\begin{aligned} \mathbb{E}_{\mathbf{s}_1, \dots, \mathbf{s}_K} \left[ \log_2 \det \left( \pi e \mathbf{Q}_{\bar{\mathbf{y}}'_i \bar{\mathbf{y}}'_i} \right) \right] &= d_i \log_2 (\pi e) + d_i \mathbb{E}_\xi \left[ \log_2 \left( \sigma_E^2 \frac{\rho_i}{d_i} \xi + 1 \right) \right] \\ &= d_i \log_2 (\pi e) + d_i \exp \left( \frac{d_i}{\sigma_E^2 \rho_i} \right) \log_2(e) \sum_{p=1}^n E_p \left( \frac{d_i}{\sigma_E^2 \rho_i} \right), \end{aligned} \tag{4.45}$$

where the last equality is from [74].

## 5 Interference Alignment in Cellular Networks

In this chapter, we consider a large cellular network with an arbitrary number of base stations equipped with multiple antennas. We evaluate the applicability of interference alignment methods to cases representative of upcoming cellular networks. This approach is motivated by the fact that, in the current generation of cellular systems, the density of the base stations and frequency reuse factors are such that the system is in most cases interference limited.

We assume that the base stations serve the users within their cell using orthogonal resource sharing. Therefore, users within the same cell do not interfere with each other whereas interference is caused by users in neighboring cells scheduled within the same resource block. We group the base stations into cooperating clusters. The clusters form a partition of the set of all base stations. Each cluster of base stations and their associated users scheduled within the same resource block form a MIMO interference channel. We propose clustered interference alignment within the group of cooperating base stations in the spatial domain while the rest of the network contributes non-aligned interference.

This strategy reduces backhaul communication among the base stations since channel state information has to be exchanged solely inside the clusters. Compared to joint transmit cooperation schemes such as network MIMO, we further save system resources that would be used for sharing the user payload data. Synchronous data exchange between  $K$  base stations would result in a  $K$ -fold increase of backhaul capacity. Using the alignment-based transmit strategy, precoding is performed locally at each base station and based only on the in cell user data.

We have shown in Chapter 4 that interference alignment based strategies over the  $K$ -user IC perform optimal in the high SNR regime, based on the assumption that all links in the network are subject to an average interference power of similar level. For the downlink of cellular networks, however, the practical range of SNR is  $5 \sim 20$  dB and interference power levels can vary by several orders of magnitude [78]. In the considered cellular network, we introduce a distance dependent pathloss factor for each link in the network, which captures more practical network deployments.

Instead of the SNR investigated in a  $K$ -user IC, the signal-to-residual interference ratio after receive filtering becomes the relevant figure of merit, due to the presence of non-aligned interference.

Interference alignment in cellular networks was considered in [79] for single-antenna terminals. The system model is comprised of  $G$  base stations, each of which simultaneously serves  $K$ -users within their cell. The model is referred to as interfering broadcast channel and the users suffer from out-of-cell and intra-cell interference. The authors of [79] show that with asymptotically many users  $K$  per cell, it is possible to approach the interference free DoF if all the  $G$  base stations cooperate. However, increasing the number of base stations  $G$  leads to long symbol extensions and the optimality of the proposed alignment scheme is restricted to the high SNR regime. Uncoordinated interference and a pathloss model is omitted in their analysis.

In our proposed clustered base station cooperation scheme, alignment is performed over the constant MIMO channel, prohibiting large symbol extensions. Furthermore, the feasibility conditions derived in Subsection 4.2.1 and the constructive alignment procedures introduced in Subsection 4.3.2 for special network settings as well as the iterative alignment algorithms described in 4.3.1 for all feasible network settings can be applied. In our model, uncoordinated interference originates from bases stations outside of the cooperating cluster.

The road map of this chapter is: We describe the model for clustered base station cooperation in Section 5.1. Feasible cluster settings and the number of antennas that need to be deployed per base station and mobile terminal are determined. In Section 6.5, we compare the performance of the proposed technique to a classical non-cooperative cellular network model, where interference is mitigated though fractional frequency reuse, while eigenwaterfilling is applied independently inside each cell (see for example [48] and references therein for descriptions of such techniques). We show improvements in terms of throughput for users located close to the base-station and an overall improvement of cell spectral efficiency of multicell alignment-based cooperation.

Results presented in this chapter were first published in [80] and [81].

## 5.1 Large Cellular Network Model

Let us consider the downlink of a cellular system. We assume intra-cell orthogonality between users. The system is assumed to incorporate  $N$  cells. Each cell is comprised of one base station with  $N_T$  transmit antennas serving one user equipped with  $N_R$  antennas within a resource block, over a frequency-flat MIMO channel. We consider the application of interference alignment in this context, involving a cluster of  $K$  base



stations among the  $N$  in the network. Hence, each cluster forms a  $K$ -user interference channel. An example of this setting are fourth-generation (4G) cellular systems based on orthogonal frequency division multiple-access (OFDMA), such as LTE-Advanced [82], the successor of the Universal Mobile Telecommunications System (UMTS) Long-Term Evolution (LTE) or WiMAX [83]. Thanks to the frequency orthogonality introduced by the OFDMA physical layer, we can apply interference alignment independently for each OFDM subband.

Under the assumption that the channel coefficients representing the MIMO channels between base stations and users within the cluster are drawn independently from a continuous distribution, the feasibility condition (4.7) derived in Subsection 4.2.1 show that the existence (with probability one) of a interference alignment solution depends solely on the dimensions of the problem  $(K, N_T, N_R, d_1 \dots d_K)$ , and not on the particular channel realization. In the particular case of clustered IA with multiplexing gain allocation  $d_1 = \dots = d_K = 1$  without receive diversity, solutions exist for the  $K$ -user interference channel if and only if

$$N_R + N_T - 1 \geq K. \quad (5.1)$$

Therefore, even for networks with a large number of cells  $N$ , the size  $K$  of a cluster of base stations involved in interference alignment is limited by (5.1) if the number of antennas  $N_T$  and  $N_R$  remain fixed. In the sequel, we analyze the operation of a cluster of  $K$  base stations (assumed geographically close to each other, since in a cellular network, interference is practically dominated by neighboring base stations [84]), in a network of  $N$  base stations, with  $N \gg K$ .

### 5.1.1 Clustered Base Station Cooperation

We propose cooperation within a finite set of base stations. Let us consider a cluster of cooperating base stations denoted by  $\Psi$  and its complement set, comprised of noncooperative base stations, by  $\Psi^c$ . We focus on the communication taking place in a cell  $i \in \Psi$ . Channel state information is exchanged within the cluster. By virtue of the intra-cluster interference alignment method, interference from neighboring base station within the set  $\Psi$  can be suppressed, but uncoordinated interference from all the other base stations within the cellular network  $\Psi^c$  is accumulated at receiver  $i$ . Fig. 5.1 shows a large network with interference coordination among three cells. The shaded area of the cells represents the cooperation horizon. In most practical scenarios, the strength of the interfering signals of distant transmitters is significantly decreased by the path loss, and the interference at receiver  $i$  is dominated by the base stations in the immediate vicinity [84]. The received signal of user  $i$  after interference

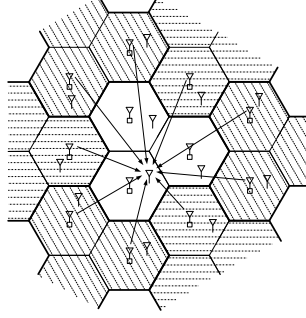


Figure 5.1: Large cellular network with base station cooperation, i.e. the three cells in the middle do not interfere with each other.

suppression filtering yields

$$\begin{aligned}
 \bar{\mathbf{y}}_i &= \sqrt{\gamma_{ii}} \mathbf{u}_i^H \mathbf{H}_{ii} \mathbf{v}_i s_i + \sum_{\substack{j \in (\Psi \cup \Psi^c) \\ j \neq i}} \sqrt{\gamma_{ij}} \mathbf{u}_i^H \mathbf{H}_{ij} \mathbf{v}_j s_j + \mathbf{u}_i^H \mathbf{n}_i \\
 &= \sqrt{\gamma_{ii}} \mathbf{u}_i^H \mathbf{H}_{ii} \mathbf{v}_i s_i + \sum_{j \in \Psi^c} \sqrt{\gamma_{ij}} \mathbf{u}_i^H \mathbf{H}_{ij} \mathbf{v}_j s_j + \bar{\mathbf{n}}_i,
 \end{aligned} \tag{5.2}$$

where  $s_j \in \mathbb{C}$  is the transmit signal of transmitter  $j$ , and  $\mathbf{v}_j \in \mathbb{C}^{N_T \times 1}$  is the associated precoding vector.  $[\mathbf{H}_{ij}]_{i,j=1 \dots K}$  are complex  $N_R \times N_T$  matrices representing the MIMO channels between transmitter  $j$  and receiver  $i$ .  $\gamma_{ij}$  is the path-loss coefficient on the same link. The second equality in (5.2) follows from the fact that the interference from transmitters within  $\Psi$  is perfectly suppressed, due to the alignment condition (4.4) introduced in Section 4.2.

Having derived the expression of the received signal of user  $i$ , let us continue with the throughput analysis. The mutual information  $I(s_i; \bar{\mathbf{y}}_i | \mathbf{H})$  given perfect channel state information, expanded into differential entropies yields

$$I(s_i; \bar{\mathbf{y}}_i | \mathbf{H}) = h(\bar{\mathbf{y}}_i | \mathbf{H}) - h(\bar{\mathbf{y}}_i | s_i, \mathbf{H}). \tag{5.3}$$

$\mathbf{H}$  in the above expectation is the short hand notation for the set of all MIMO channels, i.e.  $[\mathbf{H}]_{(i,j) \in (\Psi \cup \Psi^c)}$ . If we denote  $\bar{\mathbf{t}}_i$  as the interference plus noise term in (5.2), we can write [51]

$$I(s_i; \bar{\mathbf{y}}_i | \mathbf{H}) = \log_2 \det(\pi e \mathbf{Q}_{\bar{\mathbf{y}}_i \bar{\mathbf{y}}_i}) - \log_2 \det(\pi e \mathbf{Q}_{\bar{\mathbf{t}}_i \bar{\mathbf{t}}_i}), \tag{5.4}$$

with

$$\begin{aligned}\mathbf{Q}_{\bar{\mathbf{y}}_i \bar{\mathbf{y}}_i} &= \mathbb{E}_{s_i, s_j, \bar{\mathbf{n}}_i} [\bar{\mathbf{y}}_i \bar{\mathbf{y}}_i^H] = \gamma_{ii} \mathbf{U}_i^H \mathbf{H}_{ii} \mathbf{V}_i \mathbf{Q}_{s_i s_i} \mathbf{V}_i^H \mathbf{H}_{ii}^H \mathbf{U}_i + \\ &\quad \sum_{j \in \Psi^c} \gamma_{ij} \mathbf{U}_i^H \mathbf{H}_{ij} \mathbf{V}_j \mathbf{Q}_{s_j s_j} \mathbf{V}_j^H \mathbf{H}_{ij}^H \mathbf{U}_i + \sigma_n^2 \mathbf{I}_{d_i}, \\ \mathbf{Q}_{\bar{\mathbf{t}}_i \bar{\mathbf{t}}_i} &= \mathbb{E}_{s_j, \bar{\mathbf{n}}_i} [\bar{\mathbf{t}}_i \bar{\mathbf{t}}_i^H] = \sum_{j \in \Psi^c} \gamma_{ij} \mathbf{U}_i^H \mathbf{H}_{ij} \mathbf{V}_j \mathbf{Q}_{s_j s_j} \mathbf{V}_j^H \mathbf{H}_{ij}^H \mathbf{U}_i + \sigma_n^2 \mathbf{I}_{d_i},\end{aligned}\quad (5.5)$$

where we used the fact that  $s_i, s_j$  and  $\bar{\mathbf{n}}_i$  are jointly Gaussian and  $\mathbb{E}_{\bar{\mathbf{n}}_i} [\bar{\mathbf{n}}_i \bar{\mathbf{n}}_i^H] = \sigma_n^2 \mathbf{I}_{d_i}$ . Let us consider the ergodic mutual information, achievable by a user at a given position, i.e. the expectation of  $I(s_i; \bar{\mathbf{y}}_i | \mathbf{H})$  over the fading. The mutual information is a function of the relative position of receiver  $i$  and transmitters  $j$  via the path loss model  $\gamma_{ij}$ . Let us denote the random position of user  $i$  by  $p_i$ . We neglect the noise term in (5.5), since our focus is on the interference-limited scenario. Furthermore, we can simplify (5.4) by noticing that  $\mathbf{Q}_{\bar{\mathbf{t}}_i \bar{\mathbf{t}}_i}$  appears as a summand in  $\mathbf{Q}_{\bar{\mathbf{y}}_i \bar{\mathbf{y}}_i}$  and is invertible. Hence, the average achievable rate of user  $i$  at position  $p_i$  is

$$R_{i, \mathbf{IA}}(p_i) = \mathbb{E}_{\mathbf{H}} \left[ \log_2 \det \left( \mathbf{I}_{d_i} + \bar{\mathbf{H}}_{ii} \mathbf{Q}_{s_i s_i} \bar{\mathbf{H}}_{ii}^H \left( \sum_{j \in \Psi^c} \bar{\mathbf{H}}_{ij} \mathbf{Q}_{s_j s_j} \bar{\mathbf{H}}_{ij}^H \right)^{-1} \right) \right], \quad (5.6)$$

where we denoted  $\bar{\mathbf{H}}_{ij} = \sqrt{\gamma_{ij}} \mathbf{U}_i^H \mathbf{H}_{ij} \mathbf{V}_j \forall (i, j)$  and used the fact that  $\log_2 \det(\pi e(\mathbf{A} + \mathbf{B})) - \log_2 \det(\pi e \mathbf{B}) = \log_2 \det(\mathbf{I} + \mathbf{A} \mathbf{B}^{-1})$  if  $\mathbf{B}$  is invertible. The expectation above is taken over the channel realizations experienced at position  $p_i$ .

## 5.2 Simulation Results

In this section, we present simulation results for two clustered interference alignment scenarios as outlined in Section 5.1.1 and compare to the performance of a frequency reuse scheme that is described in the following.

### 5.2.1 Frequency Reuse Scheme

In order to provide an element of comparison for the clustered interference alignment scheme, we derive the rate of user  $i$  in the large network where frequency reuse is employed. The system bandwidth is split into  $1/\kappa$  non-overlapping bands and the base stations transmit on a fixed band. Channel state information at the transmitter is exploited independently inside of each cell. Fig. 5.2 shows a network with hexagonal cells and frequency reuse factor  $\kappa = 1/3$ . The shaded area of the cells represents the

different frequency bands. Let us partition the set of base stations according to the frequency they are using, and denote those  $1/\kappa$  partitions by  $\Psi_\ell$ , with  $\ell = 1 \dots 1/\kappa$ . The sources of interference for a user in cell  $i \in \Psi_\ell$  are therefore the base stations  $j \in \Psi_\ell$  s.t.  $j \neq i$ . Network planning normally allocates different frequency bands to cells in the immediate vicinity of each other.

We use spatial multiplexing with waterfilling (WF) power allocation within each cell. Therefore, the receive signal of user  $i \in \Psi_\ell$  yields

$$\underline{\mathbf{y}}_i = \sum_{j \in \Psi_\ell} \sqrt{\gamma_{ij}} \mathbf{H}_{ij} \underline{\mathbf{s}}_j + \underline{\mathbf{n}}_i. \quad (5.7)$$

Let us derive the mutual information between  $\underline{\mathbf{s}}_i$  and  $\underline{\mathbf{y}}_i$  under perfect channel knowledge (and again neglecting the noise term in (5.7), in the interference-limited case). The average achievable rate of user  $i$  at position  $p_i$  can be written as

$$R_{i,\mathbf{WF}}(p_i) = \mathbb{E}_{\mathbf{H}} \left[ \kappa \cdot \log_2 \det \left( \mathbf{I}_{N_R} + \gamma_{ii} \mathbf{H}_{ii} \mathbf{Q}_{\mathbf{WF},i} \mathbf{H}_{ii}^H \left( \sum_{j \in \Psi_\ell} \gamma_{ij} \mathbf{H}_{ij} \mathbf{Q}_{\mathbf{WF},j} \mathbf{H}_{ij}^H \right)^{-1} \right) \right], \quad (5.8)$$

where the covariance of the transmitted signals  $\mathbf{Q}_{\mathbf{WF},i} = \mathbb{E}_{\tilde{\mathbf{s}}_i} [\tilde{\mathbf{s}}_i \tilde{\mathbf{s}}_i^H]$  is chosen according to the eigenwaterfilling technique, independently in each cell. The covariance of the interference received from base stations  $j \in \Psi_\ell$ ,  $j \neq i$ , necessary to solve the eigenwaterfilling equations, is approximated by assuming that all interference sources are spatially white, but their powers are known exactly.

Comparing (5.8) to (5.6), the power budget per active base station is increased by  $1/\kappa$  (yielding  $\text{Tr}(\mathbf{Q}_{\mathbf{WF},i}) = (1/\kappa) \cdot \rho_i$ ), since only a fraction  $\kappa$  of the base stations are transmitting on a given frequency band. Conversely, in (5.8), the frequency reuse factor  $\kappa$  is pre-multiplying the instantaneous rate of user  $i$ . This accounts for the fact that only a fraction  $\kappa$  of the system bandwidth can be used per base station.

### 5.2.2 Performance Evaluation

In this subsection, we present simulation results for a hexagonal wrap-around-cell layout. The whole network consists of  $N > K$  hexagonal cells on a regular grid, with the considered cluster  $\Omega$  in the center. Base stations are assumed to be equipped with omnidirectional antennas (i.e. no sectoring is considered). The user positions are drawn independently according to a uniform distribution inside the area of the cells. In the interference alignment scheme, the transmit power  $\rho_i$  of each base station is transmitted in the direction set by  $\mathbf{V}_i$  (a vector in this case, since  $d_i = 1$ ).

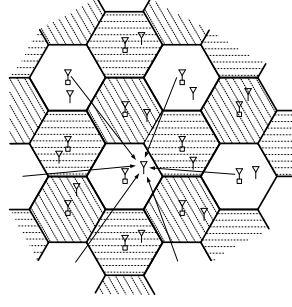


Figure 5.2: Large cellular network with frequency reuse three, i.e. interference originates from cells with the same color.

|                        | $K$ | $N$ | $N_T$ | $N_R$ |
|------------------------|-----|-----|-------|-------|
| Cooperation Scenario A | 3   | 27  | 2     | 2     |
| Cooperation Scenario B | 7   | 37  | 6     | 2     |

Table 5.1: Parameters for the considered scenarios with cooperation among  $K$  base stations along with the number of antennas needed for IA.

Two scenarios for alignment-based base station cooperation are considered, both with receivers equipped with  $N_R = 2$  antennas, reflecting realistic hardware constraints, and with unit multiplexing gains  $d_1 = \dots = d_K = 1$ . Under these assumption, the maximum number of base stations in the cluster allowed by (5.1) becomes  $K = N_T + 1$ . In scenario A, three base stations each equipped with  $N_T = 2$  antennas cooperate, while in scenario B,  $K = 7$  base stations with  $N_T = 6$  antennas are considered. Table 5.1 lists the details of the parameters for the considered scenarios, while the system parameters are described in Table 5.2. Note that for both cooperation scenarios, two rings of interfering base stations which model non-coordinated interference. We assume a Rayleigh fading channel model, i.e.  $\mathbf{H}_{ij} \in \mathbb{C}^{N_R \times N_T}$  are i.i.d.  $\mathcal{CN}(0, 1) \forall (i, j)$ .

For each position  $p_i$  inside the cluster, we average the achievable rate according to (5.6) over the channel realizations, and compare it to that achieved by the non-cooperative eigenwaterfilling scheme with frequency reuse 1/3, as given by (5.8). Fig. and Fig. we plot the ergodic rates for the two network scenarios whereas in Fig 5.5 we consider the ratio  $(R_{i,\mathbf{IA}}/R_{i,\mathbf{WF}})(p_i)$  of those quantities as our comparison metric.

Fig. 5.3(a) shows the ergodic throughput  $R_{i,\mathbf{IA}}$  of the clustered interference alignment scheme for cooperation scenario A. The x-y grid scale is in meters. Users located near the base station achieve an ergodic throughput of up to 16 bit/s/Hz whereas

| Parameter                     | Value  |
|-------------------------------|--|
| Transmit Power per Subcarrier | $\rho_i = 17 \text{ dBm } \forall i$                                       |
| Path Loss Model               | $\gamma_{ij} = 128.1 + 37.6 \cdot \log_{10}(r_{ij}[\text{km}]) \text{ dB}$ |
| Path Loss Exponent            | $\alpha = 3.76$  |
| Cell Radius                   | $r = 1 \text{ km}$   |
| Antenna Pattern               | uniform  |
| Frequency Reuse Factor        | $\kappa = 1/3$   |

Table 5.2: System parameters for the considered large cellular network with hexagonal cells.

users at the cluster edge achieve an ergodic throughput of 1 bit/s/Hz. The throughput decay towards the cell edge shows the characteristics of the pathloss. The ergodic throughput of the non-cooperative eigenwaterfilling scheme  $R_{i,\mathbf{WF}}$  ranges from 13 bit/s/Hz near the base station to 2 bit/s/Hz at the cell edge.

Fig. 5.4(b) shows the ergodic throughput  $R_{i,\mathbf{IA}}$  of the clustered interference alignment scheme for cooperation scenario B. Users located near the base station achieve an ergodic throughput of up to 16 bit/s/Hz (17.5 bit/s/Hz for the central cell) whereas users at the cluster edge achieve an ergodic throughput of 1 bit/s/Hz. The users at the cell edge between cooperating cells achieve an ergodic throughput of 2 bit/s/Hz. The throughput decay towards the cell edge shows the characteristics of the pathloss. The ergodic throughput of the non-cooperative eigenwaterfilling scheme  $R_{i,\mathbf{WF}}$  ranges from 14 bit/s/Hz near the base station to 2 bit/s/Hz at the cell edge.

Fig. 5.5(a) shows the relative ergodic throughput gain for cooperation scenario A. The grid scale is in meters. Users located near the base station experience an ergodic throughput gain of up to 30% if the clustered base station coordination scheme is employed. Users located in the central area of the cluster experience a minor ergodic throughput gain, whereas the ergodic throughput gain of users at the edge of the cluster decreases significantly.

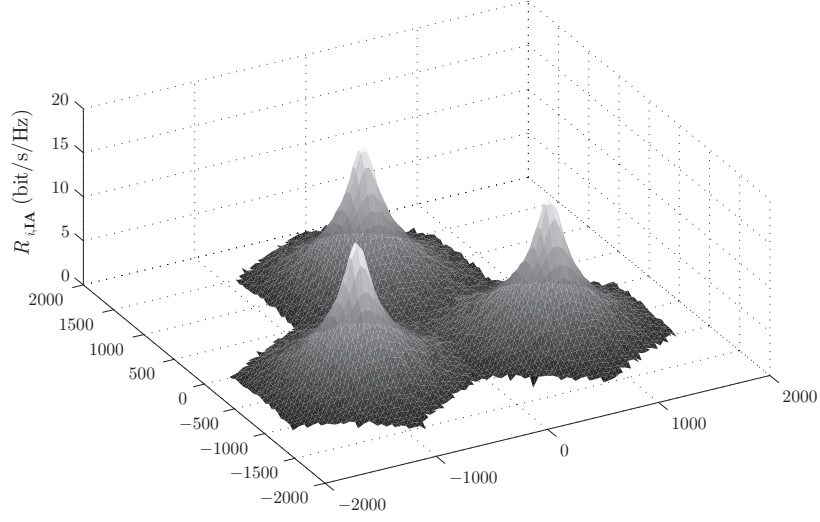
Fig. 5.5(b) shows the relative ergodic throughput gain for cooperation scenario B. Any user in the central cell experiences a positive throughput gain w.r.t. the non-cooperating scheme with frequency reuse. Averaged over all random positions inside the central cell, the throughput gain is 20%. Users located in the central area of the other six cells experience throughput gains, whereas the ergodic throughput of users at the edge of the cluster is significantly lower than in the non-cooperative, frequency reuse scheme.

For users located in the central area of the cell, both clustered base station cooperation scenarios outperform the frequency reuse scheme. An intuitive interpretation of this result is the following. The alignment of dominant interference from neighboring base stations in the cooperation scenarios increases the signal-to-interference ratio (SIR) of those users. Using the interference suppression matrix of the IA scheme, the energy of the signal part that lies in the interference subspace is lost. However, this loss is not dominant in the high SIR regime (bandwidth limited) since the users can simultaneously access the whole spectrum. On the other hand, the pre-log factor  $\kappa$  of the achievable rate (5.8) of the frequency reuse scheme significantly influences the throughput in this high signal-to-interference ratio (SIR) regime. The SIR of the user in the central cell in scenario B is further increased by the fact that the interference from all the adjacent base stations is perfectly suppressed.

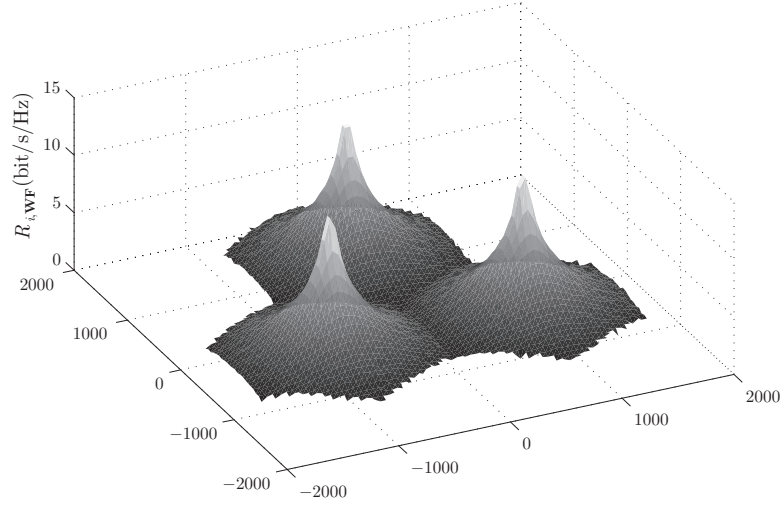
For users located at the edge of the cluster, the situation is obviously less beneficial, since they receive interference from base stations in close proximity which are not included in the cluster. For those users, the numerator of the SIR benefits from the higher multiplexing gain of the eigenwaterfilling-based scheme, while the interference is kept low by the splitting of the spectrum. The pre-log factor in (5.8) does not dominate the performance in the low SIR regime. The uncoordinated interference from 4 adjacent cells (scenario A) and 3 adjacent cells (scenario B), significantly decreases the performance of clustered IA schemes at the cluster edge.

The cell spectral efficiency defined as the throughput summed over all user positions in the cell is numerically evaluated using the simulated throughput curves. The spectral efficiency gain of the clustered interference alignment scheme with respect to non-cooperative eigenwaterfilling is approximately 16% for cluster scenario A and 12% for cluster scenario B. The spectral efficiency gain of the center cell of scenario B is 30%.

Those results show that in a large network with uniform cell locations, only certain areas can benefit from the proposed spatial interference alignment scheme, since it is not possible for all base stations in the network to participate in the alignment. However, for certain non-uniform network topologies, with certain hot spots characterized by high user density, and other areas with lower densities (and presumably non-regular cell shapes), implementation of the proposed clustered interference alignment scheme around the hot spots might be beneficial, the uncoordinated interference remaining limited to areas with low user densities.



(a)  $R_{i,\mathbf{IA}}$  of clustered interference alignment scheme.



(b)  $R_{i,\mathbf{WF}}$  of non-cooperative eigenwaterfilling scheme.

Figure 5.3: Ergodic throughput [bit/s/Hz] for cluster scenario A where cooperation among  $K = 3$  base stations is established in the presence of uncoordinated interference of  $N - K = 24$  neighboring base stations.



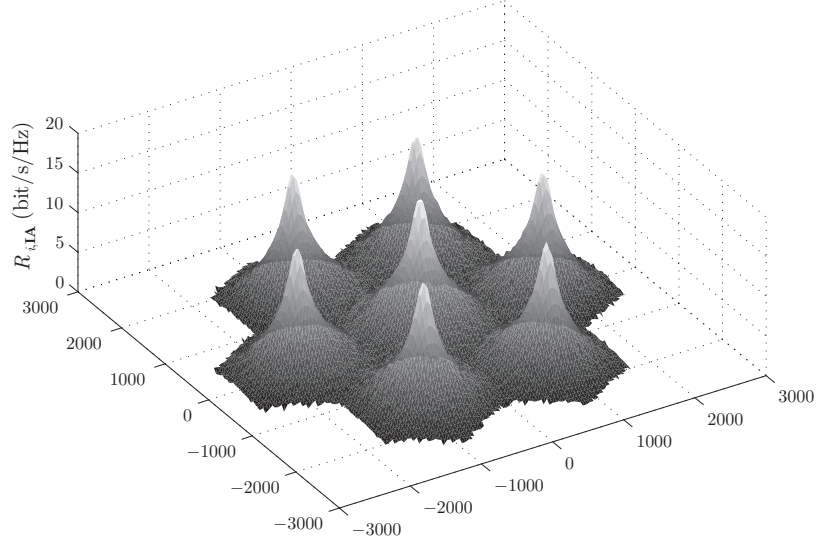
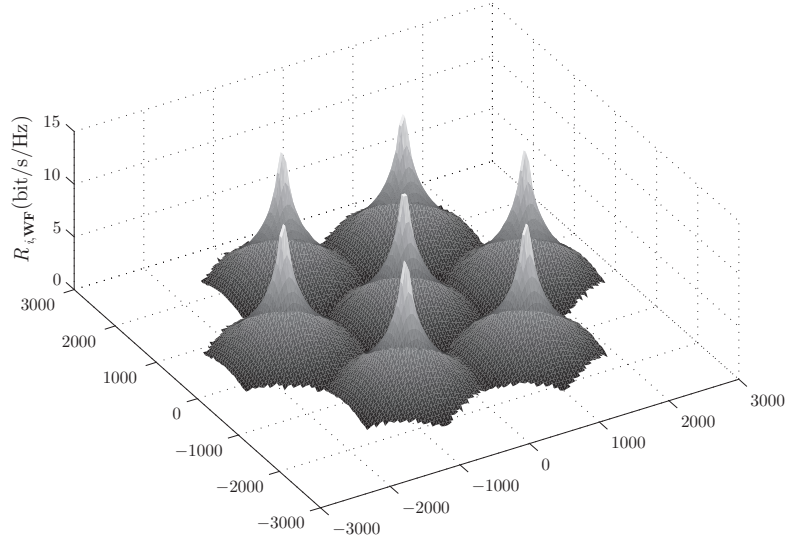
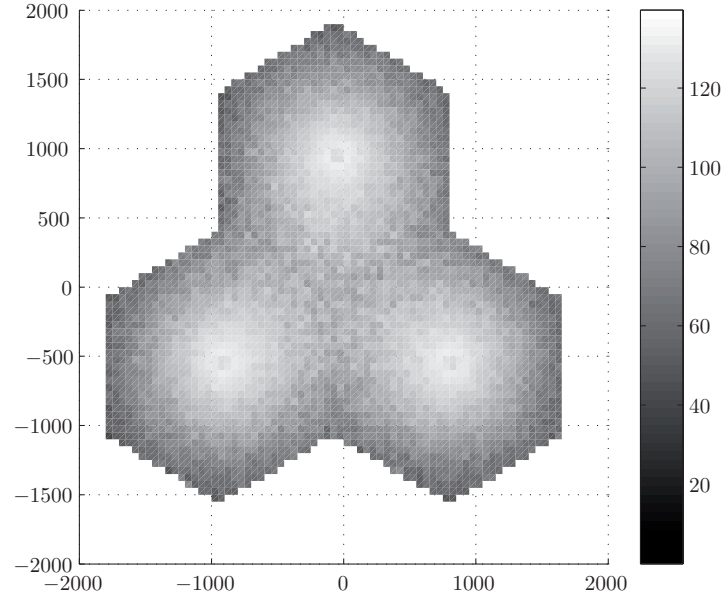
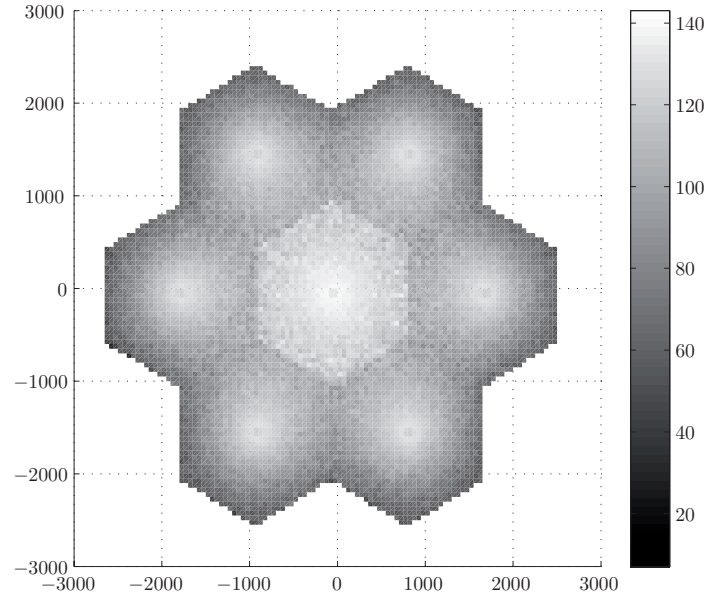

 (a)  $R_{i,IA}$  of clustered interference alignment scheme.

 (b)  $R_{i,WF}$  of non-cooperative eigenwaterfilling scheme.

Figure 5.4: Ergodic throughput [bit/s/Hz] for cluster scenario B where cooperation among  $K = 7$  base stations is established in the presence of uncoordinated interference of  $N - K = 30$  neighboring base stations.



(a) Cluster scenario A. Two rings of uncoordinated base stations around the cluster cause non-coordinated interference, i.e.  $|\Psi^c|=24$ .



(b) Cluster scenario B. Two rings of uncoordinated base stations around the cluster cause non-coordinated interference, i.e.  $|\Psi^c|=30$ .

Figure 5.5: Relative ergodic throughput w.r.t. the independent eigenwaterfilling with frequency reuse scheme  $(R_{i,\mathbf{IA}}/R_{i,\mathbf{WF}})$  [%] for the two considered network scenarios.

## 6 Interference Alignment in Clustered Ad Hoc Networks

In the previous chapter, we discussed the applicability of interference alignment among a finite number of base stations in a fixed geometry cellular networks. We assessed the performance of interference alignment in large cellular systems with clustered cooperation and the impact of uncoordinated interference on the throughput of the users. In this chapter, we consider peer-to-peer networks without infrastructure. The positions of the transmitters, equipped with multiple antennas, are modeled as a realization of a stochastic point process on the infinite plane. The considered model incorporates accumulation of transmitting nodes in geographical areas which we group into clusters. The receiving nodes, equipped with multiple antennas, are placed in the vicinity of the intended transmitters. Each cluster forms a MIMO interference channel and we apply MIMO interference alignment among the users in the clusters while the rest of the network contributes uncoordinated interference. The clustered interference alignment approach leads to a reduced feedback signaling overhead since channel state information (CSI) needs to be exchanged only among the users in the cluster. Furthermore, the number of antennas deployed per node can be reduced since we align solely the intra-cluster interference. Our analysis and simulations, currently limited to single stream transmission per user, attest improvements over known MIMO precoding strategies based on spatial diversity and array gain in terms of link-level performance.

This chapter is organized as follows. At first, some useful definitions and results from stochastic geometry are given with a focus on point processes and their underlying properties. The model for the clustered wireless ad hoc network is introduced next. The transmission success probability of interference alignment with local cooperation horizon is analyzed, and closed-form bounds for special cases are derived. As a baseline scheme, we evaluate the performance of dominant eigenmode transmission. The performance limits of interference alignment with receive diversity in the high reliability regime are described and validated through simulations. A large system analysis of the proposed transmission scheme is carried out in the high reliability regime and expressions for the area spectral efficiency are established and

the optimal SINR operating point in the network is analyzed.

Results presented in this chapter were first published in [85], [86] and [87].

## 6.1 Stochastic Geometry

As the network grows, a deterministic evaluation of connectivity, throughput and reliability becomes unfeasible and less conclusive since the performance is significantly affected by the relative distances between all the nodes. Therefore, a statistical model for the node locations based on stochastic geometry and the associated mathematical tool set for assessing spatial relationships is needed. Stochastic geometry allows to study the average behavior of a multiuser wireless network over many spatial realizations, i.e. different spatial deployments of nodes governed by a probabilistic law. The theory of point processes provides a tool set that contains laws and properties that allow to measure the interference at a particular point in the network. In the following, we introduce the underlying concepts of stochastic geometry that will be used in the course of this chapter.

### 6.1.1 Point Processes

Let us begin with the definition of a point process and a listing of associated properties. Let  $\mathbf{N}$  be the set of all sequences of points in  $\mathbb{R}^2$ , i.e.  $\{x_1, x_2, \dots\} \in \mathbf{N}$  is a sequence where  $x_i$  is the coordinate of the point in  $\mathbb{R}^2$ . Informally, a point process on  $\mathbb{R}^2$  is a random variable which takes values from the set of sequences  $\mathbf{N}$ . This can be formalized as follows.

**Definition 3.** A point process (PP) on  $\mathbb{R}^2$  is a measurable mapping  $\Phi$  from some probability space  $(\Omega, \mathcal{A}, \mathbb{P})$  to the set of sequences  $\mathbf{N}$  [36], i.e.

$$\begin{aligned} \Phi : \quad \Omega &\rightarrow \mathbf{N} \\ \omega &\mapsto \Phi(\omega) = \{x_1, x_2, \dots\}, \end{aligned} \tag{6.1}$$

with  $\Omega$  the set of all possible outcome of a random experiment,  $\mathcal{A}$  a set of events and  $\mathbb{P}$  a probability assignment to the events.

We will denote the set of indices of the points as  $\phi = \{1, 2, \dots\}$ . The definition of a PP is illustrated in Fig. 6.1. Fig. 6.1(a) depicts the mapping  $\Phi$  from a particular outcome  $\omega$  of the random experiment to a sequence  $\{x_1, x_2, \dots\} \in \mathbf{N}$ . Alternatively, a PP can be decomposed as a discrete sum of Dirac measures on  $\mathbb{R}^2$ , i.e.

$$\Phi = \sum_i \delta_{x_i}, \tag{6.2}$$

with the random variables  $\{X_i\}$  denoting the points of the PP. For any area  $B \subset \mathbb{R}^2$ , we denote the number of points in  $\Phi \cap B$  as  $\Phi(B)$ , i.e.  $\Phi(B)$  is a random variable, which maps the set of sequences inside an area  $B$  to the set of integers. The probability that the number of points inside the area  $B$  equals  $k$  is denoted as  $\mathbb{P}(\Phi(B) = k)$ . Fig. 6.1(b) shows a realization of a PP with the mapping  $\Phi(B)$  from an area  $B$  to the number of points of the PP inside the area.

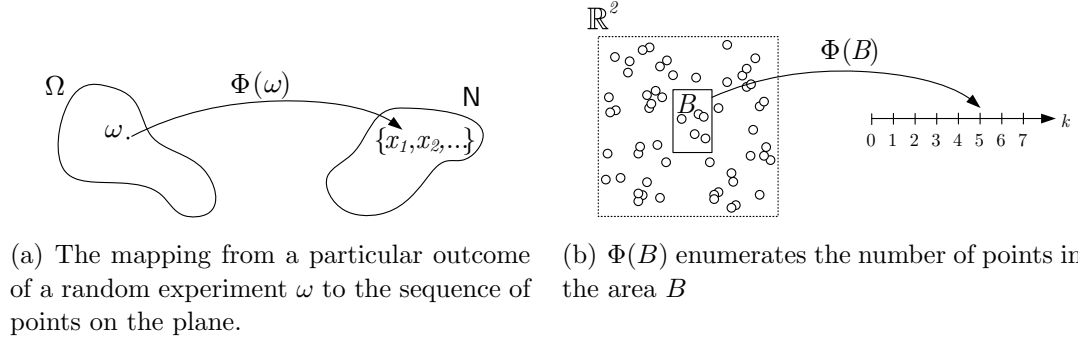


Figure 6.1: Definition of a two dimensional PP as a mapping from some probability space to the set of sequences of points on the infinite plane.

**Definition 4.** The intensity measure  $\Lambda$  of a PP  $\Phi$  in the area  $B$  is defined as

$$\Lambda(B) = \mathbb{E}[\Phi(B)]. \quad (6.3)$$

The expectation in (6.3) is taken with respect to different realizations of the PP. Hence,  $\Lambda(B)$  measures the average number of points inside a particular area  $B$  over different realizations of the PP. *Thinning* of a PP denotes a procedure where each point is retained with probability  $\eta$  and discarded with probability  $1 - \eta$ . We now list important properties of point processes:

- A PP is *stationary* if and only if the law of the PP is invariant by translation. Thus,  $\Lambda(B) = \lambda|B|$ , where  $\lambda$  is called the intensity (density) of  $\Phi$  and  $|B|$  is the surface area of  $B$ .
- A PP is *isotropic* if and only if the law of the PP is invariant to rotation. If a PP is isotropic and stationary, it is called *motion-invariant*.

The most comprehensively studied point processes are Poisson point processes due to their analytical tractability, offering a simple computational framework for different networks quantities of interest.

**Definition 5.** A PP on  $\mathbb{R}^2$  is Poisson, denoted as Poisson point process (PPP), if and only if

- For all mutually disjoint subsets  $B_1, \dots, B_n$  of  $\mathbb{R}^2$ , the random variables  $\Phi(B_i)$  are mutually independent.
- For all subsets  $B$  of  $\mathbb{R}^2$ , the random variable  $\Phi(B)$  is Poisson, i.e.

$$\mathbb{P}(\Phi(B) = k) = \exp(-\Lambda(B)) \frac{(\Lambda(B))^k}{k!}. \quad (6.4)$$

Noteworthy properties of PPP are:

- Conditioned on the fact that  $\Phi(B) = k$  for any  $B \subset \mathbb{R}^2$ , these  $k$  points are independently located in  $B$
- A PPP is *homogeneous* if and only if the density of the points is constant across space, i.e. the number of points in any subsets  $B$  of  $\mathbb{R}^2$  is a Poisson random variable with mean  $\lambda|B|$ .
- The homogeneous PPP is stationary.
- The superposition of two stationary PPPs of densities  $\lambda_1$  and  $\lambda_2$  results in a stationary PPP of density  $\lambda_1 + \lambda_2$ .
- The independent thinning of a PPP is again a PPP.

A realization of a homogeneous PPP is depicted on the left in Fig. 6.2. A Homogeneous PPP models complete spatial uniformity, i.e. the coordinates of all points are independent.

Clustered point processes model spatial arrangements with accumulation of points in certain geographical areas. In the course of this chapter we study Neyman-Scott cluster processes which are stationary and isotropic Poisson cluster processes on the infinite plane  $\mathbb{R}^2$  [34]. An example of this PP is depicted on the RHS of Fig. 6.2.

**Definition 6.** A Neyman-Scott PP  $\Phi$  is a Poisson cluster process (PCP) which results from homogeneous independent clustering applied to a stationary Poisson process [38].  $\Phi$  follows a modular construction procedure. Introducing a parent (homogeneous) PPP  $\Phi_p = \{x_1, x_2, \dots\}$  with density  $\lambda_p$  as a reference for the cluster centers (depicted by crosses in Fig. 6.2), the clusters are of the form  $\mathbf{N}_{x_i} = \mathbf{N}_i + x_i$  for each  $x_i \in \Phi_p$ . The  $\mathbf{N}_i$  are a family of i.i.d. point sets which are also independent of

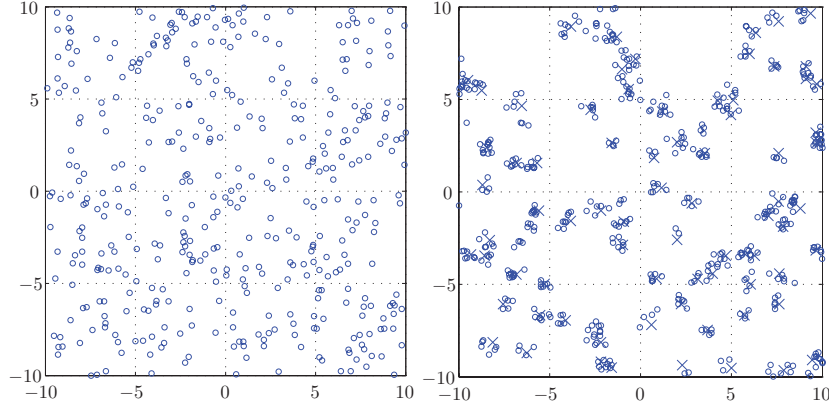


Figure 6.2: Snapshot of point processes, where the points are depicted by circles. On the LHS a homogeneous PPP with  $\lambda = 1$  is pictured, whereas the RHS shows a clustered point process with the same density. Crosses indicate the cluster centers.

$\Phi_p$ . Hence, the daughter points are scattered i.i.d around the positions of the parent points. The complete PCP is given by

$$\Phi = \bigcup_{i \in \phi_p} \mathbf{N}_{x_i}, \quad (6.5)$$

with  $\phi_p$  the set of indices of the points in  $\Phi_p$ . The number of points  $|\mathbf{N}_i|$  in a representative cluster  $\Psi \subset \Phi$  may be random or fixed.  $K$  denotes in turn the average number of cluster points or for a fixed number of points the cardinality of  $\mathbf{N}_i$ . The daughter points  $x_j \in \Psi$  are scattered with density function  $f_{cl}(x_j - x_i)$ , where  $x_j - x_i$  is the coordinate of the cluster point relative to the cluster center. The intensity measure of  $\Phi$  is

$$\Lambda(B) = \lambda_p K |B|. \quad (6.6)$$

Prevalently studied Newman-Scott PCPs are Matern and Thomas cluster processes [36]. For both PCPs, the number of points in a cluster is Poisson distributed. For the Matern cluster process, each daughter point is uniformly distributed in a disk of radius  $a$  around the parent point, whereas in the Thomas cluster process, each daughter point is scattered using a isotropic normal distribution.

## 6.2 Clustered Wireless Ad Hoc System

Let us introduce the model for the clustered wireless ad hoc network. The clustering of nodes may be due to geographical factors, hot spots with a high user density or

induced by the channel access scheme. The location of the transmitters is modeled as a Neyman-Scott cluster process  $\Phi$  with a fixed number of cluster points. Fig. 6.3 shows on the LHS a sample realization of the deployment of the transmitters in a bounded area of the clustered wireless ad hoc network. The transmitters, depicted by circles, are located inhomogeneously in the considered area. The receivers, depicted by squares, are not considered a part of the process. The distance between each transmitter and its intended receiver is constant, which is visualized on the RHS of Fig. 6.3. This transmitter-receiver setting is referred to as the bipolar model [88]. Hence, the model excludes the partner selection problem and focuses on the notion of a common distance that information travels in the network [38]. Every transmitter and receiver is equipped with  $N_T$  and  $N_R$  antennas, respectively and the transmit power is assumed to be one.  $d_{ij}$  is the distance between transmitter  $j$  and receiver  $i$ .

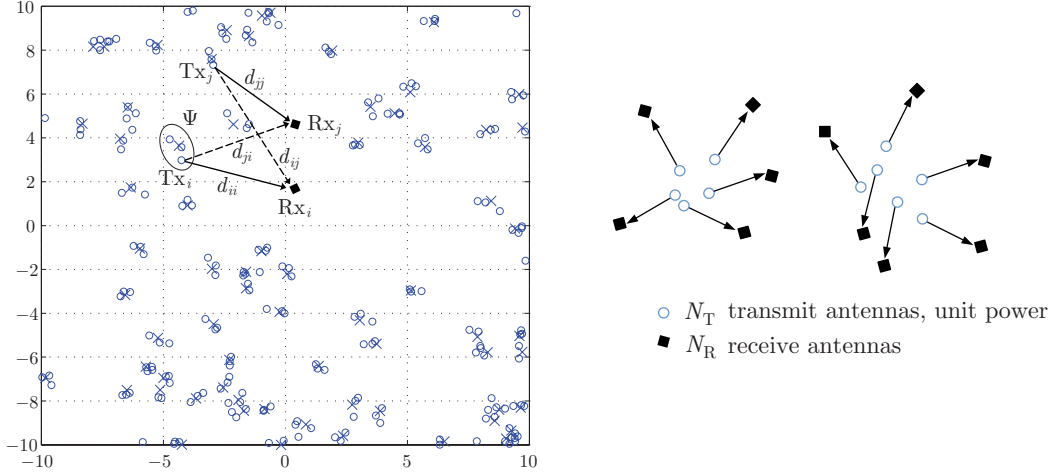


Figure 6.3: Transmitter positions modeled as a Poisson cluster process with  $\lambda_p = 0.2$ ,  $K = 3$ ,  $\sigma = 0.25$ , each transmitter (circles) conveys an independent message to its intended receiver (squares, depicted only receiver  $i$  and  $j$  for clarity) located at a fixed distance from the transmitter position.

In our system model, we consider a Neyman-Scott cluster process  $\Phi$  with a fixed number of points  $K$  in a representative cluster  $\Psi$ . In Fig. 6.3 a cluster  $\Psi$  is highlighted that contains  $K = 3$  points. The scattering density function  $f_{cl}$  is chosen as

$$f_{cl}(x_j - x_i) = \frac{1}{2\pi\sigma^2} \exp\left(-\frac{\|x_j - x_i\|^2}{2\sigma^2}\right), \quad (6.7)$$

with  $x_j - x_i$  containing the two dimensional coordinates relative to the parent point. Hence, cluster points are scattered around the parent point according to a circularly



symmetric normal distribution of variance  $2\sigma^2$ . Since the scattering density of the representative cluster is isotropic, the whole cluster process  $\Phi$  is isotropic. The clusters form a partition of  $\Phi$ . The overall density of the cluster process is denoted as  $\lambda = \lambda_p K$ .

The subset  $\psi = \{k, k+1, \dots, k+K-1\}$  of the index set of the PCP  $\phi$  contains the indices of the points in the representative cluster  $\Psi$ . Each transmitter  $j \in \phi$  is assumed to transmit at unit power. We will investigate alignment-based interference mitigation techniques with local cooperation inside of a cluster  $\Psi$ . Due to computational and analytical tractability, we assume that the rest of the network  $\Phi \setminus \Psi$  contributes non-coordinated interference. While not optimal in general, treating the inter-cluster interference as noise is, in fact, optimal in the Gaussian weak interference regime [89]. In particular, this case arises when the cluster intensity  $\lambda_p$  is small.

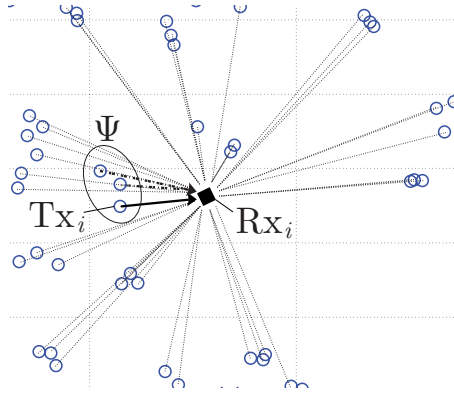


Figure 6.4: Receiver  $i$  receives a superposition of the intended signal (solid arrow) the intra-cluster interference (dash dotted arrow) and inter-cluster interference (dotted links).

Let us focus on a receiver  $i \in \psi$  in the representative cluster  $\Psi$ , see Fig. 6.4. The discrete-time signal received at a given time instant is the superposition of the signals transmitted by the  $K$  transmitters of the cluster  $\Psi$ , and the transmitters of the rest of the network  $\Phi \setminus \Psi$ , weighted by their respective channel gains and path-loss coefficients. Fig. 6.4 discriminates the intended signal, the interference coming from  $K-1$  intra-cluster nodes and the other-cluster interference originating from transmitters of neighboring clusters. Namely, the signal at receiver  $i$  can be written

as

$$\underline{\mathbf{y}}_i = \sqrt{\gamma_{ii}}\mathbf{H}_{ii}\underline{\mathbf{v}}_i s_i + \underbrace{\sum_{j \neq i \in \psi} \sqrt{\gamma_{ij}}\mathbf{H}_{ij}\underline{\mathbf{v}}_j s_j}_{\text{intra-cluster interference}} + \underbrace{\sum_{k \in (\phi \setminus \psi)} \sqrt{\gamma_{ik}}\mathbf{H}_{ik}\underline{\mathbf{v}}_k s_k}_{\text{inter-cluster interference}} + \underline{\mathbf{n}}_i, \quad (6.8)$$

where  $s_j \in \mathbb{C}$  represents the scalar signal transmitted by node  $j$  with  $\mathbb{E}[|s_j|^2] \leq 1$ , and  $\underline{\mathbf{v}}_j \in \mathbb{C}^{N_T \times 1}$  is the associated precoding vector.  $[\mathbf{H}_{ij}]_{i,j \in \phi}$  are complex  $N_R \times N_T$  matrices representing the MIMO channels between transmitter  $j$  and receiver  $i$ . The channel fading coefficients are drawn independently from a continuous distribution and kept constant for the duration of transmission.  $\gamma_{ij} = g(d_{ij})$  is the path-loss model on the same link with  $d_{ij} = \|x_j - x_i\|$  the distance between transmitter  $j$  and receiver  $i$  and  $g(\cdot)$  the path-loss function. We assume a flat-fading channel model.  $\underline{\mathbf{n}}_i$  is a noise term, accounting for the thermal noise generated in the radio frequency front-end of the receiver and interference from sources other than the considered transmitters  $j \in \phi$ .

### 6.2.1 Intra-cluster IA and Feasible Cluster Settings

Let us focus on a given cluster  $\Psi$ , where we aim to achieve IA with multiplexing gain allocation one for each of the  $K$  users in  $\Psi$ . This strategy is suboptimal in general, but chosen for analytical tractability. Channel state information has to be exchanged solely between the nodes of the cluster. Following this strategy, each transmitter is assigned a precoding vector  $\underline{\mathbf{v}}_i$  in order to steer its transmitted signal into a receive subspace of minimum dimension at each unintended intra-cluster receiver. Uncoordinated interference is caused to all inter-cluster receivers, i.e.  $i \in (\phi \setminus \psi)$ . However, for short range communication the strength of the inter-cluster interference decreases with increasing geographical distance between clusters. Fig. 6.5 shows a snapshot of a node deployment and the received signals at receiver  $i$ .

*Theorem 5.* An IA solution with multiplexing gain allocation one and diversity gain allocation  $d'$  among the users in the clusters of a peer-to-peer network whose underlying transmitter node distribution is a PCP with a fixed number of  $K$  nodes per cluster  $\Psi$  that are equipped with  $N_T$  transmit antennas and intended receivers equipped with  $N_R$  antennas, exists almost surely if and only if

$$\frac{N_T - 1}{d'} + N_R - d' + 1 \geq K \quad (6.9)$$

*Proof.* The feasibility condition (4.6) can be particularized to the cluster  $\Psi$ , leading to (6.9). Hence, for every cluster  $\Psi$  there exist  $N_T \times 1$  unit-norm vectors (precoding

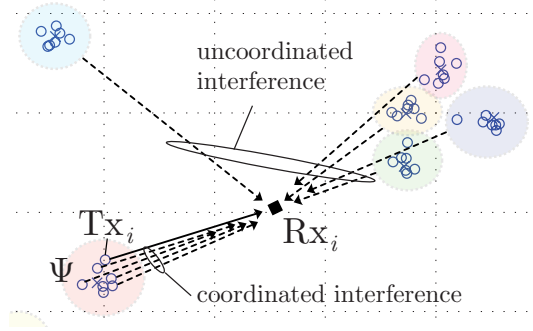


Figure 6.5: Intra-cluster interference alignment leads to coordinated interference from  $K - 1$  transmitters in  $\Psi$  at a representative receiver  $i$  and uncoordinated (non-aligned) interference from transmitters outside of the cooperation cluster.

vectors)  $\underline{\mathbf{v}}_i$  and  $N_R \times d'$  truncated unitary projection matrices (interference suppression matrices)  $\mathbf{U}_i$  such that, for all  $i \in \psi$ ,

$$\mathbf{U}_i^H \mathbf{H}_{ij} \underline{\mathbf{v}}_j = \mathbf{0}_{d'}, \forall (j \neq i) \in \psi, \quad \text{and} \quad (6.10)$$

$$\text{rank}(\mathbf{U}_i^H \mathbf{H}_{ii} \underline{\mathbf{v}}_i) = 1. \quad (6.11)$$

□

Henceforth, we assume that the cluster setting is feasible, i.e. a solution to the intra-cluster IA problem exists almost surely and can be found with the alignment procedures described in Section 4.3. Let us now introduce a receiver architecture that uses linear operations to suppress the intra-cluster interference and to achieve the feasible diversity gain.

**Definition 7.** The intra-cluster *interference decorrelator* is a linear filter comprised of the projection receiver introduced in Subsection 4.2.2 followed by the matched filter (MF) to the signal of interest in the intra-cluster interference-free subspace, i.e.

$$\underline{\mathbf{u}}_{Di} = \mathbf{U}_i \underline{\mathbf{u}}_{MF_i}, \quad (6.12)$$

with  $\mathbf{U}_i \in \mathbb{C}^{N_R \times d'}$  defined by the intra-cluster IA condition (6.10) and  $\underline{\mathbf{u}}_{MF_i} = \mathbf{U}_i^H \mathbf{H}_{ii} \underline{\mathbf{v}}_i / \|\mathbf{U}_i^H \mathbf{H}_{ii} \underline{\mathbf{v}}_i\| \in \mathbb{C}^{d' \times 1}$ .

The following example with  $d' = 2$  and  $N_R = 3$  illustrates the interference decorrelator. The three-dimensional receive signal space of user  $i$  in the cluster  $\Psi$  is shown in Fig. 6.6. The intra-cluster interference  $[\sqrt{\gamma_{ik}} \mathbf{H}_{ik} \underline{\mathbf{v}}_k s_k]_{k \neq i \in \psi}$  is aligned along a one-dimensional subspace. The intra-cluster interference decorrelator projects the

receive signal onto the plane orthogonal to  $\mathcal{S}([\sqrt{\gamma_{ik}}\mathbf{H}_{ik}\mathbf{v}_k s_k]_{k \neq i \in \psi})$ . The projection is depicted along the dashed lines and the components of the signal of interest  $\sqrt{\gamma_{ii}}\mathbf{H}_{ii}\mathbf{v}_i s_i$  and the inter-cluster interference  $[\sqrt{\gamma_{ij}}\mathbf{H}_{ij}\mathbf{v}_j s_j]_{j \in (\phi \setminus \psi)}$  parallel to the plane are highlighted. The projection of the signal of interest  $\sqrt{\gamma_{ii}}\mathbf{U}_i^H \mathbf{H}_{ii}\mathbf{v}_i s_i$  spans a one dimensional subspace in the two dimensional intra-cluster interference-free subspace of user  $i$ . The matched filter to the signal of interest achieves the diversity gain two and further mitigates the energy of the residual inter-cluster interference, i.e. the filter suppresses those parts of the interference depicted by the arrows inside the area that are perpendicular to the projected signal of interest.

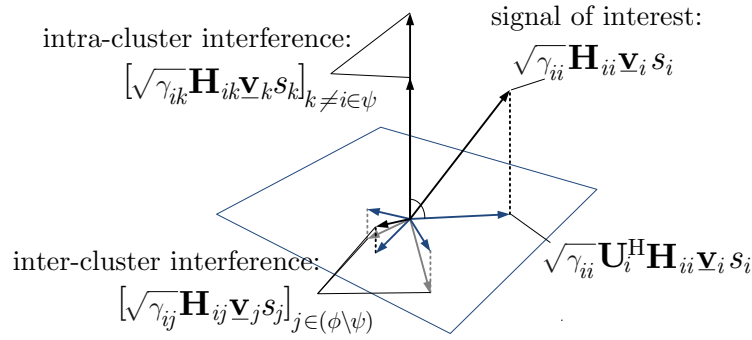


Figure 6.6: Intra-cluster IA along a one dimensional subspace in the receive signal space. Linear filtering at the receiver leads to projection of the signal of interest and inter-cluster interference along the dashed lines. Maximum ratio combining of the projected signal of interest yields diversity gain.

### 6.2.2 Analysis of the Equivalent Channel

Henceforth, we assume that  $\mathbf{H}_{ij}$  is Rayleigh fading, i.e. the channel coefficients are complex Gaussian i.i.d. random variables, with zero mean and unit variance.

Let us now analyze the input-output relation of the system after applying the intra-cluster interference decorrelator, introduced in Definition 7. The  $i^{\text{th}}$  receive signal  $\underline{\mathbf{y}}_i$  (6.8) gets filtered by  $\underline{\mathbf{u}}_{Di}$  (6.12) which yields

$$\begin{aligned} \bar{y}_i &= \underline{\mathbf{u}}_{Di}^H \underline{\mathbf{y}}_i = \sqrt{\gamma_{ii}} \underline{\mathbf{u}}_{MF i}^H \mathbf{U}_i^H \mathbf{H}_{ii} \mathbf{v}_i s_i + \sum_{j \neq i \in \phi} \sqrt{\gamma_{ij}} \underline{\mathbf{u}}_{Di}^H \mathbf{H}_{ij} \mathbf{v}_j s_j + \underline{\mathbf{u}}_{Di}^H \mathbf{n}_i \\ &= \sqrt{\gamma_{ii}} \|\mathbf{U}_i^H \mathbf{H}_{ii} \mathbf{v}_i\| s_i + \sum_{j \in (\phi \setminus \psi)} \sqrt{\gamma_{ij}} \underline{\mathbf{u}}_{Di}^H \mathbf{H}_{ij} \mathbf{v}_j s_j + \underline{\mathbf{u}}_{Di}^H \mathbf{n}_i \end{aligned} \quad (6.13)$$

Here, we used the fact that the interference from transmitters within  $\Psi$  is perfectly suppressed, due to (6.10). The effective channel  $\bar{h}_{ii} = \|\mathbf{U}_i^H \mathbf{H}_{ii} \mathbf{v}_i\|$  as seen by receiver  $i$

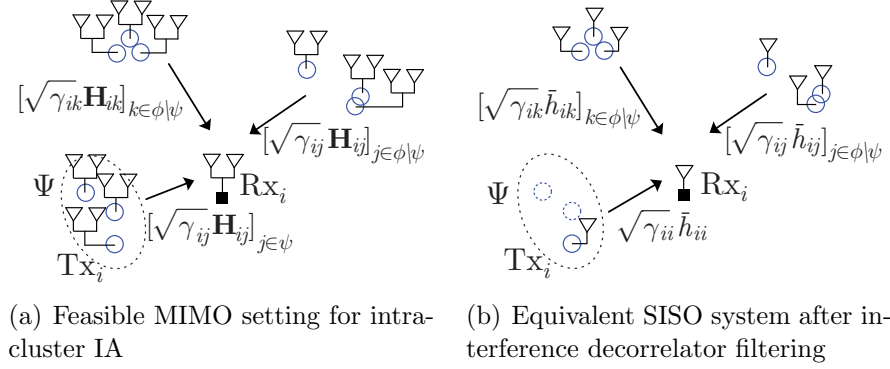


Figure 6.7: Cluster setting with  $K = 3$  cluster points,  $2 \times 2$  MIMO,  $d' = 1$ , and equivalent dimension-reduced intra-cluster interference free input-output relation.

is scalar. Furthermore, since  $\mathbf{U}_i^H \mathbf{U}_i = \mathbf{I}_{d'}$  and  $\mathbf{v}_i^H \mathbf{v}_i = 1$ , and  $\mathbf{U}_i, \mathbf{v}_i$  are independent of  $\mathbf{H}_{ii}$ ,  $\mathbf{U}_i^H \mathbf{H}_{ii} \mathbf{v}_i$  is a  $d' \times 1$  Gaussian vector whose coefficients have the same variance as the components in  $\mathbf{H}_{ii}$ . Hence,  $\|\mathbf{U}_i^H \mathbf{H}_{ii} \mathbf{v}_i\|$  is Chi distributed with  $2d'$  DoF. Similarly, since  $\mathbf{u}_{Di}^H \mathbf{u}_{Di} = \mathbf{u}_{MF i}^H \mathbf{U}_i^H \mathbf{U}_i \mathbf{u}_{MF i} = 1$  and independent of  $[\mathbf{H}_{ij}]_{j \in \phi \setminus \psi}$ , the effective channel  $\bar{h}_{ij} = \mathbf{u}_{Di}^H \mathbf{H}_{ij} \mathbf{v}_j$  is a scalar Gaussian coefficient with the same variance as the components of  $\mathbf{H}_{ij}$ . The effective noise term  $\bar{n}_i = \mathbf{u}_{Di}^H \mathbf{n}_i$ , is a scalar Gaussian coefficient with the same variance  $\sigma_n^2$  as the noise vector  $\mathbf{n}_i$ .

Thus, an equivalent scalar input-output relation of the system after interference suppression yields

$$\bar{y}_i = \sqrt{\gamma_{ii}} \bar{h}_{ii} s_i + \sum_{j \in (\phi \setminus \psi)} \sqrt{\gamma_{ij}} \bar{h}_{ij} s_j + \bar{n}_i, \quad (6.14)$$

which can be interpreted as a system with single antenna terminals where the intra-cluster interference has been completely suppressed, as pictured in Fig. 6.7. In Fig. 6.7(a), the representative cluster  $\Psi$  is depicted. Transmitter  $i \in \psi$  is serving its receiver  $i$  which gets impaired by intra-cluster interference and inter-cluster interference illustrated by two clusters in the pictured area of the PCP. All nodes are equipped with two antennas. Here, diversity gain is not achievable due to the fact that the antenna configuration allows solely for IA with  $d = d' = 1$ , according to (6.9). In Fig. 6.7(b), the equivalent SISO system (6.14) after interference decorrelator filtering is shown. Here, the intra-cluster interference-free subspace of receiver  $i$  is one dimensional. Therefore,  $\bar{h}_{ii}$  is Rayleigh distributed.

### 6.3 Transmission Success Probability

After having derived the scalar input-output relation for intra-cluster IA (6.14), we proceed in this section with the analysis of the transmission success probability. We assume that all transmitters use a common data-rate  $R = \log_2(1 + T)$  and outage-based transmission, i.e. we define the outage probability as the probability that a receiver cannot correctly decode its packet, which is equivalent to the probability that the received SINR falls below the required threshold  $T$  during packet transmission. We use the tool set of stochastic geometry to derive formulas for the transmission success probability of a transmitter-receiver pair in our clustered wireless model for the following schemes.

- In Subsection 6.3.1, we derive a numerical integrable expression for the transmission success probability of intra-cluster IA without additional diversity gain, i.e.  $d' = 1$  along with a simplified bound which can be written in closed-form for a particular pathloss function. We compare to the numerical integrable expression of the transmission success probability of the corresponding clustered SISO network derived in [38].
- In Subsection 6.3.3 we establish a numerical integrable expression for the transmission success probability of intra-cluster IA with diversity gain  $d' > 1$  in the high reliability regime where the density of interfering clusters goes to zero. We argue that analytical expressions for the transmission success probability in dense networks are analytically intractable.
- The expression for the probability of successful transmission of dominant eigenmode transmission is introduced in Subsection 6.3.4. We identify the power fading statistics of the signal of interest and the interference. This opportunistic transmission scheme will be analyzed as a reference architecture to intra-cluster IA.

#### 6.3.1 Intra-Cluster IA with $d'=1$ and Bounds

Let the desired transmitter be located at the origin and the receiver at location  $z$  and distance  $d_{ii} = \|z\|$  from the intended transmitter [38]. Communication is successful, if the SINR exceeds the threshold  $T = 2^R - 1$  which is a function of the fixed data rate in the network. Thus, the probability of success for this pair is given by [38, eq. (31)]

$$\mathbb{P}(\text{success}) = \mathbb{P}\left(\frac{|\bar{h}_{ii}|^2 \gamma_{ii}}{\sigma_n^2 + I_\Phi} \geq T \mid \text{intended transmitter at the origin}\right), \quad (6.15)$$

where the accumulated interference from the rest of the network  $I_\Phi$  is

$$I_\Phi = \begin{cases} \sum_{j \in (\phi \setminus \psi)} |\bar{h}_{ij}|^2 \gamma_{ij} & \text{for intra-cluster IA with } d' = 1 \text{ according to (6.14)} \\ \sum_{j \in (\phi \setminus i)} |\bar{h}_{ij}|^2 \gamma_{ij} & \text{for the corresponding network with single antenna} \\ & \text{terminals, i.e. } N_T = N_R = 1 \end{cases} \quad (6.16)$$

The intended received signal and interference power fading terms  $|\bar{h}_{ij}|^2 \forall (i, j)$  (according to (6.14) which assumes non line-of-sight situations with dense scattering and Rayleigh fading channels) in (6.15) and (6.16) are exponentially distributed.

*Theorem 6.* Using intra-cluster IA in a feasible cluster setting without additional diversity gain, i.e.  $d' = 1$  and the IA criteria (6.9) is  $N_R + N_T - 1 \geq K$ , the success probability (when we neglect the noise  $\sigma_n^2$ ) is given by

$$\mathbb{P}(\text{success}) = \exp \left( -\lambda_p \int_{\mathbb{R}^2} \left[ 1 - \tilde{\beta}(z, y)^K \right] dy \right), \quad (6.17)$$

where

$$\tilde{\beta}(z, y) = \int_{\mathbb{R}^2} \frac{f_{cl}(x)}{1 + \frac{Tg(x-y-z)}{g(z)}} dx, \quad (6.18)$$

where  $x, y, z$  are two-dimensional coordinates. In the case of single-antenna terminals ( $N_T = N_R = 1$ ), the expression for  $\mathbb{P}(\text{success})$  has to account for intra-cluster interference via an additional the term in (6.17)  $\int \tilde{\beta}(z, y)^{K-1} f_{cl}(y) dy$ .

The proof is outlined in Appendix 6.6 using tools from stochastic geometry along the lines of the analysis proposed in [38].

### 6.3.2 Bounds on the Transmission Success Probability for $d'=1$

In this subsection, we fix the path-loss model  $g(d_{ij}) = d_{ij}^{-\alpha}$  with  $2 \leq \alpha \leq 4$  and seek bounds on the transmission success probability, for the particular case of  $d' = 1$ , i.e. no receive diversity. We seek a simple upper bound on  $\mathbb{P}(\text{success})$  as defined in (6.17). Henceforth, we denote  $\xi(z) = \int 1 - \tilde{\beta}(z, y)^K dy$ , the two dimensional integral in (6.17). Therefore, we are looking for an upper bound on  $\tilde{\beta}(z, y)$  (6.18). If one considers  $x$  in (6.18) to be a random vector  $X$  with two-dimensional density function  $f(\cdot)$ , we can write

$$\tilde{\beta}(z, y) = \mathbb{E} \left[ \frac{1}{1 + \frac{T\|X-y-z\|^{-\alpha}}{\|z\|^{-\alpha}}} \right] = \mathbb{E} \left[ \frac{1}{1 + \frac{T(U^2)^{-\alpha/4}}{\|z\|^{-\alpha}}} \right], \quad (6.19)$$

where the second equality comes from a change of variable  $U = \|X - y - z\|^2$ . Since  $X$  is assumed to have a circularly symmetric normal distribution with variance  $2\sigma^2$ , the random variable  $U$  has a non-central chi-square distribution with mean  $2\sigma^2 + \|y + z\|^2$  and variance  $4\sigma^4 + 4\sigma^2\|y + z\|^2$ . Furthermore, since  $1/(1 + TV^{-\alpha/4}/\|z\|^{-\alpha})$  is concave for  $V > 0$  and  $\alpha \leq 4$ , we apply Jensen's inequality to get

$$\tilde{\beta}(z, y) = \mathbb{E} \left[ \frac{1}{1 + \frac{T(U^2)^{-\alpha/4}}{\|z\|^{-\alpha}}} \right] \leq \frac{1}{1 + \frac{T\mathbb{E}[U^2]^{-\alpha/4}}{\|z\|^{-\alpha}}} = \frac{1}{1 + \frac{T((2\sigma^2 + \|y + z\|^2)^2 + 4\sigma^4 + 4\sigma^2\|y + z\|^2)^{-\alpha/4}}{\|z\|^{-\alpha}}}, \quad (6.20)$$

where we used the fact that the second raw moment of  $U$  is  $(2\sigma^2 + \|y + z\|^2)^2 + 4\sigma^4 + 4\sigma^2\|y + z\|^2$ . Since we found an upper bound on  $\tilde{\beta}(z, y)$ , we lower bound  $\xi(z)$  in (6.17) with (6.20) as

$$\xi(z) \geq \int_{\mathbb{R}^2} \left[ 1 - \left( \frac{1}{1 + \frac{T((2\sigma^2 + \|y + z\|^2)^2 + 4\sigma^4 + 4\sigma^2\|y + z\|^2)^{-\alpha/4}}{\|z\|^{-\alpha}}} \right)^K \right] dy. \quad (6.21)$$

Shifting the integrand in (6.21) towards direction  $-z$  and change of variables leads to an equivalent expression for the lower bound on  $\xi(z)$ , i.e.

$$\begin{aligned} & \int_{\mathbb{R}^2} \left[ 1 - \left( \frac{1}{1 + \frac{T((2\sigma^2 + \|y\|^2)^2 + 4\sigma^4 + 4\sigma^2\|y\|^2)^{-\alpha/4}}{\|z\|^{-\alpha}}} \right)^K \right] dy \\ &= 2\pi \int_0^\infty \left[ 1 - \left( \frac{1}{1 + \frac{T((2\sigma^2 + r^2)^2 + 4\sigma^4 + 4\sigma^2 r^2)^{-\alpha/4}}{\|z\|^{-\alpha}}} \right)^K \right] r dr \\ &= \pi \int_{4\sigma^2}^\infty \left[ 1 - \left( \frac{1}{1 + \frac{T(s^2 - 8\sigma^4)^{-\alpha/4}}{\|z\|^{-\alpha}}} \right)^K \right] ds, \end{aligned} \quad (6.22)$$

where the first equality comes from a change of the Cartesian coordinates  $y = (y_1, y_2)$  into polar coordinates, i.e.  $y_1 = r \cos \varphi$  and  $y_2 = r \sin \varphi$ . The second equality follows from change of variable  $s = r^2 + 4\sigma^2$ . Thus, the upper bound on the transmission probability reads

$$\mathbb{P}(\text{success}) \leq \exp \left( -\lambda_p \pi \int_{4\sigma^2}^\infty \left[ 1 - \left( \frac{1}{1 + \frac{T(s^2 - 8\sigma^4)^{-\alpha/4}}{d_{ii}^{-\alpha}}} \right)^K \right] ds \right), \quad (6.23)$$

where we replaced  $\|z\|$  by  $d_{ii}$ . Hence, the upper bound for probability of success depends only on the distance between transmitter  $i$  and receiver  $i$  and does not depend on the relative position  $z$ .



### 6.3.2.1 Closed-form Solution for a Special Case

If we consider  $\alpha = 4$  and  $\sigma^2 \ll 1$ , i.e. the cluster size is typically small, we can find a closed-form upper bound for  $\mathbb{P}(\text{success})$ . Neglecting  $8\sigma^4$  in the integrand of (6.22) and changing of variables  $t = 1/s$  leads to

$$\begin{aligned}\xi(z) &\geq \pi \int_0^{1/(4\sigma^2)} \sum_{k=1}^K \frac{\frac{T}{d_{ii}^{-\alpha}}}{\left(\frac{T}{d_{ii}^{-\alpha}} t^2 + 1\right)^k} dt \\ &= \pi \left( \delta(K) d_{ii}^2 \sqrt{T} \tan^{-1} \left( \frac{d_{ii}^2 \sqrt{T}}{4\sigma^2} \right) + \mathcal{R}(d_{ii}, T, \sigma^2) \right),\end{aligned}\quad (6.24)$$

with  $\delta(K) = \sum_{k=0}^{K-1} (-1)^k \binom{-1/2}{k}$  and a residual term  $\mathcal{R}(d_{ii}, T, \sigma^2)$ . Neglecting the term  $\mathcal{R}(d_{ii}, T, \sigma^2)$  leads to

$$\mathbb{P}(\text{success}) \leq \exp \left( -\lambda_p \pi \delta(K) d_{ii}^2 \sqrt{T} \tan^{-1} \left( \frac{d_{ii}^2 \sqrt{T}}{4\sigma^2} \right) \right). \quad (6.25)$$

### 6.3.3 Intra-Cluster IA with Diversity Receiver

Let us now consider intra-cluster IA with receive diversity, i.e.  $d' > 1$ . The transmission success probability (if we neglect the noise) is

$$\mathbb{P}(\text{success}) = \mathbb{P} \left( \frac{|\bar{h}_{ii}|^2 \gamma_{ii}}{\sum_{j \in (\phi \setminus \psi)} |\bar{h}_{ij}|^2 \gamma_{ij}} \geq T \right). \quad (6.26)$$

By virtue of intra-cluster IA, only the inter-cluster interference is added in the denominator of (6.26) with exponentially distributed power fading terms  $|\bar{h}_{ij}|^2$ . The CCDF of the intended receive signal power  $|\bar{h}_{ii}|^2$  is  $\chi^2$  with  $2d'$  DoF, i.e. [90]

$$F_{|\bar{h}_{ii}|^2}^c(t) = e^{-t} \sum_{k=0}^{d'-1} \frac{t^k}{k!}. \quad (6.27)$$

We show in Appendix 6.6, that numerically integrable expressions for the transmission success probability of intra-cluster IA with diversity receivers using the analysis in [38] are analytically intractable. However, the outage probability can be analyzed in the high-reliability regime for any  $d'$ . As the underlying MAC protocol, we assume highly clustered ALOHA [42], i.e. keeping or removing entire clusters with a fixed medium access probability  $\eta$ . Due to the thinning property of Poisson point

processes, this scheme leads to a process with decreased cluster density (parent thinning). The high reliability regime is attained by letting  $\eta \rightarrow 0$ .

Let us denote the parent process  $\Phi_p = \{x_1, x_2, \dots\}$  with  $x_i$  the coordinate of the cluster center and  $\phi_p = \{1, 2, \dots, \infty\}$  is the set of indices of the clusters. In the asymptotic regime as the density of residual inter-cluster interferers goes to zero, we use a cluster fusion approach to derive the intrinsic spatial contention of the network. Hence, we replace the daughter points by a representative point at the coordinates of the cluster center. Assuming finite cluster size, the accumulated interference for receiver  $i$  in (6.15) is approximated by

$$I_{\phi \setminus \psi} \approx \sum_{j \in \phi_p \setminus i} |\bar{h}'_{ij}|^2 \gamma'_{ij}, \quad (6.28)$$

with  $|\bar{h}'_{ij}|^2 = \sum_{k \in \Psi_j} |\bar{h}_{ik}|^2$  being the compound channel power gain and  $\gamma'_{ij} = g(\|z - x_j\|)$  being the path-loss coefficient from a fictitious transmitter at the cluster center.  $|\bar{h}'_{ij}|^2$  is the sum of i.i.d. exponentially distributed random variables and therefore Gamma distributed, i.e. the density function writes  $f_{|\bar{h}'_{ij}|^2}(h) = h^{K-1} \exp(-h)/\Gamma(K)$  [90].  $\Phi_p$  is a homogeneous Poisson point process with second order product density  $\rho^{(2)}(x) = \lambda_p^2$  and according to [41, Theorem 3] the asymptotic success probability writes  $\mathbb{P}(\text{success}) \sim 1 - \gamma\eta$  with the so called spatial contention

$$\gamma = \frac{1}{\lambda_p} \int_{\mathbb{R}^2} \left[ 1 - \mathbb{E}_{|\bar{h}'_{ij}|^2} F_{|\bar{h}_{ii}|^2} \left( h \frac{Tg(x)}{g(d_{ii})} \right) \right] \rho^{(2)}(x) dx. \quad (6.29)$$

The integrand in (6.29) can be simplified to

$$\begin{aligned} & \lambda_p \left[ 1 - \int_0^\infty F_{|\bar{h}_{ii}|^2}(h') (h\vartheta) \left( \frac{h'}{\vartheta} \right)^{K-1} e^{-h'/\vartheta} \frac{1}{\Gamma(K)\vartheta} dh' \right] \\ &= \lambda_p \left[ 1 - \frac{1}{\Gamma(K)\vartheta^K} \left( \frac{d}{dK-1} (-1)^{K-1} \mathcal{L}(F_{|\bar{h}_{ii}|^2}(s)) \Big|_{s=\frac{1}{\vartheta}} \right) \right] \\ &= \lambda_p \left[ 1 - \frac{1}{\Gamma(K)\vartheta^K} \left( \frac{d}{dK-1} (-1)^{K-1} \sum_{k=0}^{d'-1} \frac{1}{(1+\vartheta^{-1})^{K+k}} \right) \right], \end{aligned} \quad (6.30)$$

with  $\vartheta = Tg(x)/g(d_{ii})$ . For the first expression we used the substitution  $h' = h\vartheta$ , the first equality comes from the Laplace equivalence  $t^n f(t) \longleftrightarrow (-1)^n \mathcal{L}(f)^{(n)}(s)$  and the second equality from the equivalence  $(t^n/n!)e^{-t} \longleftrightarrow 1/(s+1)^{n+1}$ . Above steps turn (6.29) into

$$\gamma = \lambda_p \int_{\mathbb{R}^2} \left[ 1 - \left( \frac{g(d_{ii})}{Tg(x)} \right)^K \left( \sum_{k=0}^{d'-1} \frac{\binom{K-1+k}{K-1}}{\left( 1 + \frac{g(d_{ii})}{Tg(x)} \right)^{K+k}} \right) \right] dx. \quad (6.31)$$

For the special case of  $g(d_{ij}) = d_{ij}^{-\alpha}$  with  $\alpha = 4$ , (6.31) is equivalent to

$$\gamma = \lambda_p \pi^2 / 2\delta(K) \mu(d') d_{ii}^2 \sqrt{T}, \quad (6.32)$$

with  $\delta(K)$  from (6.25) and  $\mu(d') = \left( \frac{2(d' - 1)}{d' - 1} \right) / 4^{d'-1}$ . Hence,  $\epsilon(d')$  in (6.32) captures the impact of diversity gain on the success probability. We note that for  $d' = 1$ ,  $1 - \gamma\eta$  with  $\gamma$  according to (6.32) coincides with a first-order Taylor approximation of (6.25) for  $\sigma \rightarrow 0$ .

### 6.3.4 Dominant Eigenmode Transmission

As a reference architecture, we analyze the link level performance of dominant eigenmode (EM) transmission [49]. This scheme is based only on channel state information of the link between transmitter  $i$  and receive  $i$ . In a single-user MIMO channel, this precoding method achieves an array gain according to the largest eigenvalue of  $\mathbf{H}_{ii} \mathbf{H}_{ii}^H$ . In the clustered network, the signaling overhead for channel state feedback is significantly reduced compared to clustered IA. However, dominant eigenmode transmission leads to uncoordinated intra- and inter-cluster interference.

The precoding vector of transmitter  $i$  is  $\mathbf{v}_i$ , i.e. the right singular vector corresponding to the largest singular value  $\sigma_1$  of the SVD of  $\mathbf{H}_{ii}$  (3.9) introduced in Section 3.3. For analytical tractability, we choose as the receive filter the matched filter to the signal of interest, i.e.  $\mathbf{u}_{\text{MF}i} = \mathbf{H}_{ii} \mathbf{v}_i / \|\mathbf{H}_{ii} \mathbf{v}_i\| \in \mathbb{C}^{N_R \times 1}$ .

Here, an equivalent scalar input-output relation of the system after matched filtering yields

$$\bar{y}_i = \mathbf{u}_{\text{MF}i}^H \mathbf{y}_i = \sum_{j \in \phi} \mathbf{u}_{\text{MF}i}^H \mathbf{H}_{ij} \mathbf{v}_j s_j + \mathbf{u}_{\text{MF}i}^H \mathbf{n}_i = \sqrt{\gamma_{ii}} \bar{h}_{ii} s_i + \sum_{j \neq i \in \phi} \sqrt{\gamma_{ij}} \bar{h}_{ij} s_j + \bar{n}_i. \quad (6.33)$$

The squared effective channel  $|\bar{h}_{ii}|^2 = \|\mathbf{H}_{ii} \mathbf{v}_i\|^2$  in (6.33) is distributed as the largest eigenvalue of a complex Wishart matrix [40]. The sum of interference terms  $[\sqrt{\gamma_{ij}} \bar{h}_{ij} s_j]_{j \neq i \in \phi}$  in (6.33) consist of intra-cluster and inter-cluster interference.  $\bar{h}_{ij} = \mathbf{u}_{\text{MF}i}^H \mathbf{H}_{ij} \mathbf{v}_j$  are scalar Gaussian coefficients with the same variance as the components of  $\mathbf{H}_{ij}$  since  $\mathbf{v}_i^H \mathbf{v}_i = \mathbf{u}_{\text{MF}i}^H \mathbf{u}_{\text{MF}i} = 1$  and independent of  $\mathbf{H}_{ij}$ .  $\bar{n}_i$  is an equivalent Gaussian noise term with the same variance  $\sigma_n^2$  as the noise vector  $\mathbf{n}_i$ .

We follow the derivation according to the SINR model for link outages introduced in (6.15). The probability of successful transmission for dominant EM transmission (if we neglect the noise) is

$$\mathbb{P}(\text{success}) = \mathbb{P} \left( \frac{|\bar{h}_{ii}|^2 \gamma_{ii}}{\sum_{j \in (\phi \setminus i)} |\bar{h}_{ij}|^2 \gamma_{ij}} \geq T \right). \quad (6.34)$$

The interference term in (6.34) contains inter- and intra-cluster interference. The interference power factors  $|\bar{h}_{ij}|^2$  are exponentially distributed. The CCDF of the power factor  $|\bar{h}_{ii}|^2$  related to the intended signal is the square of the maximum singular value of  $H_{ii}$  or equivalently the largest eigenvalue of a complex *Wishart* matrix [91]. Hence, the CCDF of the intended receive signal power cannot be given explicitly for arbitrary  $N_T$  and  $N_R$ . Therefore, we will evaluate the performance of dominant EM transmission through Monte-Carlo simulation of (6.34).

## 6.4 Transmission Capacity

In order to assess the performance of intra-cluster IA with receive diversity from a viewpoint of the whole clustered network, we introduce in this section the transmission capacity [39] and the closely related area spectral efficiency. These two metrics capture the maximum achievable transmissions density in the network given a constraint on the link outage probability and the corresponding achievable network throughput.

Let us first define  $\lambda_\epsilon(T)$  as the maximum density of transmissions in the network such that the link outage probability is smaller than  $\epsilon$  relative to a SIR threshold  $T$ . The transmission capacity  $\text{TC}(\epsilon, T)$  is the maximum density of transmissions times the probability of successful transmission and measured in transmissions per unit area, i.e.

$$\text{TC}(\epsilon, T) = \lambda_\epsilon(1 - \epsilon). \quad (6.35)$$

The area spectral efficiency takes into account the per user data-rate which is in the order of  $\log_2(1 + T)$ , i.e.

$$\text{TC} \cdot \log_2(1 + T) \quad \left[ \frac{\text{bit/s/Hz}}{\text{m}^2} \right]. \quad (6.36)$$

Note that the area spectral efficiency depends on the SIR threshold  $T$  though both the transport capacity which is a function of the threshold and the per user data rate that is determined by the SIR threshold.

In general, closed form expressions for the transmission capacity in a clustered networks are difficult to obtain. However, for intra-cluster IA with diversity gain allocation  $d'$ , it is possible to find closed form results if we relate to the high reliability regime and the framework introduced in [41]. The asymptotic transmission capacity is obtained in [41] by inverting the asymptotic of  $\mathbb{P}(\text{success}) \approx 1 - \eta\gamma$  to solve for the density  $\eta$  corresponding to  $\mathbb{P}(\text{success}) = 1 - \epsilon$ . For the intra-cluster IA scheme with

highly clustered ALOHA as underlying MAC protocol, the inversion is formalized by [41, Theorem 4] since the  $\mathbb{P}(\text{success})$  is only depending on the inter-cluster IA which is strictly increasing when decreasing the ALOHA parameter  $\eta$ . Hence we can find the maximum spatial density of transmissions as

$$\lambda_\epsilon = K\lambda_p\eta = \frac{\epsilon K\lambda_p}{\gamma}, \quad (6.37)$$

where the second equality follows from the inversion of the asymptotic  $\mathbb{P}(\text{success})$  and with  $\gamma$  according to (6.31). Thus, the asymptotic transmission capacity writes

$$\text{TC}(\epsilon, T) = \frac{\epsilon K\lambda_p}{\gamma} + \mathcal{R}(\epsilon), \quad \epsilon \rightarrow 0. \quad (6.38)$$

where  $\mathcal{R}(\epsilon)$  is a term of order strictly higher than one in  $\epsilon$ .

If we consider the pathloss function  $g(d_{ij}) = d_{ij}^{-\alpha}$  with  $\alpha = 4$  we can further simplify the expression for the transmission capacity. Inserting (6.32) into (6.38) leads to

$$\text{TC}(\epsilon, T) = \frac{\epsilon K}{\pi^2/2\delta(K)\mu(d')d_{ii}^2\sqrt{T}} + \mathcal{R}(\epsilon). \quad (6.39)$$

## 6.5 Simulation Results

In this section, we present simulation results for different settings of the Poisson cluster process. The standard power law  $g(d_{ij}) = d_{ij}^{-\alpha}$  with  $\alpha = 3, 4$  and a SIR threshold  $T = 0.1, 1$  is used. Monte-Carlo simulation of the transmission success probability are averaged over 1000 realizations of the PCP. In Subsection 6.5.1, we plot link level performance results for the intra-cluster IA scheme without receive diversity and investigate the tightness of the closed-form upper bound derived in Subsection 6.3.2. We compare to the performance of the corresponding SISO network. Curves of the transmission success probability for intra-cluster IA with receive diversity are plotted in Subsection 6.5.2 and compared to the performance of dominant eigenmode transmission. Furthermore, in Subsection 6.5.3, we validate the high SIR formulas for intra-cluster IA with receive diversity derived in 6.3.3 and investigate the area spectral efficiency of the network.

### 6.5.1 Link Level Performance of IA for $d'=1$ and Bounds

In Fig. 6.8 the probability of success of the intra-cluster IA ("MIMO IA") without receive diversity and the corresponding single-antenna network ("SISO") with the

same underlying node distribution suffering from intra- and inter-cluster interference is plotted versus  $d_{ii}$ . The curves for the probability of success were derived by numerical integration of (6.17) and verified by Monte-Carlo simulation of (6.15) over different transmitter positions and fading coefficients. The curves overlap and we plot only the results of the numerical integration. The overall intensity of the network  $\lambda = \lambda_p K$  is fixed. The pathloss coefficient is set to  $\alpha = 4$  and a SIR threshold  $T = 0.1$  is used. Possible antenna configurations can be deduced with the feasibility condition (6.9), e.g.  $2 \times 2$  for  $K = 3$ ,  $4 \times 2$  for  $K = 5$  and  $6 \times 2$  for  $K = 7$ .

The relative gain of MIMO IA compared to non-cooperative SISO is increasing for increasing number of cluster points. If we focus on the case of seven cluster points, the probability of success for  $d_{ii} \in [0.5, 1]$  is increased by more than a factor of two. Therefore, local cooperation significantly increases the performance of the system whenever the signals of many strong interfering nodes can be aligned.

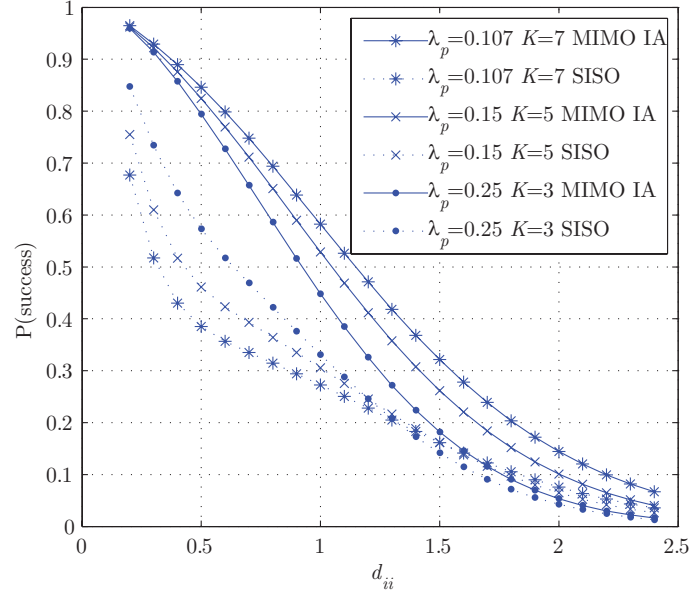
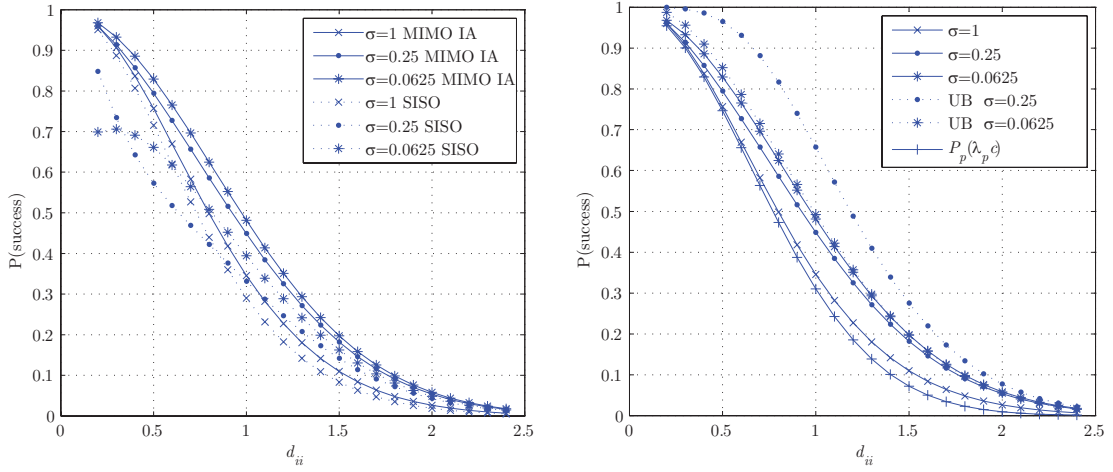


Figure 6.8:  $\mathbb{P}(\text{success})$  versus  $d_{ii}$  for  $\lambda = \lambda_p K$  fixed,  $\sigma=0.25$ ,  $T = 0.1$ , and  $\alpha = 4$ , comparison of SISO clustered network with MIMO intra-cluster IA with  $d' = 1$ .

Fig. 6.9 plots the transmission success probability  $\mathbb{P}(\text{success})$  versus  $d_{ii}$  for a network with parent process intensity  $\lambda_p = 0.25$ , three cluster points  $K = 3$  and varying cluster size. Again, we plot the numerical integration of (6.17) and omit the overlapping curves of the Monte-Carlo simulation of (6.15). In Fig. 6.9(a), we evaluate the performance gain of the MIMO intra-cluster IA scheme with  $d' = 1$  compared to the corresponding SISO network with the same network intensity for varying cluster spread. The smaller the scattering parameter  $\sigma$  the better the IA strategy performs

in terms of probability of success over the whole range of  $d_{ii}$ . However, for the non-cooperative SISO settings that suffer from intra- and inter-cluster interference, the performance is not monotonous with  $\sigma$ . E.g. the SISO network with  $\sigma = 0.0625$  outperforms the other SISO settings only in the range  $d_{ii} > 0.6$ . The intra-cluster interference dominates the performance for small distances, i.e.  $d_{ii} < 0.6$ . Here, the use of multiple antennas at each node, coupled with intra-cluster IA can significantly increase the performance. For  $\sigma = 0.25$  a maximum relative gain of 40% is achieved at  $d_{ii} = 0.5$ . If the scattering of the cluster points becomes larger (see  $\sigma = 1$  in Fig. 6.9(a)), the benefit of intra-cluster interference suppression decreases. In Fig. 6.9(b) the closed-form upper bound (6.25) for the same network setting as in Fig. 6.9(a) is plotted. For  $\sigma = 0.0625$  the upper bound is tight for  $d_{ii} > 1$ . We also compare



(a) Comparison of SISO clustered network with MIMO intra-cluster IA with  $d' = 1$ . (b) Intra-cluster IA with  $d' = 1$  (solid lines), closed-form upper bound ("UB") according to (6.25) and comparison with  $P_p(\lambda_p K)$ .

Figure 6.9:  $\mathbb{P}(\text{success})$  versus  $d_{ii}$  for a network configuration with cluster density  $\lambda_p = 0.25$ , three cluster nodes  $K = 3$ , threshold  $T = 0.1$ , and inverse power law pathloss with  $\alpha = 4$ .

the probability of success of the intra-cluster IA scheme with the performance of a SISO network whose underlying node distribution is a corresponding homogeneous Poisson point process with intensity  $\lambda = \lambda_p K$ . The probability of success for that case  $P_p(\lambda_p K) = \exp(-\lambda_p K d_{ii}^2 T^{2/\alpha} C(\alpha))$  with  $C(\alpha) = 2\pi^2/\alpha \csc(2\pi/\alpha)$  [38] is also plotted in Fig. 6.9(b). It performs only slightly worse than the MIMO IA for  $\sigma = 1$ . Increasing the spreading of the cluster points increases the overall spatial randomness in the network. Therefore, we conjecture that  $P_p(\lambda_p K)$  is the limiting  $\mathbb{P}(\text{success})$  for  $\sigma \rightarrow \infty$ .

### 6.5.2 Link Level Performance of IA with Receive Diversity

We now evaluate the transmission success probability of intra-cluster IA with receive diversity ("IA  $d' = 2$ ") and compare with the outage performance of dominant eigenmode transmission ("dominant EM"). The SIR threshold is set to  $T = 1$ . The results are presented in Fig. 6.11 and Fig. 6.12 for a network with a fixed cluster density  $\lambda_p = 0.05$  and two different cluster scattering parameters realizing mostly non-overlapping  $\sigma = 0.25$  and mostly overlapping  $\sigma = 1$  clusters in the network. The pathloss coefficient is set to  $\alpha = 4$  in Fig. 6.11, whereas Fig. 6.12 shows results with  $\alpha = 3$ . Depending on  $d'$  and the antenna configuration, a different number of users can be accommodated. We consider the case of  $N_R = 3$  receive antennas and two different transmit antenna deployments, i.e.  $N_T = 5, 7$ . Table 6.1 lists the number of

| $K$ | $d'$ | $N_T$ | $N_R$ |
|-----|------|-------|-------|
| 4   | 2    | 5     | 3     |
| 5   | 2    | 7     | 3     |
| 7   | 1    | 5     | 3     |
| 9   | 1    | 7     | 3     |

Table 6.1: Feasible number of cluster points for intra-cluster IA depending on diversity gain and antenna configuration.

cluster points that can be accommodated in the intra-cluster IA scheme depending on the diversity gain allocation  $d'$  and the antenna configuration. All network settings listed in Table 6.1 achieve the intra-cluster IA criteria (6.9) with equality. Fig. 6.10 shows sample realizations of the transmitting nodes in the clustered network with different cluster sizes. We depict the case with  $K = 7$  transmitters per cluster. For the smaller cluster size with  $\sigma = 0.25$  (Fig. 6.10(a)) almost all clusters are not overlapping, except for a few clusters where the cluster centers are close-by. For the larger cluster size with  $\sigma = 1$  (Fig. 6.10(b)) the transmitting nodes are scattered further apart from the cluster center and clusters are more likely to be overlapping.

Let us first focus on  $\alpha = 4$  in Fig. 6.11 and the case with mostly non-overlapping clusters in Fig. 6.11(a). For all network configurations considered, intra-cluster IA outperforms dominant EM transmission for small transmitter–receiver distances  $d_{ii}$ . IA with receive diversity substantially improves the transmission success probability. For a fixed outage probability target, the maximum achievable  $d_{ii}$  is increased significantly for both antenna configurations, e.g.  $\mathbb{P}(\text{success}) > 0.9$ , the maximum  $d_{ii}$  increases by about 60%. However, decreasing diversity allows for more users per



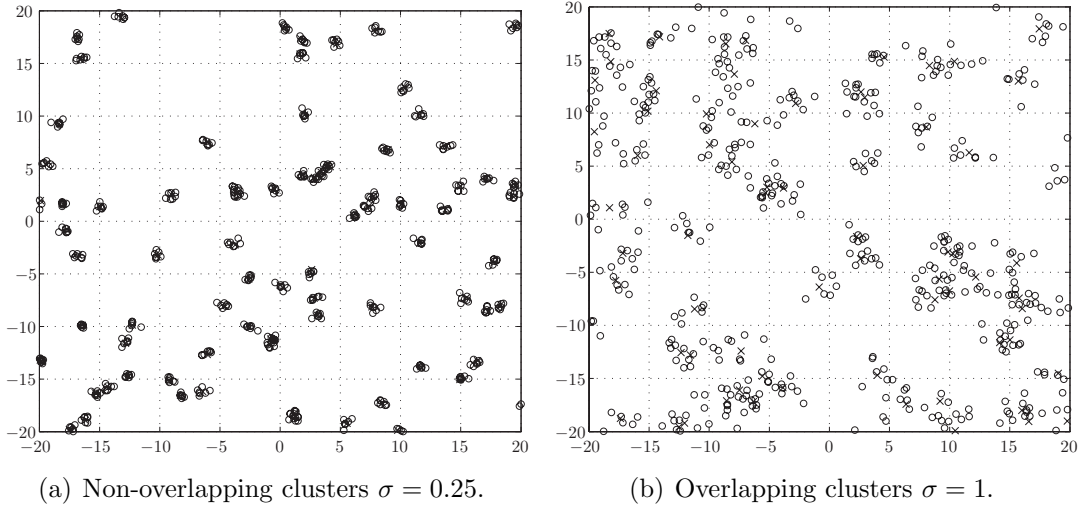


Figure 6.10: Sample realization of a clustered network with cluster intensity  $\lambda_p = 0.05$  and different cluster sizes.

cluster that can be supported while still fulfilling the IA condition. Dominant EM outperforms intra-cluster IA for large distances between transmitter–receiver pairs. For large distances, the inter-cluster interference is predominant and the performance of intra-cluster IA is suffering from the diminishing received intended signal power caused by the alignment procedure. In that case, maximizing the receive signal power of the intended transmitter should be preferred to IA. In all considered cases, the equivalent SISO system performs worst. Clearly, an increasing number of cluster nodes decreases the transmission success probability, as can be verified from Fig. 6.11(a).

Fig. 6.11(b) shows the link level performance evaluation of the network configurations in Table 6.1 for the case where the clusters size is increased, i.e.  $\sigma = 1$ . In this case, clusters are more likely to be overlapping. The benefit of coordinated intra-cluster interference due to the alignment is vanishing. Dominant EM outperforms intra-cluster IA for the whole range of considered transmitter–receiver distances. The inter-cluster interference is predominant even for small transmitter–receiver distances  $d_{ii}$ .

In Fig. 6.12, we use a pathloss coefficient  $\alpha = 3$  and show the link level performance comparison of intra-cluster IA, dominant eigenmode transmission and the corresponding SISO network for the configurations in Table 6.1. Fig. 6.12(a) plots the probability of successful transmission curve for the cluster size  $\sigma = 0.25$ . Similar to 6.11(a), intra-cluster IA outperforms dominant EM transmission for small transmitter–receiver distance  $d_{ii}$ . Increasing  $d_{ii}$ , we observe a crossover of the cor-

responding curves for intra-cluster IA and dominant EM transmission. Compared to the case of  $\alpha = 4$ , the interception points for  $\alpha = 3$  are at smaller transmitter–receiver distances. Fig. 6.12(b) depicts the case with likely overlapping clusters, i.e.  $\sigma = 1$ . Dominant EM outperforms intra-cluster IA for the whole range of  $d_{ii}$ .

### 6.5.3 High Reliability Regime and Large System Analysis

We consider next the high SIR regime. The inverse power pathloss law with  $\alpha = 4$  is used. For the network settings listed in Table 6.1, Fig. 6.13 plots the derived asymptotic expression  $1 - \gamma\eta$  for intra-cluster IA with diversity gain  $d' = 1, 2$  with  $\gamma$  according to (6.32) and  $d_{ii} = 2$  along with Monte-Carlo simulations. We observe a close match between simulation and asymptotic expression for small  $\eta$ .

Fig. 6.14 shows the term related to the receive diversity  $\mu(d')$  derived in (6.32). Taking diversity gain allocation  $d' = 2$  decreases the slope of the  $\mathbb{P}(\text{success})$  curve by a factor of two compared to alignment without receive diversity ( $d' = 1$ ). However, we observe a diminishing incremental gain when intra-cluster IA is carried out with higher-order diversity.

Fig. 6.15 plots the area spectral efficiency [bit/s/Hz/m<sup>2</sup>] formula (6.36) as a function of the SIR threshold  $T$  for the network configurations listed in Table 6.1.  $d_{ii} = 2$  and an outage constraint  $\epsilon = 0.1$  was used. The network configurations with  $d' = 2$  outperform the corresponding configurations with classical IA. Hence, decreasing the number of simultaneously transmitting nodes per cluster increases the network spectral efficiency significantly. There exists an optimal SIR threshold  $T$  for which the area spectral efficiency is maximized. For the given network, we note that the spectral efficiency curve around the maximum is relatively flat, indicating that the choice of an operational point in  $T$  is robust to minor errors.

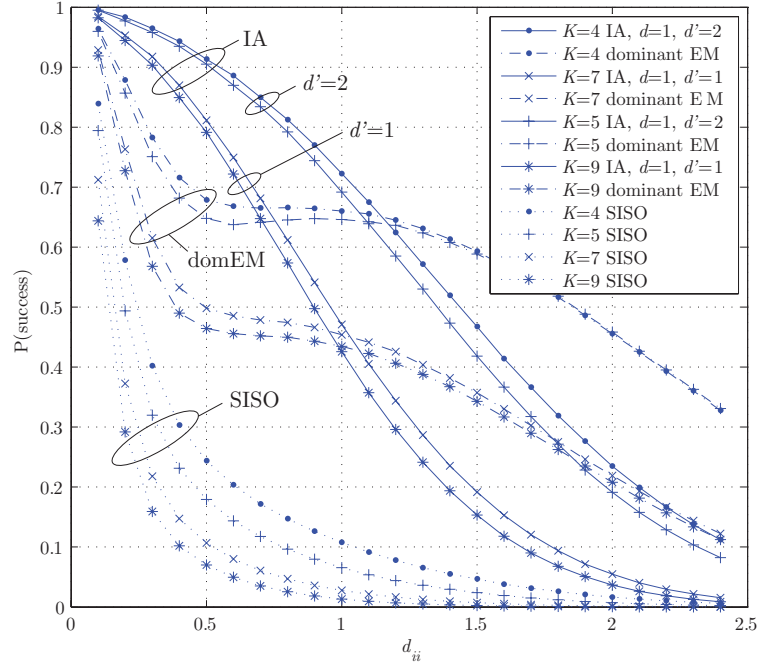
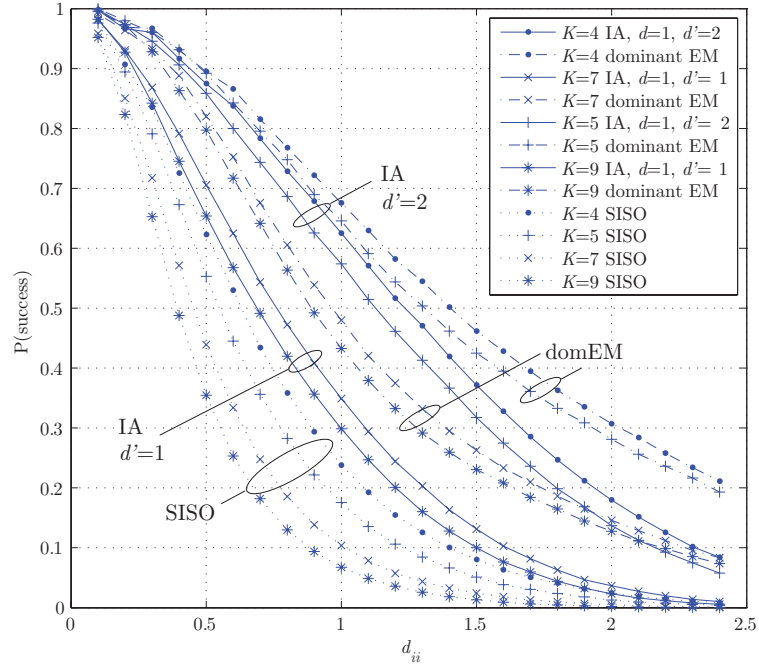
(a) Non-overlapping clusters  $\sigma = 0.25$ .(b) Overlapping clusters  $\sigma = 1$ .

Figure 6.11:  $\mathbb{P}(\text{success})$  versus  $d_{ii}$ ,  $\lambda_p = 0.05$ ,  $\alpha = 4$ . Comparison of link level performance of intra-cluster IA, dominant eigenmode transmission and the corresponding SISO network.

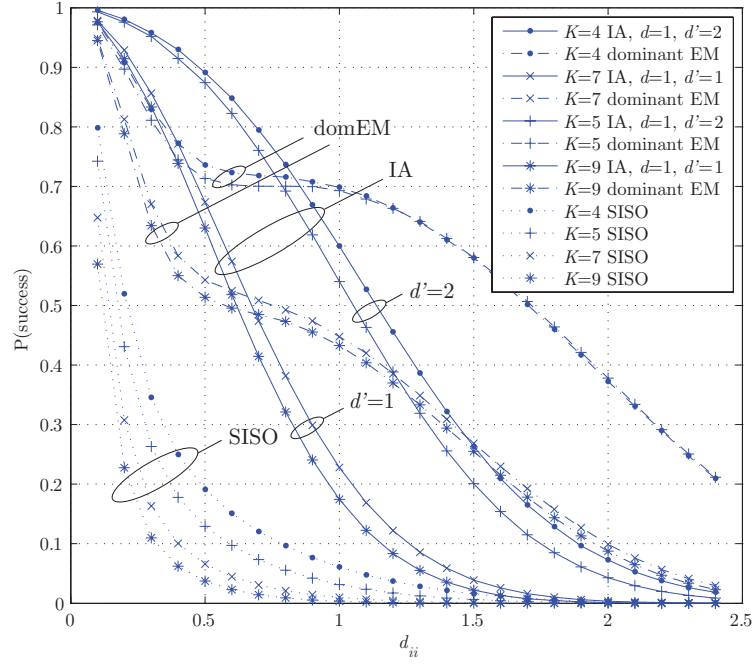
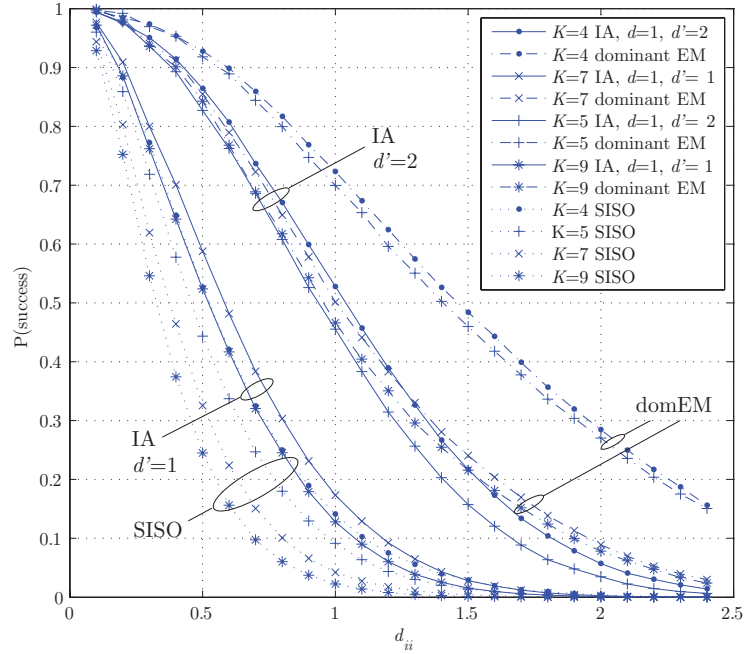

 (a) Non-overlapping clusters  $\sigma = 0.25$ .

 (b) Overlapping clusters  $\sigma = 1$ .

Figure 6.12:  $\mathbb{P}(\text{success})$  versus  $d_{ii}$ ,  $\lambda_p = 0.05$ ,  $\alpha = 3$ . Comparison of link level performance of intra-cluster IA, dominant eigenmode transmission and the corresponding SISO network.

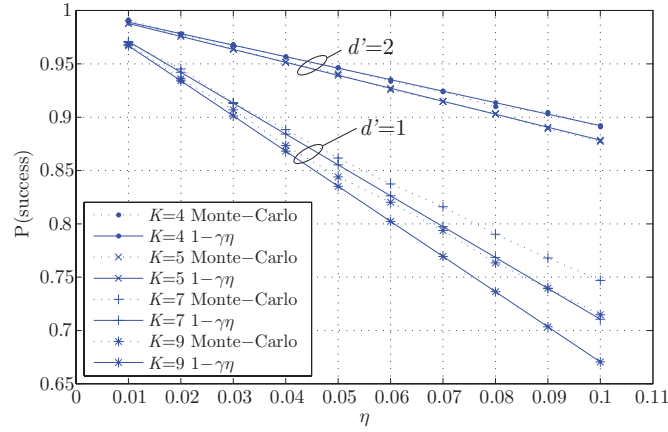


Figure 6.13:  $\mathbb{P}(\text{success})$  versus  $\eta$  in the high-reliability regime. Comparison of Monte-Carlo simulation of the SIR expression and closed-form approximation with  $\gamma$  derived in (6.32).

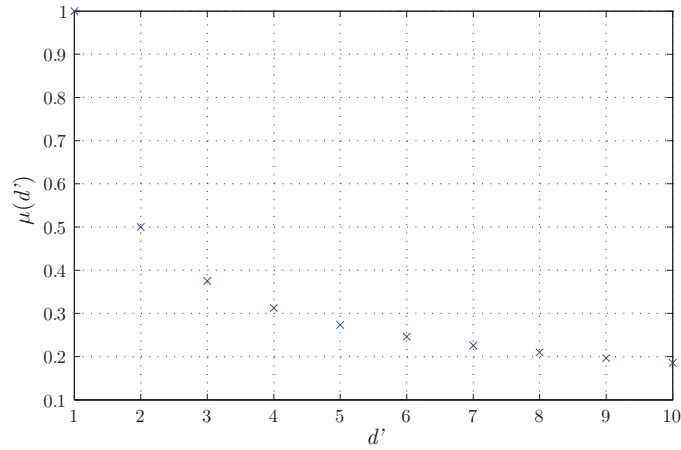


Figure 6.14: Term in the expression of the transmission success probability (6.32) related to the diversity gain as a function of the diversity gain allocation.

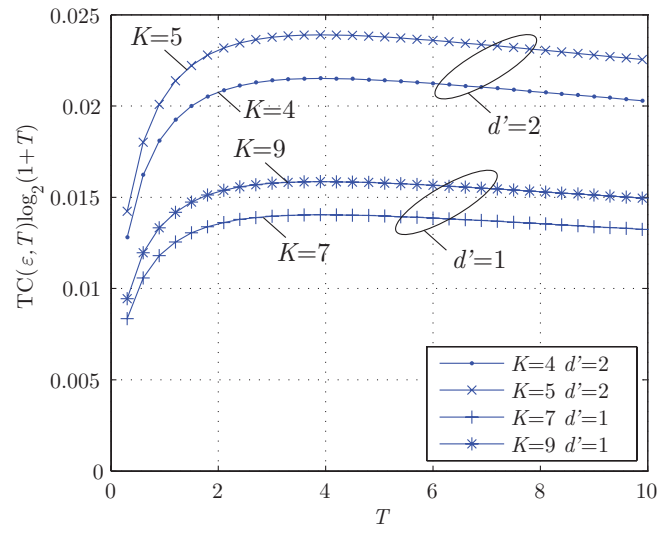


Figure 6.15: Area spectral efficiency [bit/s/Hz/m<sup>2</sup>] as a function of the SIR threshold  $T$  for the network configurations introduced in Table 6.1.

## 6.6 Appendix: Integral Expressions for $\mathbb{P}(\text{success})$

In this section, we proof Theorem 6 which finds numerically integrable expression for the transmission success probability of intra-cluster MIMO-IA without diversity gain ( $d' = 1$ ) and for the corresponding SISO network without intra-cluster interference mitigation. We measure the interference conditioned on having the intended transmitter at a fixed geographical location (henceforth the origin for mathematical convenience). Here, we use the fact that PCP are stationary and utilize the framework of *Palm* probabilities. Informally, Palm distributions for PP are the counterparts of conditional distributions for random variables. Furthermore, we use the conditional *probability generating functional* (PGFL) of a PP that is instrumental for interference characterization. We will show that the outage probability is derived as the Laplace transform of the interference evaluated at a particular point conditioned on the intended transmitter located at the origin. The expression for the Laplace transform of the interference is established using the PGFL of the clustered PP.

Let us begin with the definition of the PGFL. It fully characterizes the PP and is equivalent to the *moment generating function* for random variables.

**Definition 8.** Let  $\nu(x) : \mathbb{R}^2 \rightarrow [0, \infty)$ . The conditional *probability generating functional* PGFL of the PP  $\Phi$  is defined as

$$\tilde{\mathcal{G}}(\nu) = \mathbb{E}^{\text{lo}} \left[ \prod_{i \in \phi} \nu(x_i) \right]. \quad (6.40)$$

where  $\mathbb{E}^{\text{lo}}[\cdot]$  is the conditional expectation for PP, given that there is a point of the process at the origin but without including the point. The unconditional PGFL  $\mathcal{G}(\nu)$  is similarly defined with an unconditional expectation in the RHS of (6.40). For a homogeneous PPP with density  $\lambda$ , the conditional PGFL equals the PGFL and reads [34]

$$\mathcal{G}(\nu) = \exp \left( -\lambda \int_{\mathbb{R}^2} [1 - \nu(x)] dx \right). \quad (6.41)$$

We now tackle the derivation of the transmission success probability and prove Theorem 6.

*Proof.* The probability of success for a transmitter located at the origin and the receiver at location  $z$  and distance  $d_{ii} = \|z\|$  is given by (6.15), i.e.

$$\begin{aligned} \mathbb{P}(\text{success}) &= \mathbb{P} \left( \frac{|\bar{h}_{ii}|^2 \gamma_{ii}}{\sigma_n^2 + I_\Phi} \geq T \mid \text{intended transmitter at the origin} \right) \\ &= \mathbb{P}^{\text{lo}} \left( \frac{|\bar{h}_{ii}|^2 \gamma_{ii}}{\sigma_n^2 + I_\Phi} \geq T \right), \end{aligned} \quad (6.42)$$

with  $I_\Phi$  according to (6.16) and  $\mathbb{P}^{!o}$  in (6.42) is the probability conditioned on the fact that the PP has a point at the origin. Following [37], the probability of successful transmission for the receiver served by the transmitter at the origin (when we neglect the noise) is

$$\begin{aligned}\mathbb{P}(\text{success}) &= \mathbb{P}^{!o}(|\bar{h}_{ii}|^2 \geq T\gamma_{ii}^{-1}I_\Phi) = \int_0^\infty \mathbb{P}(|\bar{h}_{ii}|^2 \geq tT\gamma_{ii}^{-1}) f_{I_\Phi}(t) dt \\ &= \int_0^\infty F_{|\bar{h}_{ii}|^2}^c(tT\gamma_{ii}^{-1}) f_{I_\Phi}(t) dt,\end{aligned}\quad (6.43)$$

with  $F_{|\bar{h}_{ii}|^2}^c$  the complementary cumulative distribution function (CCDF) of the received signal power and  $f_{I_\Phi}(t)$  the density function of the interference. In (6.43)  $F_{|\bar{h}_{ii}|^2}^c(tT\gamma_{ii}^{-1}) = \exp(-tT\gamma_{ii}^{-1})$  so that

$$\mathbb{P}(\text{success}) = \int_0^\infty \exp(-tT\gamma_{ii}^{-1}) f_{I_\Phi}(t) dt = \mathcal{L}_{I_\Phi}^{!o}(T\gamma_{ii}^{-1}), \quad (6.44)$$

with  $\mathcal{L}_{I_\Phi}^{!o}$  the conditional *Laplace transform* of the interference.

It is shown in [38, Lemma 2] that the conditional Laplace transform of the interference (6.44) is

$$\mathcal{L}_{I_\Phi}^{!o}(s) = \tilde{\mathcal{G}}(\mathcal{L}_{|\bar{h}_{ij}|^2}(sg(x-z))), \quad (6.45)$$

with  $\tilde{\mathcal{G}}(\cdot)$  the conditional PGFL and  $|\bar{h}_{ij}|^2$  the power received from the interfering transmitters. Since  $|\bar{h}_{ij}|^2$  is exponentially distributed,  $\mathcal{L}_{|\bar{h}_{ij}|^2}(sg(x-z)) = 1/(1 + sg(x-z))$  and with (6.44)

$$\mathbb{P}(\text{success}) = \mathcal{L}_{I_\Phi}^{!o}(s)|_{s=T\gamma_{ii}^{-1}} = \tilde{\mathcal{G}}\left(\frac{1}{1 + T\gamma_{ii}^{-1}g(\cdot - z)}\right). \quad (6.46)$$

Now, we have to distinguish the two interference situations given by the above settings with interference terms according to (6.16). Firstly, if only inter-cluster interference is accumulated, the conditional PGFL is equal to the unconditional PGFL which can be calculated for Neyman-Scott cluster processes with a constant number of cluster points as [34]

$$\mathcal{G}(\nu) = \exp\left(-\lambda_p \int_{\mathbb{R}^2} \left[1 - \left(\int_{\mathbb{R}^2} \nu(x+y) f_{cl}(y) dy\right)^K\right] dx\right), \quad (6.47)$$

with  $\nu(x) : \mathbb{R}^2 \rightarrow [0, \infty)$  any function. In (6.47) we used the fact that the parent process is a homogeneous PPP with density  $\lambda_p$  (for which the PGFL is (6.41)). Equation (6.46) with  $\tilde{\mathcal{G}}(\nu) = \mathcal{G}(\nu)$  according to (6.47) where  $\nu(x) = 1/(1 + T\gamma_{ii}^{-1}g(x -$



$z$ )) leads to (6.17). Secondly, in the case of single-antenna terminals where inter-cluster and intra-cluster interference is accumulated, the conditional PGFL writes [38]

$$\tilde{\mathcal{G}}(\nu) = \exp \left( \mathcal{G}(\nu) \int_{\mathbb{R}^2} \left( \int_{\mathbb{R}^2} \nu(x-y) f_{\text{cl}}(x) dx \right)^{(K-1)} f_{\text{cl}}(y) dx \right). \quad (6.48)$$

Equation (6.46) together with (6.48) and (6.47) where  $\nu(x) = 1/(1 + T\gamma_{ii}^{-1}g(x-z))$  leads to the additional term  $\int \tilde{\beta}(z, y)^{K-1} f_{\text{cl}}(y) dy$  in the expression for  $\mathbb{P}(\text{success})$ , in line with [38, Appendix II].  $\square$

Let us now apply the above derivation to the case of intra-cluster IA with receive diversity and opportunistic dominant eigenmode transmission. In the case of IA, the CCDF of the power fading term  $|\bar{h}_{ii}|^2$  is according to (6.27)  $F_{|\bar{h}_{ii}|^2}^c(t) = e^{-t} \sum_{k=0}^{d'-1} \frac{t^k}{k!}$ . Due to the Laplace transform property  $t^n f(t) \leftrightarrow (-1)^n \frac{d^n}{ds^n} \mathcal{L}_f(s)$ , the transmission success probability corresponding to (6.46) writes

$$\mathbb{P}(\text{success}) = \sum_{k=0}^{d'-1} \frac{(-1)^k}{k!} \frac{d^k}{ds^k} \mathcal{L}_{I_\Phi}^{\text{lo}}(s) \big|_{s=T\gamma_{ii}^{-1}}. \quad (6.49)$$

The derivatives involved in (6.49) make the derivation of along the lines presented above analytically intractable. In the case of dominant eigenmode transmission the CCDF of the power fading term  $|\bar{h}_{ii}|^2$  is [91]

$$F_{|\bar{h}_{ii}|^2}^c(t) = 1 - \frac{\det(\Upsilon(t))}{\prod_{k=1}^{N^{\min}} \Gamma(N^{\min} - k - 1) \Gamma(N^{\max} - k - 1)}, \quad (6.50)$$

where  $N^{\min} = \min\{N_T, N_R\}$ ,  $N^{\max} = \max\{N_T, N_R\}$ , and the entries of the  $N^{\min} \times N^{\min}$  matrix  $\Upsilon(t)$  are given by  $[\Upsilon(t)]_{(i,j)} = \gamma(N^{\max} - N^{\min} + i + j - 1, t)$ ,  $i, j = 1, \dots, N^{\min}$  where  $\gamma(\cdot, \cdot)$  is the lower incomplete *Gamma* function and  $\Gamma(\cdot)$  the *Gamma* function. The CCDF cannot be given explicitly for arbitrary  $N_T$  and  $N_R$  and prohibits the derivation of analytically tractable expressions.



## 7 Summary and Conclusions

In this thesis, I devised, assessed and analyzed interference management techniques for the multiple antenna broadcast and interference channels. The contributions and key findings are summarized in the following.

- My improved SINR feedback metric for random beamforming based on noisy MIMO channel measurements provides a noticeable decrease in outage probability. In practical scenarios such as the  $4 \times 2$  ( $N_T \times N_R$ ) antenna case, it incurs only a marginal goodput loss compared to state-of-the-art rate back-off schemes. The metric is designed as a conservative estimate of the actual SINR, based on expectations of bounds on the signal and interference power.
- Interference alignment with diversity receivers significantly increases the ergodic per-user rate in the  $K$ -user MIMO interference channel at medium SNR. However, this gain has to be traded-off with the number of simultaneous users that are active in the network.
- I derived a closed-form solution for interference alignment in the  $M \times M$  interference channel for an arbitrary number of users  $K$  with single-stream transmission per user under the assumption that the number of antennas is  $M = N_T = N_R = K - 1$ . My constructive method for finding the interference alignment precoders significantly reduces the computational complexity compared to iterative schemes. It does not require the channel/network reciprocity assumption and can be applied in frequency division duplex systems.
- In a large cellular system with clustered base station cooperation, I identified that uncoordinated interference causes the inferior performance of interference alignment for users located at the base station cooperation edge. However, users located in the central area of the cells enjoy throughput gains of up to 30% with respect to non-cooperating base stations. This gain comes at the cost of cooperation overhead and signaling feedback. For the cluster-edge users, prevalent techniques based on frequency reuse outperform alignment-based schemes.

- I modeled the positions of concurrent transmitters in a peer-to-peer network as realizations of a stochastic point process on the infinite plane. This approach facilitated link-level performance analysis of clustered cooperation using tools of stochastic geometry. I found numerically integrable expression for the outage probability of intra-cluster IA. For certain network settings, I devised closed-form bounds for the outage probability as a function of the underlying network model, signal attenuation and link-level communication parameters.
- Per-cluster interference alignment is inferior to egoistic transmission along the dominant eigenmode of the intended channel in a large network with overlapping clusters. The same holds for the case of isolated clusters if the distances between transmitter-receiver pairs is large. Interference alignment is beneficially applied if the clusters are separated and the distances between transmitter receiver pairs is small. In this case, alignment with receive diversity reveals its full potential, i.e. the suppression of coordinated intra-cluster interference in the vicinity of the intended transmitter and an increased link reliability. A distance dependent pathloss with inverse power law and pathloss coefficients three and four was used in my analysis.
- I found a diminishing incremental gain when intra-cluster interference alignment is carried out with higher order diversity. I studied the case where the density of the inter-cluster interferers is negligible. When using per-cluster ALOHA, I showed that the probability of successful transmission (as a function of the ALOHA medium access probability) can be approximated in the high reliability regime by an affine function of the cluster transmission probability. I derived a numerically integrable expression for its slope. For a special network setting with power-law pathloss, we derived the slope in closed-form and identified the term related to the diversity gain.
- Intra-cluster interference alignment with diversity gain can increase the aggregated network throughput per unit area. I established formulas for the transmission capacity, i.e. the maximum spatial density of active links given an outage constraint in the high reliability regime. For the aforementioned network setting with power-law pathloss four, I derived a closed form expression and found that the optimal SIR operating point is robust to minor errors.

Based on the work of my thesis, I draw the following conclusions regarding practically feasible interference management protocols for interference limited communication networks.

---

**Channel state information (CSI):** I observed that accurate CSI significantly influences the performance gains of interference mitigation techniques. I assessed the diminishing effects of imperfect CSI in the random beamforming scheme and for alignment-based precoding. My investigations showed that theoretical performance gains of interference alignment can only be achieved with considerable effort in CSI acquisition and feedback. The performance of noncooperative schemes are less sensitive to imperfect channel knowledge. This is especially relevant in large networks where channel knowledge of all interfering links is practically infeasible. Therefore, I conclude that cooperative interference mitigation techniques in practical systems require compressed CSI feedback that allows nearly optimal channel adaptation and minimum cooperation overhead.

**Low complexity interference alignment schemes:** I investigated interference alignment schemes that require low computational complexity. I found an explicit solution for the alignment precoders that can be applied in frequency division duplex systems. The explicit solution is derived using a global network formulation and is based on explicit feedback of the channel gains. Albeit the restriction that it is solely applicable to particular MIMO settings, this method has the advantage that it avoids a potentially long training phase and calibration methods that are needed for schemes based on network reciprocity. I deduce that low complexity interference alignment algorithms with low-rate CSI feedback have to be developed further in order to be included in standards of future wireless systems. Approaches in combination with diversity techniques will gain significance due to the inferior performance of interference alignment in the low-to-medium SNR regime.

**Clustering:** In large interference networks, I deduced that suitable clustering of cooperating transmitters in a distributed and adaptive way is a key challenge. I restricted my investigations to static clusters that partition the network. In dense network scenarios, I found a superior performance of opportunistic transmission schemes compared to local alignment-based cooperation whose performance is significantly impaired by the presence of uncoordinated interference. In the context of base station cooperation, hybrid solutions where interference alignment and frequency reuse schemes are simultaneously used inside of one cell have the potential to increase the network spectral efficiency. I propose network planning that applies interference alignment for users with high SIR (bandwidth limited regime) and frequency reuse schemes in a separate subband for users at the edge of the cooperation cluster at low SIR (power-limited regime). My modeling approach, based on two-dimensional stochastic point processes led to a more accurate assessment of the

benefits of node cooperation than prevalent one-dimensional or grid-based models. I showed that the applicability of interference alignment in large interference limited networks that render benefits for all users need to include scalable grouping strategies with possibly flexible formation of cooperation clusters.

# A Notation, Abbreviations

Symbols and notation used in this manuscript are listed in Table A.1 and Table A.2.

| Symbol                    | Description   |
|---------------------------|---|
| $\gamma_{ij}$             | pathloss on the link between transmitter $j$ and receiver $i$               |
| $\Phi$                    | stochastic point process on $\mathbb{R}^2$                                  |
| $d$                       | multiplexing gain allocation per user                                       |
| $d'$                      | diversity gain allocation per user  |
| $d_{\mathbf{H}}$          | multiplexing gain of the multiuser network                                  |
| $K$                       | number of user pairs present in the network                                 |
| $\mathbf{H}_{ij}$         | MIMO channel of the link between transmitter $j$ and receiver $i$           |
| $\tilde{\mathbf{H}}_{ij}$ | estimated MIMO channel of the link between transmitter $j$ and receiver $i$ |
| $L_h$                     | maximum number of channel taps with significant energy                      |
| $N_T$                     | number of transmit antennas   |
| $N_R$                     | number of receive antennas  |
| $M$                       | number of transmit and receive antennas in a symmetric MIMO system          |
| $T_c$                     | coherence time  |
| $T_d$                     | delay spread  |
| $\mathbf{v}_j$            | precoding/beamforming vector of transmitter $j$                             |
| $W_{ij}$                  | message from transmitter $j$ to receiver $i$                                |

Table A.1: Symbols used throughout this manuscript.

| Symbol   | Description  |
|--|--|
| $\mathbb{P}(A)$                                  | probability of an event $A$  |
| $\mathbb{E}_x[\cdot]$                            | expectation operator taken over the variable $x$   |
| $(\cdot)^*$                                      | complex conjugate operator   |
| $(\cdot)^T$                                      | transpose operator   |
| $(\cdot)^H$                                      | Hermitian transpose operator (transpose + complex conjugate)   |
| $\text{Tr}(\cdot)$                               | trace operator   |
| $\mathcal{S}(\mathbf{v}_1, \dots, \mathbf{v}_n)$ | subspace spanned by vectors $\mathbf{v}_1, \dots, \mathbf{v}_n$  |
| $\sim$   | distributed as   |
| $ S $  | cardinality of a set $S$   |
| $\mathbf{I}_n$                                   | $n \times n$ identity matrix   |
| $\mathbf{O}_{m \times n}$                        | $m \times n$ all zero matrix   |
| $\mathbf{0}_n$                                   | $n \times 1$ all zero vector   |
| $\ \cdot\ $                                      | Euclidean norm   |
| $\ \cdot\ _F$                                    | Frobenius norm   |
| $\mathbb{R}$                                     | set of real numbers  |
| $\mathbb{C}$                                     | set of complex numbers   |
| $\mathcal{N}(a, \sigma^2)$                       | normal (Gaussian) distribution of mean $a$ and variance $\sigma^2$   |
| $\mathcal{CN}(a, \sigma^2)$                      | complex normal distribution of mean $a$ and variance $\sigma^2$  |
| $\delta[\cdot]$                                  | discrete-time (Kronecker) delta function   |
| $[x_i]_{i=1, \dots, n}$                          | a list containing $x_1, x_2, \dots, x_n$   |
| $[\mathbf{A}]_{(k:l, m:n)}$                      | a submatrix of $\mathbf{A}$ containing the elements of rows $k - l$ and columns $m - n$  |
| $\text{diag}\{\mathbf{A}\}$                      | main diagonal of $M \times M$ $\mathbf{A}$ , i.e. $[A_{11}, A_{22}, \dots, A_{MM}]$  |
| $\text{diag}\{\mathbf{v}\}$                      | diagonal matrix with the main diagonal $\mathbf{v}$ , i.e. $\text{diag}\{\mathbf{v}\} = \mathbf{A}$ such that $[A]_{(1,1)} = \mathbf{v}_{(1,1)}, [A]_{(2,2)} = \mathbf{v}_{(2,1)}, \dots, [A]_{(M,M)} = \mathbf{v}_{(M,1)}$ and $[A]_{(i,j)} = 0 \ \forall i \neq j$ |
| $\mathbb{I}[g]$                                  | indicator function, i.e. $\mathbb{I}[g] = \{1, 0\}$ if statement $g$ is true or false  |
| $\Re\{c\}$                                       | the real part of $c \in \mathbb{C}$  |
| $\Im\{c\}$                                       | the imaginary part of $c \in \mathbb{C}$   |
| $\mathcal{L}(f(t))$                              | Laplace transform of $f(t)$  |

Table A.2: Notation used throughout this manuscript.



---

Abbreviations used in this manuscript are listed in Table A.3 and A.4.

| Abbreviation | Description                                    |
|--------------|--|
| AWGN         | additive white Gaussian noise                  |
| BC           | broadcast channel                              |
| CCDF         | complementary cumulative distribution function |
| CDMA         | code division multiple access                  |
| CCI          | co-channel interference                        |
| CSI          | channel state information                      |
| DMT          | diversity-multiplexing trade-off               |
| DoF          | degrees of freedom                             |
| EM           | eigenmode                                      |
| FDD          | frequency division duplexing                   |
| GSM          | global system for mobile communications        |
| IA           | interference alignment                         |
| IC           | interference channel                           |
| i.i.d.       | independent and identically distributed        |
| ISI          | inter-symbol interference                      |
| LHS          | left-hand side                                 |
| LMMSE        | linear minimum mean square error               |
| LTE          | long term evolution                            |

Table A.3: Abbreviations A-L used throughout this manuscript.

| Abbreviation | Description                                     |
|--------------|---|
| MF           | matched filter                                  |
| MIMO         | multiple-input multiple-output                  |
| MISO         | multiple-input single-output                    |
| OFDM         | orthogonal frequency division multiplexing      |
| PCP          | Poisson cluster process                         |
| PDF          | probability density function                    |
| PGFL         | probability generating functional               |
| PP           | point process                                   |
| PPP          | Poisson point process                           |
| RHS          | right-hand side                                 |
| SIMO         | single-input multiple-output                    |
| SINR         | signal-to-interference-plus-noise ratio         |
| SISO         | single-input single-output                      |
| SIR          | signal-to-interference ratio                    |
| SNR          | signal-to-noise ratio                           |
| SVD          | singular value decomposition                    |
| TC           | transport capacity                              |
| TDD          | time division duplexing                         |
| UMTS         | universal mobile telecommunications system      |
| WiMAX        | worldwide interoperability for microwave access |
| w.p.         | with probability                                |

Table A.4: Abbreviations M-Z used throughout this manuscript.

# Bibliography

- [1] E. Dahlmann, S. Parkvall, J. Sköld, and P. Beming, *3G evolution: HSPA and LTE for mobile broadband*. Academic Press, 2007.
- [2] D. Astely, E. Dahlman, A. Furuskär, I. Jading, M. Lindström, and S. Parkvall, “LTE: The evolution of mobile bradband,” *IEEE Communications Magazine*, vol. 47, no. 4, pp. 44–51, Apr. 2009.
- [3] S. Parkvall and D. Astely, “The evolution of LTE towards ITM-advanced,” *Journal of Communications (JCM)*, vol. 4, no. 3, pp. 146–154, Apr. 2009.
- [4] T. Cover, “Broadcast channels,” *IEEE Trans. Information Theory*, vol. 18, no. 1, pp. 2–14, Jan. 1972.
- [5] H. Weingarten, Y. Steinberg, and S. S. (Shitz), “The capacity region of the Gaussian MIMO broadcast channel,” in *Proc. IEEE Int. Symp. on Information Theory (ISIT)*, Chicago, IL, USA, Jun. 2004.
- [6] B. M. Hochwald, C. B. Peel, and A. L. Swindlehurst, “A vector-perturbation technique for near-capacity multiantenna multiuser communication - part ii: Perturbation,” *IEEE Trans. Information Theory*, vol. 53, no. 3, pp. 537–544, Mar. 2005.
- [7] D. J. Love, J. R. W. Heath, V. K. N. Lau, D. Gesbert, B. D. Rao, and M. Andrews, “An overview of limited reedback in wireless communication systems,” *IEEE Journal on Sel. Areas in Comm., Special Issue on Exploiting Limited Feedback in Tomorrow’s Wireless Communication Networks*, vol. 26, pp. 1341–1365, Oct. 2008.
- [8] D. Tse and P. Viswanath, *Fundamentals of wireless communication*. Cambridge, 2005.
- [9] M. Sharif and B. Hassibi, “On the capacity of MIMO broadcast channels with partial side information,” *IEEE Trans. Information Theory*, vol. 51, no. 2, pp. 506–522, Feb. 2005.

- [10] P. Viswanath, D. Tse, and R. Laroia, "Opportunistic beamforming using dumb antennas," *IEEE Trans. Information Theory*, vol. 48, no. 6, pp. 1277–1294, Jun. 2002.
- [11] A. Vakili, M. Sharif, and B. Hassibi, "The effect of channel estimation error on the throughput of broadcast channels," in *Proc. International Conference on Acoustics, Speech, and Signal Processing (ICASSP)*, 2006.
- [12] A. Vakili and B. Hassibi, "On the throughput of broadcast channels with imperfect CSI," in *Proc. 7th IEEE Workshop on Signal Processing Advances in Wireless Communications (SPAWC)*, 2006.
- [13] M. Kobayashi, G. Caire, and D. Gesbert, "Impact of multiple transmit antennas in a queued SDMA/TDMA downlink," in *Proc. IEEE Workshop on Signal Processing Advances in Wireless Communications (SPAWC)*, New York, NY, USA, Jun. 2005.
- [14] G. Kramer, "Outer bounds on the capacity of Gaussian interference channels," *IEEE Trans. Information Theory*, vol. 50, no. 3, pp. 581–586, Mar. 2004.
- [15] A. B. Carleial, "Interference channels," *IEEE Trans. Information Theory*, vol. 24, no. 1, pp. 60–70, Jan. 1978.
- [16] M. Costa, "On the Gaussian interference channel," *IEEE Trans. Information Theory*, vol. 31, no. 5, pp. 607–615, Sep. 1985.
- [17] V. R. Cadambe and S. A. Jafar, "Interference alignment and degrees of freedom of the  $K$ -user interference channel," *IEEE Trans. Information Theory*, vol. 54, no. 8, pp. 3425–3441, Aug. 2008.
- [18] A. Host-Madsen and A. Nosratinia, "The multiplexing gain of wireless networks," in *Proc. IEEE Int. Symp. on Information Theory (ISIT)*, Adelaide, Australia, Sep. 2005.
- [19] S. A. Jafar and S. Shamai, "Degrees of freedom region of the MIMO X channel," *IEEE Trans. Information Theory*, vol. 54, no. 1, pp. 151–170, Jan. 2008.
- [20] V. R. Cadambe and S. A. Jafar, "Reflections on interference alignment and the degrees of freedom of the  $K$  user interference channel," *IEEE Information Theory Society Newsletter*, vol. 59, no. 4, pp. 5–9, Dec. 2009.

- [21] —, “Interference alignment and degrees of freedom of the  $K$ -user interference channel,” in *Proc. of the IEEE International Conference on Communications (ICC 2008)*, Beijing, China, May 2008.
- [22] K. Gomadam, V. R. Cadambe, and S. A. Jafar, “Approaching the capacity of wireless networks through distributed interference alignment,” *IEEE Trans. Information Theory*, 2008, accepted for publication. [Online]. Available: <http://arxiv.org/abs/0803.3816>
- [23] K. S. Gomadam, V. R. Cadambe, and S. A. Jafar, “Approaching the capacity of wireless networks through distributed interference alignment,” in *Proc. of IEEE Global Communications Conference (GLOBECOM)*, Dec. 2008.
- [24] D. A. Schmidt, C. Shi, R. A. Berry, M. L. Honig, and W. Utschick, “Minimum mean squared error interference alignment,” in *Proc. of the 43th Asilomar Conference on Signals, Systems and Computers*, Nov. 2009.
- [25] S. W. Peters and J. Robert W. Heath, “Interference alignment via alternating minimization,” in *Proc. IEEE International Conference on Acoustics, Speech and Signal Processing (ICASSP)*, Taipei, Taiwan, Apr. 2009.
- [26] —, “Cooperative algorithms for MIMO interference channels,” *IEEE Trans. on Vehicular Technology*, 2010, to appear.
- [27] C. M. Yetis, T. Gou, S. A. Jafar, and A. H. Kayran, “Feasibility conditions for interference alignment,” in *Proc. IEEE Global Telecommunications Conference 2009 (GLOBECOM)*, 2009.
- [28] —, “On feasibility of interference alignment in MIMO interference networks,” *IEEE Transactions on Signal Processing*, vol. 58, no. 9, pp. 4771–4782, Sep. 2010.
- [29] K. R. Kumar and X. Feng, “An iterative algorithm for joint signal and interference alignment,” in *Proc. IEEE Int. Symp. on Information Theory (ISIT)*, Austin, Texas, USA, Jun. 2010.
- [30] T. Gou and S. A. Jafar, “Degrees of freedom of the  $K$ -user  $M \times N$  MIMO interference channel,” *IEEE Trans. Information Theory*, 2008, accepted for publication. [Online]. Available: <http://arxiv.org/abs/0809.0099>

- [31] M. Guillaud, "Receive diversity and ergodic performance of interference alignment on the MIMO Gaussian interference channel," in *Proc. Allerton Conference on Communication, Control, and Computing*, Monticello, IL, USA, Sep. 2010.
- [32] M. Haenggi, J. G. Andrews, F. Baccelli, O. Dousse, and M. Franceschetti, "Stochastic geometry and random graphs for the analysis and design of wireless networks," *IEEE Journal on Selected Areas in Communications*, vol. 27, pp. 1029–1046, Sep. 2009.
- [33] J. G. Andrews, R. K. Ganti, M. Haenggi, N. Jindal, and S. Weber, "A primer on spatial modeling and analysis in wireless networks," *IEEE Communications Magazine*, Nov. 2010, accepted. Available at <http://www.nd.edu/~mhaenggi/pubs/commag10.pdf>.
- [34] D. Stooyan, W. Kendall, and J. Mecke, *Stochastic geometry and its applications, 2nd edition*. John Wiley and Sons, 1996.
- [35] F. Baccelli and B. Błaszczyszyn, "Stochastic geometry and wireless networks volume 1: THEORY," *Foundations and Trends in Networking*, vol. 3–4, no. 3, pp. 249–449, 2009.
- [36] M. Haenggi and R. K. Ganti, "Interference in large wireless networks," *Foundations and Trends in Networking*, vol. 3, no. 2, pp. 127–248, 2009.
- [37] F. Baccelli, B. Błaszczyszyn, and P. Mühlethaler, "An ALOHA protocol for multihop mobile wireless networks," *IEEE Trans. Inf. Theory*, vol. 52, pp. 421–436, 2006.
- [38] R. K. Ganti and M. Haenggi, "Interference and outage in clustered wireless *ad hoc* networks," *IEEE Trans. Information Theory*, vol. 55, no. 9, pp. 4067–4086, Sep. 2009.
- [39] S. P. Weber, X. Yang, J. G. Andrews, and G. de Veciana, "Transmission capacity of wireless *ad hoc* networks with outage constraints," *IEEE Trans. Information Theory*, vol. 51, no. 12, pp. 4091–4102, Dec. 2005.
- [40] A. Hunter, J. Andrews, and S. Weber, "Transmission capacity of *ad hoc* networks with spatial diversity," *Wireless Communications, IEEE Transactions on*, vol. 7, no. 12, pp. 5058–5071, Dec. 2008.

- [41] R. K. Ganti, J. G. Andrews, and M. Haenggi, “High-SIR transmission capacity of wireless networks with general fading and node distribution,” *IEEE Trans. Information Theory*, 2010, submitted.
- [42] R. Giacomelli, R. K. Ganti, and M. Haenggi, “Outage probability of general ad hoc networks in the high-reliability regime,” *IEEE/ACM Transactions on Networking*, 2010, submitted.
- [43] R. K. Ganti and J. G. Andrews, “A new method for computing the transmission capacity of non-Poisson wireless networks,” in *Proc. IEEE Int. Symp. on Information Theory (ISIT)*, Austin, Texas, USA, Jun. 2010.
- [44] V. Chandrasekhar and J. G. Andrews, “Uplink capacity and interference avoidance for two-tier femtocell networks,” *IEEE Transactions on Wireless Communications*, vol. 8, no. 7, pp. 3498–3509, Jul. 2009.
- [45] O. Johnson, M. Aldridge, and R. Piechocki, “Interference alignment-based sum capacity bounds for random dense Gaussian interference networks,” *IEEE Trans. Information Theory*, vol. 57, no. 1, pp. 282–290, Jan. 2011.
- [46] U. Niesen, “Interference alignment in dense wireless networks,” in *Proc. IEEE Information Theory Workshop (ITW)*, Dublin, Ireland, Jan. 2010.
- [47] B. Nazer, M. Gastpar, S. A. Jafar, and S. Vishwanath, “Ergodic interference alignment,” in *Proc. IEEE Int. Symp. Information Theory (ISIT)*, Jun. 2009, pp. 1769–1773.
- [48] T. Rappaport, *Wireless communications: principles & practice*. Prentice Hall, 1996.
- [49] A. Paulraj, R. Nabar, and D. Gore, *Introduction to Space-Time Wireless Communications*. Cambridge University Press, 2003.
- [50] H. Bölcskei, “Principles of MIMO-OFDM Wireless Systems,” *Chapter in CRC handbook on signal processing for mobile communications*, M. Ibnkahla, Ed., 2004.
- [51] I. E. Telatar, “Capacity of multi-antenna Gaussian channels,” *European Transactions on Telecommunications*, vol. 10, no. 6, pp. 585–595, 1999.
- [52] G. W. Stewart, “Stochastic perturbation theory,” *SIAM Review*, vol. 32, no. 4, pp. 579–610, 1990.

- [53] M. Kountouris, R. de Francisco, D. Gesbert, D. Slock, and T. Salzer, “Efficient metrics for scheduling in MIMO broadcast channels with limited feedback,” in *Proc. International Conference on Acoustics, Speech, and Signal Processing (ICASSP)*, Honolulu, USA, Apr. 2007.
- [54] R. Tresch and M. Guillaud, “SINR estimation in random beamforming with noisy MIMO channel measurements,” in *Proc. IEEE International Conference on Communications (ICC)*, Beijing, China, May 2008.
- [55] W. Yu and J. Cioffi, “Sum capacity of Gaussian vector broadcast channels,” *IEEE Trans. Information Theory*, vol. 50, pp. 1875–1892, Sep. 2004.
- [56] F. P. Kelly, A. Maulloo, and D. Tan, “Rate control in communication networks: shadow prices, proportional fairness and stability,” *Journal of the Operational Research Society*, vol. 49, pp. 237–252, 1998.
- [57] J. Wagner, Y.-C. Liang, and R. Zhang, “Random beamforming with systematic beam selection,” in *Proc. International Symposium on Personal, Indoor and Mobile Radio Communications (PIMRC)*, Helsinki, Finland, Sep. 2006.
- [58] R. Etkin, D. Tse, and H. Wang, “Gaussian interference channel capacity to within one bit,” *IEEE Trans. Information Theory*, vol. 54, no. 12, pp. 5534–5562, Dec. 2008.
- [59] T. Han and K. Kobayashi, “A new achievable rate region for the interference channel,” *IEEE Trans. Information Theory*, vol. 27, pp. 49–60, Jan. 1981.
- [60] M. Maddah-Ali, A. Motahari, and A. Khandani, “Signaling over MIMO multi-base systems: Combination of multi-access and broadcast schemes,” in *Proc. IEEE Int. Symp. Information Theory (ISIT)*, Seattle, WA, USA, Jul. 2006, pp. 2104–2108.
- [61] Z. K. M. Ho and D. Gesbert, “Balancing egoism and altruism on interference channel: the MIMO case,” in *Proc. IEEE International Conference on Communications (ICC)*, Cape Town, South Africa, May 2010.
- [62] —, “Spectrum sharing in multiple antenna channels: a distributed cooperative game theoretic approach,” in *Proc. International Symposium on Personal, Indoor and Mobile Radio Communications (PIMRC)*, Cannes, France, Sep. 2008.



- [63] E. A. Jorswieck, E. G. Larsson, and D. Danev, "Complete characterization of the Pareto boundary for the MISO interference channel," *IEEE Transactions on Signal Processing*, vol. 56, no. 10, pp. 5292–5296, Oct. 2008.
- [64] R. Tresch, M. Guillaud, and E. Riegler, "On the achievability of interference alignment in the  $K$ -user constant MIMO interference channel," in *Proc. IEEE Workshop on Statistical Signal Processing (SSP)*, Cardiff, Wales, UK, Sep. 2009.
- [65] I. Csiszár and G. Tusnády, "Information geometry and alternating minimization procedures," *Statistics and Decisions*, pp. 205–237, 1984.
- [66] T. M. Cover and J. A. Thomas, *Elements of Information Theory*. Wiley, 2006.
- [67] S. W. Choi, S. A. Jafar, and S.-Y. Chung, "On the beamforming design for efficient interference alignment," *IEEE Communications Letters*, vol. 13, no. 11, pp. 847–849, Nov. 2009.
- [68] J. Thukral and H. Bölcskei, "Interference alignment with limited feedback," in *Proc. of IEEE International Symposium on Information Theory (ISIT)*, Jun. 2009, pp. 1759–1763.
- [69] K. K. Mukkavilli, A. Sabharwal, E. Erkip, and B. Aazhang, "On beamforming with finite rate feedback in multiple-antenna systems," *IEEE Trans. Information Theory*, vol. 49, no. 10, pp. 2562–2579, Oct. 2003.
- [70] O. E. Ayach, S. W. Peters, and J. Robert W. Heath, "The feasibility of interference alignment over measured MIMO-OFDM channels," *IEEE Transactions on Vehicular Technology*, 2010, accepted for publication.
- [71] R. Tresch and M. Guillaud, "Cellular interference alignment with imperfect channel knowledge," in *International Workshop on LTE Evolution, Proc. IEEE International Conference on Communications (ICC)*, Dresden, Germany, Jun. 2009.
- [72] L. Zheng and D. N. Tse, "Diversity and multiplexing: a fundamental tradeoff in multiple-antenna channels," *IEEE Trans. Information Theory*, vol. 49, no. 5, pp. 1073–1096, May 2003.
- [73] R. A. Horn and C. R. Johnson, *Matrix Analysis*. Cambridge University Press, 1985.

- [74] H. Shin and J. H. Lee, "Capacity of multiple-antenna fading channels: spatial fading correlation, double scattering, and keyhole," *IEEE Trans. Information Theory*, vol. 49, no. 10, pp. 2636–2647, Oct. 2003.
- [75] M. Médard, "The effect upon channel capacity in wireless communications of perfect and imperfect knowledge of the channel," *IEEE Trans. Information Theory*, vol. 46, no. 3, pp. 933–946, May 2000.
- [76] S. M. Kay, *Fundamentals of Statistical Signal Processing, Vol. 1: Estimation Theory*. Prentice Hall, 1993.
- [77] T. Yoo and A. Goldsmith, "Capacity and power allocation for fading MIMO channels with channel estimation error," *IEEE Trans. Information Theory*, vol. 52, no. 5, pp. 2203–2214, May 2006.
- [78] J. Xu, J. Zhang, , and J. G. Andrews, "On the accuracy of the Wyner model in cellular networks," *IEEE Transactions on Wireless Communications*, 2010, submitted, Available at <http://arxiv.org/abs/1009.5900>.
- [79] C. Suh and D. Tse, "Interference alignment for cellular networks," in *Proc. 46th Annual Allerton Conference on Communication, Control, and Computing*, Monticello, IL, USA, Sep. 2008.
- [80] R. Tresch and M. Guillaud, "Clustered interference alignment in large cellular networks," in *IEEE International Symposium On Personal, Indoor and Mobile Radio Communications (PIMRC)*, Tokyo, Japan, Sep. 2009.
- [81] M. Guillaud and R. Tresch, "Alignment-based interference mitigation technique for cellular networks," in *Newcom++ - ACoRN Joint Workshop*, Barcelona, Spain, Mar. 2009.
- [82] 3GPP, "Technical specification group radio access network; requirements for further advancements for E-UTRA (LTE-advanced)," 3GPP, Tech. Rep. 36.913 V8.0.0, Jun. 2008.
- [83] IEEE 802.16m-08/0004r2, "IEEE802.16m evaluation methodology document (EMD)," Tech. Rep., Jul. 2008.
- [84] 3GPP, "Technical specification group radio access network; feasibility study on interference cancellation for UTRA FDD user equipment (UE)," 3GPP, Tech. Rep. 25.963 V.7.0.0, Apr. 2007.

- [85] R. Tresch and M. Guillaud, “Performance of interference alignment in clustered wireless ad hoc networks,” in *Proc. IEEE Int. Symp. on Information Theory (ISIT)*, Austin, Texas, USA, Jun. 2010.
- [86] R. Tresch, G. Alfano, and M. Guillaud, “Interference alignment in clustered wireless ad hoc networks: high reliability regime and per-cluster ALOHA,” in *Proc. IEEE International Conference on Acoustics, Speech and Signal Processing (ICASSP)*, Prague, Czech Republic, May 2011, submitted.
- [87] —, “Large system analysis of interference alignment in clustered wireless ad hoc networks,” in *Proc. NEWCOM++/COST 2100 Joint Workshop on Wireless Communications (JNCW)*, Paris, France, Mar. 2011, submitted.
- [88] F. Baccelli and B. Błaszczyszyn, “A new phase transitions for local delays in MANETs,” in *Proc. IEEE Conference on Computer Communications (INFOCOM)*, San Diego, CA, Mar. 2010.
- [89] X. Shang, G. Kramer, and B. Chen, “A new outer bound and the noisy-interference sum-rate capacity for Gaussian interference channels,” *IEEE Trans. Information Theory*, vol. 55, pp. 689–699, Feb. 2009.
- [90] A. Papoulis and S. U. Pillai, *Probability, Random Variables and Stochastic Processes*. Mc Graw Hill, 2002.
- [91] M. Kang and M.-S. Alouini, “Largest eigenvalue of complex Wishart matrices and performance analysis of MIMO MRC systems,” *IEEE Journal on Selected Areas in Communications*, vol. 21, no. 3, pp. 418–426, Apr. 2004.